

# **The Split Luciferin Reaction: From Bioorthogonal Chemistry to Bioluminescence Imaging**

THÈSE N° 7224 (2017)

PRÉSENTÉE LE 17 FÉVRIER 2017

À LA FACULTÉ DES SCIENCES DE BASE

LABORATOIRE DE CHIMIE BIO-ORGANIQUE ET D'IMAGERIE MOLÉCULAIRE  
PROGRAMME DOCTORAL EN CHIMIE ET GÉNIE CHIMIQUE

ÉCOLE POLYTECHNIQUE FÉDÉRALE DE LAUSANNE

POUR L'OBTENTION DU GRADE DE DOCTEUR ÈS SCIENCES

PAR

**Aurélien GODINAT**

acceptée sur proposition du jury:

Prof. J. Zhu, président du jury  
Prof. E. Dubikovskaya, directrice de thèse  
Prof. C. W. Löwik, rapporteur  
Dr P. C. Böhni, rapporteur  
Prof. K. Johnsson, rapporteur



ÉCOLE POLYTECHNIQUE  
FÉDÉRALE DE LAUSANNE

Suisse  
2016







*À mon papa*



The work presented in this thesis has been performed in the laboratory of Bioorganic Chemistry and Molecular Imaging (LCBIM) at the Swiss Federal Institute of Technology in Lausanne (EPFL) under the supervision of Prof. Dr. Elena A. Dubikovskaya.

Part of the work described in this dissertation has been published in peer-review journals or presented at conferences. Texts, figures or drawings have been adapted or reused from published material (adapted with permission from Godinat *et al.*, *ACS Chemical Biology* **2013**, *8*, 987-999. Copyright 2016 American Chemical Society and from Godinat *et al.*, *Current protocols in chemical biology* **2014**, *6*, 169-189. Copyright 2016 JohnWiley & Sons, Inc.).

#### Journal publications.

Godinat, A.; Park, H. M.; Miller, S. C.; Cheng, K.; Hanahan, D.; Sanman, L. E.; Boggyo, M.; Yu, A.; Nikitin, G. F.; Stahl, A.; Dubikovskaya, E. A. A biocompatible in vivo ligation reaction and its application for noninvasive bioluminescent imaging of protease activity in living mice. *Acs Chemical Biology* **2013**, *8*, 987.

Godinat, A.; Budin, G.; Morales, A. R.; Park, H. M.; Sanman, L. E.; Boggyo, M.; Yu, A.; Stahl, A.; Dubikovskaya, E. A. A biocompatible "split luciferin" reaction and its application for non-invasive bioluminescent imaging of protease activity in living animals. *Current protocols in chemical biology* **2014**, *6*, 169.

Godinat, A.; Ruscitti, F.; Yevtodiyenko, A.; Budin, G.; Collins, J.; Regenscheit, N.; Stellari, F. F.; Dubikovskaya, E. A. *In vivo* Bioluminescence imaging of Neutrophil Elastase. *Manuscript in preparation*.

#### Oral presentation.

Godinat, A.; A biocompatible in vivo ligation reaction and its application for noninvasive bioluminescent imaging of protease activity in living mice. *European Molecular Imaging Meeting 2013 - European Society for Molecular Imaging (ESMI), Torino, Italy, 26-28 May 2013*.

#### Poster presentation.

Godinat, A.; Park, H. M.; Miller, S. C.; Cheng, K.; Hanahan, D.; Sanman, L. E.; Boggyo, M.; Yu, A.; Nikitin, G. F.; Stahl, A.; Dubikovskaya, E. A biocompatible in vivo ligation reaction and its application for noninvasive bioluminescent imaging of protease activity in living mice. *Fall Meeting of the Swiss Chemical Society 2013, Lausanne EPFL, Switzerland, 6 September 2013*.

Godinat, A.; Budin, G.; Frigell, J.; Dubikovskaya, E. A. Bioluminescence imaging of various proteases using split luciferin reaction. *European Molecular Imaging Meeting 2014 - European Society for Molecular Imaging (ESMI), Antwerp, Belgium, 4-6 June 2014*.





# Acknowledgements

First of all, I would like to thank Professor Elena A. Dubikovskaya, my supervisor, for giving me the opportunity to work on this fascinating research project at the frontier between chemistry, biology and imaging. I am particularly grateful for her precious scientific advices, her trust and her unconditional support throughout my Ph.D. studies.

I would like to express my gratitude to the members of my thesis Jury, Professor Kai Johnsson, Professor Clemens W.G.M. Löwik and Dr. Peter Böhni, for reviewing my thesis as well as Professor Jieping Zhu for Chairing the committee.

I wish to thank all the LCBIM lab members for the everyday help and support, the good atmosphere and the nice time spent together. I am particularly thankful to Dr. Ghyslain Budin, Dr. Hacer Karatas, Anzhelika Vorobyeva, Dr. Aleksey Yevotodiyenko, Dr. James Collins, Dr. Jens Frigell, Gennady Nikitin and Dr. Riccardo Sinisi for the fruitful collaborations. I would like to warmly thank Dr. Hacer Karatas, Dr. James Collins, Dr. Gerorgy Mikhaylov and Sleem Tawffik for proof-reading this thesis dissertation.

I also would like to acknowledge Professor Douglas Hanahan, Dr. Ke Chen, Dr Elizabeth Allen and Ehud Drori for the precious help on biological experiments as well as leading my first steps in working with laboratory animals. Moreover, I would like to thank Professor Theo Lasser, Dr. Stefan Geissbuehler and Azat Sharipov for the very interesting and successful collaboration.

Many thanks also to the EPFL histology core facility, especially to Dr. Jessica Sordet-Dessimoz and Dr. Nadine Regenscheit for the help on histology samples preparation and analysis.

I wish to thank Professor Andreas Stahl and Hyo Min Park from University of California Berkeley for welcoming me in their lab and for the great collaboration on *in vivo* caspase imaging. Similarly, I would like to thank Professor Matthew Bogoy and Laura E. Sanman for the help on the first *in vitro* caspase 3 experiments.

I also wish to thank Dr. Fabio Stellari and Francesca Ruscitti for their warm welcome in their lab in Parma and for the productive collaboration on neutrophil elastase *in vivo* imaging.

I would also like to express my gratitude to Professor Christopher Contag and Dr. Tobi Lyn Schmidt for hosting me in their laboratory at Stanford University for a few weeks.

I also thank all the members of the Heinis lab and Johnsson lab for the help and availability as well as the good moments.

Many thanks to the UDP team and Dr. Gisèle Ferrand for taking care of our mice as well as for the help and advice. Moreover, I wish to thank Dr. Isabelle Desbaillets Hakimi and Dr. Eleonora Simeoni for the precious support concerning the writing of animal licenses.

I wish to express my gratitude for the precious help, support, advices and availability to the members of the ISIC faculty, especially to the BCH Magasin team, Annelise Carrupt, Gladys Pache and Benjamin Kronenberg as well as Donald Zbinden, the mechanical workshop team, the mass spectrometry facility team and finally to Pascal Mieville from the NMR service.

Je tiens évidemment à remercier de tout mon cœur mes parents pour m'avoir toujours beaucoup soutenu et encouragé durant mes longues études. Une pensée va à mon papa, qui nous a quittés récemment et à qui je dédie cette thèse. Un grand merci également à tous les autres membres de ma famille, qui ont toujours été très présents et qui m'ont beaucoup soutenu. Merci infiniment à celle avec qui je partage ma vie, Isabelle, pour son aide, sa patience et son soutien inconditionnel. Finalement, un immense merci à tous mes amis, ceux que je vois tous les jours, et ceux que je vois moins souvent, ceux qui habitent à côté et ceux qui sont à l'autre bout du monde.

Merci à vous tous pour votre soutien et votre amour. None of this would have been possible without you.

*Aurélien*

# Abstract

Studying biological processes on the level of live cells with the help of biocompatible reactions has tremendously advanced our understanding of basic biology. However, the great complexity of many human pathologies such as cancer, diabetes and neurodegenerative diseases requires new tools that would allow investigation of biological processes throughout the organism.

The 2-cyanobenzothiazole (CBT)-based ligation reaction has received a recent interest in the chemical biology community. It has been reported in the literature for various applications, ranging from fluorescent labelling of proteins to nanostructures formation, and, most importantly, the reaction was shown to proceed in cells. This selective reaction between D-cysteine and hydroxy-CBT (HO-CBT) or amino-CBT (H<sub>2</sub>N-CBT), also named as *split luciferin reaction*, generates as product a D-luciferin analogue, one of the most commonly used substrates for bioluminescence imaging (BLI). Therefore, the split luciferin reaction has high potential for BLI applications.

In this work, we have shown that production of a luciferin substrate via the split luciferin reaction can be visualized in live mice using BLI. Furthermore, the split luciferin approach allows interrogation of target tissues using a masking approach, where D-luciferin is formed only under certain conditions. This reaction was successfully applied to real-time non-invasive imaging of apoptosis, associated with caspase 3/7 activity. Caspase-dependent release of free D-cysteine from a caspase 3/7 specific peptide substrate allowed selective reaction with H<sub>2</sub>N-CBT *in vivo* to form 6-amino-D-luciferin with subsequent light emission in the presence of the firefly luciferase enzyme. Importantly, this strategy was found to be superior to the use of the commercially available DEVD-aminoluciferin substrate for imaging caspase 3/7 activity. The same methodology was extended to imaging activity of other caspases as well as thrombin enzyme in an *in vitro* set-up. Furthermore, the split luciferin approach enables dual imaging, where each reaction partner would be individually caged to report on separate biological events. This approach was used for simultaneous imaging of caspase 3 and  $\beta$ -galactosidase *in vitro*, validating the use of the split luciferin reaction for imaging multiple processes. Moreover, the split luciferin reaction was also successfully applied to both quantification of Neutrophil Elastase activity *in*

*vitro* and real-time non-invasive imaging of Neutrophil Elastase in an *in vivo* inflammation model. Altogether, the present study suggests that the split luciferin approach is an efficient and versatile tool for *in vivo* applications.

## Keywords

Biocompatible reaction; Bioorthogonal reaction; Bioluminescence imaging; Luciferase; D-luciferin; Split luciferin reaction; *in vivo* imaging; Protease imaging; Enzymatic assay; Caspase; Neutrophil Elastase; Bioluminogenic probes.

# Résumé

L'étude des processus biologiques dans les cellules vivantes grâce aux réactions biocompatibles a énormément amélioré notre compréhension de la biologie fondamentale. Cependant, la grande complexité de nombreuses pathologies humaines telles que le cancer, le diabète et les maladies neurodégénératives requiert de nouveaux outils indispensables à l'étude des processus biologiques à l'échelle d'un organisme.

La réaction de ligature basée sur le 2-cyanobenzothiazole (CBT) a perçu un récent intérêt de la part de la communauté de biologie chimique. L'utilisation de cette réaction a été rapportée dans la littérature pour des applications variées, allant de la modification de protéines avec des marqueurs fluorescents à la formation de nanostructures. Mais aussi et surtout, il a été démontré que cette réaction peut avoir lieu dans un milieu cellulaire. Cette réaction sélective entre la D-cystéine et le hydroxy-CBT (HO-CBT) ou amino-CBT ( $H_2N$ -CBT), également appelée réaction de split luciférine, génère comme produit un analogue de la D-luciférine, qui est l'un des substrats les plus couramment employés pour l'imagerie par bioluminescence. Par conséquent, la réaction de split luciférine présente un fort potentiel pour des applications d'imagerie par bioluminescence.

Dans le cadre de ce travail, nous avons montré que la production de luciférine, via la réaction de split luciférine, peut être visualisée dans des souris vivantes, au moyen de l'imagerie par bioluminescence. En outre, l'utilisation de la réaction de split luciférine permet l'interrogation de tissus cibles par le biais d'une approche qui consiste à masquer la D-cystéine. Celle-ci ne peut donc réagir avec le CBT qu'après avoir été libérée par un processus biologique spécifique, se traduisant par une formation de D-luciférine, dans certaines conditions particulières. Cette approche a été appliquée avec succès à l'image non-invasive en temps réel de l'apoptose, associée à l'activité des caspases 3/7. La libération de D-cystéine d'un peptide substrat des caspases 3/7 permet la réaction sélective avec  $H_2N$ -CBT *in vivo* afin de former la 6-amino-D-luciférine, qui, en présence de luciférase, produit une émission de lumière qui est donc dépendante de l'activité des caspases. Il est notable que cette stratégie se révèle être supérieure à l'utilisation de la sonde bioluminogène DEVD-aminoluciférine, laquelle est commercialisée pour l'imagerie de l'activité des caspases 3/7. La même méthodologie a ensuite été étendue à l'imagerie d'autres caspases ainsi que de la thrombine dans des conditions *in vitro*.

En outre, la réaction de split luciférine permet une double imagerie, où chaque partenaire de réaction serait individuellement masqué, permettant de détecter simultanément des événements biologiques séparés. Cette approche a été adoptée pour l'imagerie simultanée de la caspase 3 et de la  $\beta$ -galactosidase *in vitro*, validant ainsi l'utilisation de la réaction de split luciférine pour l'imagerie de processus multiples. Enfin, la réaction de split luciférine a été appliquée avec succès, d'une part, à la quantification de l'activité de la neutrophile élastase *in vitro* en temps réel et d'autre part, à l'imagerie non-invasive de la neutrophile élastase dans un modèle *in vivo* d'inflammation. En conclusion, la présente étude suggère que la réaction de split luciférine est un outil efficace et polyvalent pour diverses applications *in vivo*.

## Mots-clés

Réaction biocompatible; Réaction bioorthogonale; Imagerie par bioluminescence; Luciférase; D-luciférine; Réaction de Split luciférine; Imagerie de protéase; Analyse enzymatique; Caspase; Neutrophile élastase; Sonde bioluminogénique.

# Contents

<b>Acknowledgements .....</b>	<b>ix</b>
<b>Abstract .....</b>	<b>xi</b>
<b>Keywords.....</b>	<b>xii</b>
<b>Résumé.....</b>	<b>xiii</b>
<b>Mots-clés .....</b>	<b>xiv</b>
<b>List of Figures.....</b>	<b>xvii</b>
<b>List of Tables.....</b>	<b>xix</b>
<b>List of Schemes .....</b>	<b>xix</b>
<b>List of Movies .....</b>	<b>xix</b>
<b>Abbreviation.....</b>	<b>xxi</b>
<b>Chapter 1     Introduction .....</b>	<b>1</b>
1.1     Bioluminescence imaging .....	1
1.2     The firefly luciferin (D-luciferin) .....	4
1.3     Analogs of D-luciferin .....	6
1.4     Caged luciferins for sensing molecular changes <i>in vivo</i> .....	7
1.4.1     Bioluminescence imaging of protease activity.....	8
1.4.2     Caged-luciferin probes for imaging biological processes .....	11
1.5     Bioorthogonal click reactions .....	16
1.6     Condensation reaction between 2-cyanobenzothiazole (CBT) and 1,2-aminothiols.....	20
<b>Chapter 2     Bioluminescence Imaging Using Biocompatible Split Luciferin Reaction .....</b>	<b>25</b>
2.1 <i>In vitro</i> formation of D-luciferin and D-aminoluciferin in physiological solutions .....	26
2.1.1     Kinetic studies of the reaction between CBT derivatives and L-cysteine.....	27

2.2	Real time non-invasive imaging and quantification of the split luciferin ligation reaction in living cells .....	28
2.3	Real time non-invasive imaging and quantification of split luciferin ligation reaction in living animals .....	33
2.3.1	Optimization studies of split luciferin ligation reaction in living mice .....	34
2.3.2	<i>In vivo</i> comparative studies of signal stability of split luciferin ligation reaction with D-luciferin .....	35
2.4	Conclusion .....	37
2.5	Experimental section .....	38
2.6	Supplementary figures .....	41
<b>Chapter 3</b>	<b>Application of the Split Luciferin Reaction for Non-Invasive Bioluminescent Imaging of Protease Activity</b>	<b>45</b>
3.1	<i>In vitro</i> imaging of thrombin and caspase 3 protease activity .....	46
3.2	<i>In vitro</i> real time imaging of caspase activity .....	50
3.2.1	<i>In vitro</i> simultaneous imaging of caspase 3 and $\beta$ -galactosidase using the split luciferin reaction ....	54
3.3	Real time non-invasive imaging of caspase 3/7 activities in living animals .....	56
3.4	Conclusion .....	60
3.5	Experimental section .....	61
3.6	Supplementary figures .....	67
<b>Chapter 4</b>	<b>Bioluminescence Imaging of Neutrophil Elastase Activity Using the Split Luciferin Reaction</b> .....	<b>71</b>
4.1	Probe design .....	73
4.2	<i>In vitro</i> real time imaging of neutrophil elastase activity in enzymatic assays .....	74
4.3	Real time non-invasive imaging and quantification of neutrophil elastase activity in mouse neutrophils using the split luciferin ligation reaction .....	77
4.4	Real time non-invasive imaging of neutrophil elastase activity in living animals .....	79
4.5	Conclusion .....	85
4.6	Experimental section .....	86
4.7	Supplementary figures .....	92
<b>Chapter 5</b>	<b>Conclusion</b> .....	<b>95</b>
<b>Chapter 6</b>	<b>References</b> .....	<b>99</b>
<b>Chapter 7</b>	<b>Annexes</b> .....	<b>113</b>
7.1	Curriculum Vitae .....	113



## List of Figures

Figure 1.1: Bioluminescent firefly in nature	1
Figure 1.2: In vitro light emission in function of the time by Fluc with D-luciferin substrate	6
Figure 1.3: Examples of synthetic D-luciferin analogues as substrates for firefly luciferase	7
Figure 1.4: Structures of caged-luciferin probes for imaging furin activity	10
Figure 1.5: Caged substrates for imaging carboxypeptidases activity	10
Figure 1.6: Bioorthogonal reactions	17
Figure 1.7: Functionalization of targeting moieties with imaging reporters via the CBT-based ligation reaction	23
Figure 2.1: Overall schematic of the split luciferin ligation reaction in various biological environments	26
Figure 2.2: Formation of D-luciferin in vitro	27
Figure 2.3: Light emission resulting from the split luciferin reaction in living cells	29
Figure 2.4: Split luciferin ligation reaction in living SKOV3-Luc-D3 cells	30
Figure 2.5: Split luciferin ligation reaction in living MDA-MB-231-Luc-D3H2LN cells	31
Figure 2.6: Effect of high D-cysteine concentrations on bioluminescence emission in SKOV3-Luc-D3 and MDA-MB-231-luc- D3H2LN living cells	32
Figure 2.7: Imaging split luciferin reaction in living mice	33
Figure 2.8: Split luciferin ligation reaction in living mice	34
Figure 2.9: Split luciferin ligation reaction in living mice	36
Figure S2.1: In vitro formation of luciferins	41
Figure S2.2: Pseudo-first order rate constant determination for the reaction of HO-CBT with different concentrations of L-cysteine	41
Figure S2.3: Pseudo-first order rate constant determination for the reaction of H2N-CBT with different concentrations of L-cysteine	42
Figure S2.4: Pseudo-first order rate constant determination for the reaction of N-succinamidyl CBT derivative 1 with different concentrations of L-cysteine	42
Figure S2.5: Split luciferin ligation reaction in SKOV3-Luc-D3 living cells	43
Figure S2.6: Split luciferin ligation reaction in living MDA-MB-231-Luc-D3H2LN cells	43
Figure 3.1: <i>In vitro</i> enzymatic assay of caspase 3 activity using DEVD-(D-Cys) peptide and H <sub>2</sub> N-CBT	49
Figure 3.2: <i>In vitro</i> enzymatic assay of Thrombin activity using GGR-(D-Cys) peptide and H <sub>2</sub> N-CBT	49
Figure 3.3: <i>In vitro</i> enzymatic assay of caspase 3 activity using z-DEVD-(D-Cys) peptide and HO-CBT	50
Figure 3.4: <i>In vitro</i> enzymatic assay of caspase 6, caspase 8 and caspase 9 activities imaging with respectively z-VEID-(D-Cys), z-LETD-(D-Cys) or z-LEHD-(D-Cys) peptide and HO-CBT	51
Figure 3.5: Cross reactivity assay of the caspases specific split luciferin probes with different caspases	53
Figure 3.6: Dual enzyme imaging using the split luciferin reaction	55
Figure 3.7: Caspase 3/7 activity imaging using luciferin ligation reaction in living transgenic reporter mice	57
Figure 3.8: Caspase 3/7 activity imaging using luciferin ligation reaction in living transgenic reporter mice	58
Figure 3.9: Observed luminescence emission as a function of the time from caspase 3/7 selective bioluminescent probes after LPS and D-GalN or vehicle injection of FVB+Luc mice	58

Figure 3.10: Overall representation of the dual imaging concept for luciferin ligation	60
Figure S3.1: <i>In vitro</i> enzymatic assay of caspase 6, caspase 8 and caspase 9 activities imaging with respectively z-VEID-(D-Cys), z-LETD-(D-Cys) or z-LEHD-(D-Cys) peptide and HO-CBT	67
Figure S3.2: Colorimetric assay of caspases activities	68
Figure S3.3: Dual enzyme imaging using the split luciferin reaction	68
Figure S3.4: Flow cytometry data with a caspase 3/7 activation assay	68
Figure S3.5: Docetaxel treatment on subcutaneous SKOV3-Luc-D3 xenografts model in nude mice for caspase 3/7 activation imaging	69
Figure 4.1: Imaging NE activity using split luciferin reaction	74
Figure 4.2: <i>In vitro</i> enzymatic assay of HNE activity imaging with Ac-AAPV-(D-Cys) and HO-CBT split luciferin probe	75
Figure 4.3: <i>In vitro</i> enzymatic assay of HNE activity imaging with Ac-AAPV-(D-Cys) peptide and HO-CBT in presence of sivelestat inhibitor	76
Figure 4.4: <i>In vitro</i> enzymatic assay of HNE effect on luminescence emission using the split luciferin reaction	77
Figure 4.5: Imaging NE activity in activated mice neutrophils	78
Figure 4.6: NE activity imaging using split luciferin reaction in a mouse model of acute lung injury	81
Figure 4.7: Imaging NE activity in a LPS/fMLP induced mouse acute lung injury model	81
Figure 4.8: Observed luminescence emission over 60 min from NE bioluminescent probes in a LPS/fMLP induced mouse acute lung injury model	82
Figure 4.9: Hematoxylin and eosin (HE) staining of formalin fixed paraffin embedded tissue sections from BalbC mice lungs after intratracheal treatment with LPS or saline as control	83
Figure 4.10: Immunohistochemical (IHC) staining of Ly6G antigen revealed by Bluemap on paraffin fixed histology sections from BalbC mice lungs after intratracheal treatment with LPS or saline as control	83
Figure 4.11: Imaging NE activity in a LPS/fMLP induced mouse FVB-Luc+ acute lung injury model	84
Figure S4.1: Colorimetric assay of HNE activity	92
Figure S4.2: Background assessment resulting from the reaction between HO-CBT and cysteine present in different buffers	93
Figure S4.3: Determination of luciferase expression in BalbC transfected mice 1 day, 4 days, 5 days and 7 days after DNA delivery	93
Figure S4.4: Plasmid map of pLenti-UbC-RedFLuc-T2A-Puro (RedLuc-puro) that expresses Luciferase under UbC promoter	94

## List of Tables

Table 1.1: Commonly used luciferases for BLI with their respective substrates	3
Table 1.2: List of reported caged-luciferin probe for imaging processes of interest (target)	12-13
Table 1.3: Reported probes caged on the carboxylic acid of luciferin scaffold	15
Table 1.4: Bioorthogonal ligation reactions for <i>in vivo</i> applications	18-19
Table 2.1: Reaction rate constants between 2-cyanobenzothiazoles derivatives and L-cysteine	28
Table 2.2: Signal variability of D-luciferin and its derivatives upon I.P. injection in living mice	35

## List of Schemes

Scheme 1.1: Mechanism of D-luciferin oxidation by firefly luciferase	4
Scheme 1.2: Dehydroluciferyl adenylate and hydrogen peroxide production by FLuc	5
Scheme 1.3: Proposed biosynthesis pathway of D-luciferin from L-luciferin.	5
Scheme 1.4: Caged-luciferin strategy	8
Scheme 1.5: DEVD-aminoluciferin probe for imaging Caspase 3/7 activity	8
Scheme 1.6: Condensation reaction between 6-hydroxy-2-cyanobenzothiazole or 6-amino-2-cyanobenzothiazole with D-cysteine	21
Scheme 1.7: Reaction mechanism between 6-hydroxy-2-cyanobenzothiazole (HO-CBT) and cysteine	21
Scheme 1.8: 2-cyanobenzothiazole condensation reaction with 1,2-aminothiols	22
Scheme 2.1: Split luciferin reaction	25
Scheme 3.1: Imaging protease activity using the split luciferin reaction	48
Scheme 3.2: Dual caging on luciferin precursors for imaging multiple biomolecular activities using the split luciferin reaction	55

## List of Movies

Movie S3.1: Imaging caspase activity with the split luciferin reaction	69
--	----



# Abbreviation

AAPV	Ala-Ala-Pro-Val
AAPV-pNA	N-Methoxysuccinyl-Ala-Ala-Pro-Val- <i>para</i> -Nitroanilide
Ac-AAPV-(D-Cys)	Ac-L(Ala-Ala-Pro-Val)-D-(Cys)-OH
ALI	Acute lung injury
AMP	Adenosine monophosphate
ARDS	Acute respiratory distress syndrome
ATP	Adenosine triphosphate
AUC	Area under the curve
BAL	bronchoalveolar lavage
BalbC	BALB/cAnNCrl
BL	Bioluminescence
BLI	Bioluminescence imaging
CBT	2-cyanobenzothiazole
CoA	Coenzyme A
D-aminoluciferin	6'-amino-D-luciferin
DCM	Dichloromethane
DEVD	Asp-Glu-Val-Asp
DEVD-(D-Cys)	H <sub>2</sub> N-L(Asp-Glu-Val-Asp)-D-Cys-OH
D-GalN	D-galactosamine
DIBO	Dibenzocyclooctyne
DIFO	Difluorinated cyclooctyne

---

DMF	<i>N,N</i> -Dimethylformamide
DMSO	Dimethyl sulfoxide
DNA	Deoxyribonucleic acid
EtOH	Ethanol
FLuc	Firefly luciferase
fMLP	<i>N</i> -Formylmethionyl-leucyl-phenylalanine
FMNH <sub>2</sub>	Reduced flavin mononucleotide
FRET	Förster resonance energy transfer
FVB-Luc+	FVB-Tg(CAG-luc,-GFP)L2G85Chco/J
GGR-(D-Cys)	H <sub>2</sub> N-L(Gly-Gly-Arg)-D-Cys-OH
H <sub>2</sub> N-CBT	6-amino-2-cyanobenzothiazole
HE	Hematoxylin and eosin
HNE	Human neutrophil elastase
HO-CBT	6-hydroxy-2-cyanobenzothiazole
HPLC	High-performance liquid chromatography
i.p.	Intraperitoneal
IED DA	Inverse electron demand Diels-Alder reaction
IHC	Immunohistochemistry
LPS	Lipopolysaccharides
Lugal	1- <i>O</i> -galactopyranosyl-luciferin
MeCN	Acetonitrile
MeOH	Methanol
NE	Neutrophil elastase
NIR	Near-infrared
PBS	Phosphate-buffered saline
PET	Positron emission tomography

Abbreviation

---

pNA	4-nitroaniline
PR3	Proteinase 3
SL	Staudinger ligation reaction
SPAAC	Strain-promoted azide-alkyne cycloaddition
U	Enzymatic units
z-DEVD-(D-Cys)	Cbz-L(Asp-Glu-Val-Asp)-D-Cys-OH
z-LEHD-(D-Cys)	Cbz-L(Leu-Glu-His-Asp)-D-Cys-OH
z-LETD-(D-Cys)	Cbz-L(Leu-Glu-Thr-Asp)-D-Cys-OH
z-VEID-(D-Cys)	Cbz-L(Val-Glu-Ile-Asp)-D-Cys-OH
B-Gal	$\beta$ -galactosidase
$\lambda$	Wavelength





# Chapter 1 Introduction

## 1.1 Bioluminescence imaging

Bioluminescence is the naturally occurring form of chemiluminescence where the light is released upon a chemical reaction. It occurs in various organisms such as marine vertebrates or invertebrates and terrestrial insects. Majority of bioluminescent organisms lives in the seas and include fishes, crustaceans as well as microorganisms. Fireflies (**Figure 1.1**), click beetles, glow worms and some types of mushrooms can be cited as examples of terrestrial bioluminescent organisms. These organisms use bioluminescence for a number of purposes including camouflage, attracting mates, communication and repulsion.<sup>[1,2]</sup>

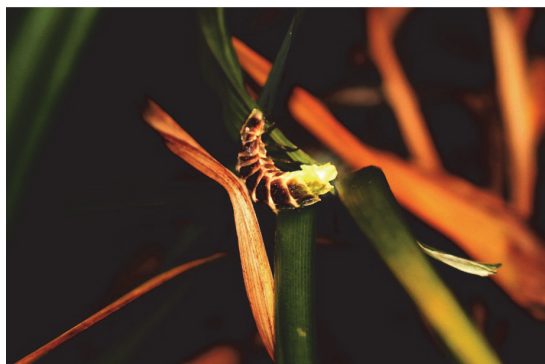


Figure 1.1: Bioluminescent firefly in nature (Photos courtesy of Jack Moreh and copyright Free Range Stock, [www.freerangestock.com](http://www.freerangestock.com)).

Basic research was carried to understand the biology of light-emitting organisms. Fundamental knowledge acquired on the molecular mechanisms of bioluminescence resulted in the translation from nature to laboratories applications. Understanding living systems requires tools to explore molecular processes in cells and animals. Chemical or genetic approach coupled to different imaging modalities are now widely used for molecular imaging applications. Among these imaging techniques, Bioluminescence imaging (BLI) is nowadays popular for sensing molecular and cellular functions in cells and *in vivo*. The principle of Bioluminescence (BL) relies on the reaction of a class of enzymes, *luciferases*, with their respective substrate, *luciferins*. Luciferases are oxidative enzymes that catalyze the oxidation

of their substrates, luciferins, to an oxidation product in an excited-state that decays with light emission. Some luciferases require cofactors such as ATP or magnesium cations.<sup>[3,4]</sup> BLI is a powerful methodology for molecular imaging and is now routinely used both *in vitro* and *in vivo* for a wide range applications including imaging gene expression, tumor growth monitoring and biological processes.<sup>[3,5]</sup> Although many different luciferase/luciferin pairs were identified in nature, only a few of them (e.g. Firefly luciferase (FLuc), Click beetle luciferase, Renilla and Gaussia luciferases) have been employed for molecular imaging (**Table 1.1**).

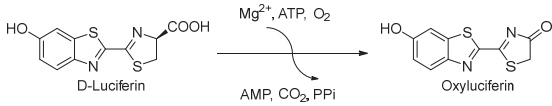
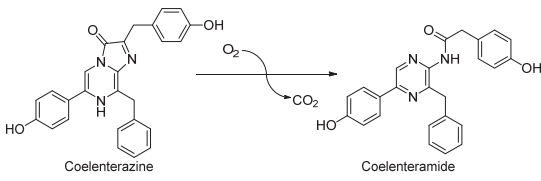
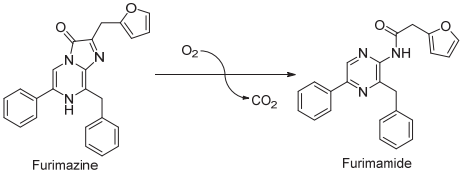
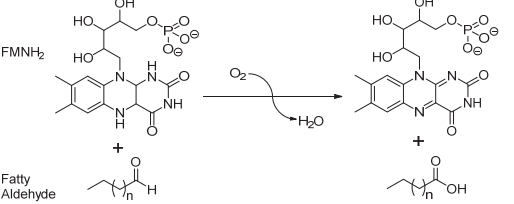
Firefly, Green click beetle and Red click beetle luciferases utilize D-luciferin ((S)-2-(6-Hydroxy-2-benzothiazolyl)-2-thiazoline-4-carboxylic acid, also called firefly luciferin) as substrate and require dioxygen and ATP as cofactors (**Table 1.1**, entry **1**). D-luciferin is oxidized to oxyluciferin in an electronically excited state, whose decay to the ground state generates a photon emission. Insect luciferases all use the D-luciferin as substrate, while having different light emission spectrum (**Table 1.1**, entry **1-3**). The exact emission wavelength is determined by both the substrate molecule and the enzyme internal microenvironment of the active site.<sup>[6]</sup>

Luciferases native of marine organisms such as Renilla or Gaussia luciferases use coelenterazine as substrate (**Table 1.1**, entry **4-6**). In the presence of a molecular oxygen, bioluminescent light is emitted upon luciferase-catalyzed oxidation of coelenterazine to coelenteramide.<sup>[7]</sup> Recently, NanoLuc was added to this class of enzyme. A native luciferase enzyme from the deep sea shrimp *Oplophorus* was engineered for stability and optimal luminogenic substrate resulting in NanoLuc enzyme which uses a coelenterazine derivative, Furimazine, as substrate (**Table 1.1**, entry **7**).<sup>[8]</sup> This class of luciferases are ATP independent and do not require exogenous cofactors to produce light. Their light emission peaks in the blue-green region of the light spectrum.

Finally, the last family of luciferases that has been used for molecular imaging is bacterial luciferases. Luminous bacteria mainly come from marine environment and are often isolated as organ symbionts of fishes. Interestingly, these bacterial luciferases produce light in a two-step mechanism, where a reduced flavin mononucleotide (FMNH<sub>2</sub>) bound to the luciferase enzyme reacts with dioxygen to produce a peroxy-intermediate that will then react with an aliphatic aldehyde to generate a second intermediate. This excited-state product then reaches ground state while generating a photon of light (**Table 1.1**, entry **8**).<sup>[9]</sup> The bacterial luciferase genes *luxA* and *luxB* (*luxAB*) encode for proteins involved in the light emission process, and the so called *lux* operon (*luxCDABE*) encode for both the luciferases and all the proteins that produce the necessary substrates. Therefore, *lux* operon provides all the nec-

essary components for light emission, resulting in a luminescent system that does not require an external luciferin substrate.<sup>[10]</sup> While this *Lux* operon had initially been limited to bacterial applications, it was recently adapted for use in mammalian cells.<sup>[11]</sup>

Table 1.1: Commonly used luciferases for BLI with their respective substrates, and the resulting BL emission wavelength (table adapted from [6] and [12]).

	Luciferase	Substrate (luciferin)	Enzymatic reaction	$\lambda^*$ [nm]	Ref.
1	Firefly (Photinus Pyralis)	D-luciferin		612	13
2	Click beetle red (Pyrophorus Plagiophthalmus)			611	13,14
3	Click beetle green (Pyrophorus Plagiophthalmus)			544	13,14
4	Renilla reniformis (native, RLuc8)	Coelenterazine		480	15
5	Renilla reniformis (RLuc8.6-535)			535	16
6	Gaussia princeps (GLuc)			480	17,18
7	NanoLuc	Furimazine		460	8
8	<i>Lux</i> AB	FMNH <sub>2</sub> + Aliphatic aldehyde		490	19

\* At 37 °C, represent the peak of emission.

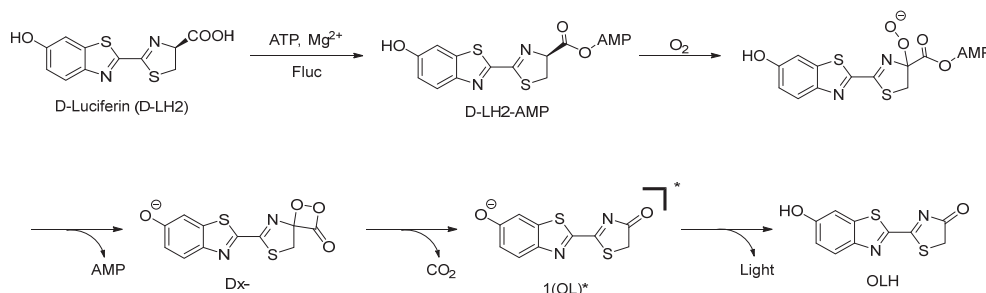
Mammalian tissues are not transparent and thus attenuate optical signal by both absorbing and scattering light. The changes in refractive index between tissue boundaries, cell membranes or organelles are responsible for scattering of light in living systems but the influence of wavelength is minor within the visible light spectrum. Absorption of photons depends on the type of tissue and endogenous chromophores such as hemoglobin that absorbs principally in the blue-green region (460-570 nm) of the visible spectrum,<sup>[20,21]</sup> which hinders the signal detection from deep tissues. In the red

and near-infrared spectrum ( $\lambda > 600$  nm), absorption by hemoglobin is lower, allowing red light penetration through tissue with a depth of a few centimeters.<sup>[13]</sup> Since Renilla, Gaussia and bacterial luciferases emit light in the blue/green region (460-570 nm) that yields lower tissue penetration, they are less suitable for *in vivo* studies compared to the FLuc/D-luciferin pair which produces a more red-shifted light. Nevertheless, the ATP independence of Renilla or Gaussia luciferases is still attractive for *in vitro* applications as they could sense both intra- and extra-cellular environments. Moreover, multiple luciferase/luciferin pairs having different emission wavelengths can be combined and used simultaneously for multicolor imaging.<sup>[3]</sup> This would allow monitoring several processes at the same time by recording different wavelengths of light emission.

## 1.2 The firefly luciferin (D-luciferin)

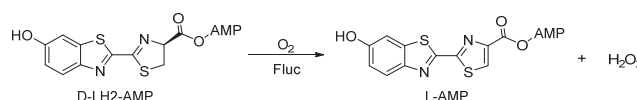
The FLuc/D-luciferin pair is one of the main luciferase/luciferin system used in bioluminescence imaging *in vitro* and *in vivo*. Due to its light emission wavelength, FLuc/D-luciferin pair is particularly suited for applications in living animals. The reaction between D-luciferin and FLuc in the presence of ATP,  $Mg^{2+}$  and a molecular oxygen produces a photon of light.<sup>[22]</sup> The intensity of the light output is closely correlated with the amount of D-luciferin available for the enzyme, and therefore it is possible to quantify the amount of D-luciferin by measuring the light emission.

The catalytic reaction, shown in Scheme 1.1, starts with the adenylation of D-luciferin (D-LH<sub>2</sub>) by FLuc to yield D-luciferin-adenylate (D-LH<sub>2</sub>-AMP), followed by oxygenation. The AMP substituent on D-LH<sub>2</sub>-AMP increases the acidity of the C4 proton, resulting in the formation of a carbanion intermediate, further performing a nucleophilic attack on molecular oxygen. In the following step, a luciferin dioxetanone anion (Dx<sup>-</sup>), which consists of a four membered strained ring formed upon AMP release. Thereafter, light emitter intermediate, the excited singlet state of oxyluciferin OL<sup>-</sup> [<sup>1</sup>(OL<sup>-</sup>)\*], is generated. Finally, the luminescent light is produced with a peak intensity around 560 nm (at pH 7.6) upon <sup>1</sup>(OL<sup>-</sup>)\* relaxation to the ground state.<sup>[23,24]</sup> The emission wavelength is dependent on a number of factors including the pH and temperature.<sup>[13,24,25]</sup>



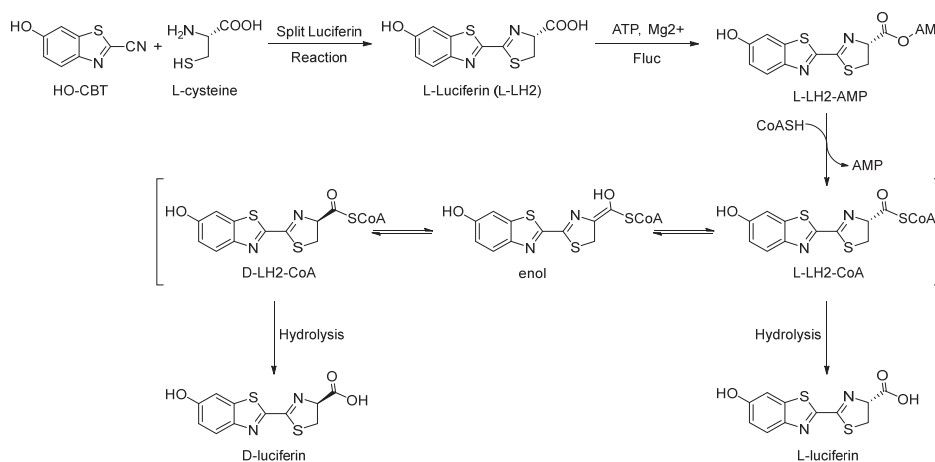
Scheme 1.1: Mechanism of D-luciferin oxidation by firefly luciferase.

Beside its oxidase activity in bioluminescent reaction, FLuc enzyme displays several lateral reactions. An alternative to the bioluminescent reaction is the reaction of D-LH2-AMP with dioxygen yielding an oxidized product, dehydroluciferyl-AMP (L-AMP), a process in which hydrogen peroxide is produced (**Scheme 1.2**). This is a dark process where no light is generated during the reaction.<sup>[26,27]</sup>



Scheme 1.2: Dehydroluciferyl adenylate and hydrogen peroxide production by FLuc.

FLuc enzyme could also act as acyl-CoA ligase.<sup>[23,28,29]</sup> Biosynthesis of the D-luciferin is not yet fully understood. As in nature only L-amino acids occur in proteins, it was proposed that D-luciferin could be produced from L-luciferin via an enzyme-mediated inversion of configuration. L-luciferin would be produced by the reaction of HO-CBT with L-cysteine, then L-luciferin would be adenylated to form L-luciferin-AMP (L-LH2-AMP). This compound would be further converted to L-luciferin-CoA which can racemize to the D-enantiomer via enolization (**Scheme 1.3**). Hydrolysis of the D-luciferin-CoA by esterases would yield the D-luciferin molecule. This pathway could also explain the capability of FLuc to produce light with L-luciferin as substrate.<sup>[30]</sup> Moreover, the production of luciferin-CoA is stereospecific and only occurs with the L-luciferin. This indicates that FLuc distinguishes the L- and D-isomer of luciferin and thus acts as Acyl-CoA synthetase only for L-luciferin, saving the use of the D-isomer for the bioluminescent reaction.<sup>[31,32]</sup>



Scheme 1.3: Proposed biosynthesis pathway of D-luciferin from L-luciferin. The split luciferin reaction between HO-CBT and L-cysteine yield L-luciferin, that further undergo a FLuc-mediated adenylation reaction resulting in the formation of L-luciferin-AMP (L-LH2-AMP). CoA reacts then with L-LH2-AMP, yielding the L-luciferin-CoA (L-LH2-CoA) which is racemized by enolization to the D-enantiomer. Hydrolysis of D-luciferin-CoA by esterases yield to the product D-luciferin (Scheme Adapted from [32]).

The CoA addition reaction also occurs with L-AMP to yield dehydroluciferl-CoA (L-CoA). As L-AMP is a strong-binding inhibitor of FLuc ( $K_i = 3.8 \pm 0.7$  nM), while L-CoA is a less powerful inhibitor ( $K_i$

=  $0.88 \pm 0.03 \mu\text{M}$ ), the formation of the acyl-adenylate in which the thiol of CoA displaces the AMP moiety favors the bioluminescent pathway.<sup>[23,32-35]</sup> Besides L-AMP, the product of the bioluminescent reaction, oxyluciferin, also has an inhibitory effect on FLuc ( $K_i = 0.50 \pm 0.03 \mu\text{M}$ ). Both of these compounds are mainly responsible for the light emission pattern of FLuc with D-Luciferin as substrate *in vitro*. It consists of an initially highly intense signal (flash of light) which quickly decays to a sustained lower intensity luminescence (**Figure 1.2**). However, addition of coenzyme A (CoA) yields a more stable, high-intensity luminescence that decays over a longer duration period.<sup>[23]</sup>

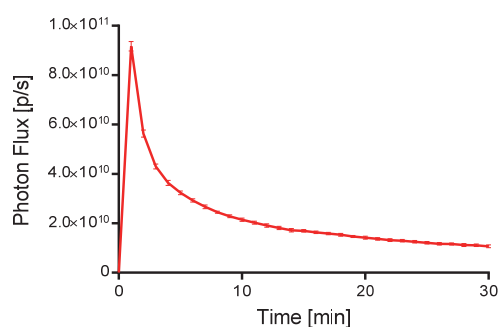


Figure 1.2: *In vitro* light emission in function of the time by FLuc with D-luciferin substrate. D-luciferin ( $10 \mu\text{M}$ ) was added to FLuc ( $40 \mu\text{g/mL}$ ) solution containing  $\text{MgSO}_4$  ( $3.3 \text{ mM}$ ) and ATP ( $3.3 \text{ mM}$ ) in Tris-HCl buffer at pH8. After rapidly reaching the maximum, a fast decay is observed. Error bars are  $\pm$  SD for three independent measurements.

### 1.3 Analogs of D-luciferin

Replacement of the aromatic hydroxyl group in D-Luciferin (**Figure 1.3**, compound **1**) with an amino group, yielded 6'-amino-D-luciferin (D-aminoluciferin) (**Figure 1.3**, compound **2**), with an emission wavelength ( $605 \text{ nm}$ ) independent of the pH upon reaction with FLuc.<sup>[25]</sup> Additionally, the D-aminoluciferin has higher affinity to FLuc than the natural D-luciferin.<sup>[36]</sup> Successive groups have attempted to synthesize analogues of D-luciferin to produce higher affinity molecules, but the high substrate specificity of FLuc does not tolerate large modifications on the scaffold without reduction or loss of affinity. Structure-activity studies showed that an electron-donating substituent at the 6'-position is essential for light emission. Alkylation or acylation of D-luciferin at the 6'-phenol position or acylation of D-aminoluciferin at the 6'-amino position has been shown to affect the luciferase/substrate reaction and such analogues have no BL capacity.<sup>[25]</sup> In another study, a series of N-mono and N-di-alkylated aminoluciferins have been proven to be substrates for FLuc. A number of analogs including molecules **3-5** (**Figure 1.3**), showed stronger light emission than the D-aminoluciferin.<sup>[37]</sup> More recent studies evaluated the bioluminescent properties of conformation-restricted cyclic alkylaminoluciferin substrates **6-9** (**Figure 1.3**) which produced red-shifted photon flux. However, most of these novel luciferins require mutant luciferases to have acceptable light emitting properties and thus cannot be conveniently used

for *in vivo* studies, with the exception of compound **6**.<sup>[38-41]</sup> Another approach that consists of replacing the sulfur atom in the thiazolin ring with selenium (**Figure 1.3**, compound **10**), resulted in a red-shifted bioluminescent signal but much lower quantum yield compared to the D-aminoluciferin.<sup>[42]</sup> Examples for modifications on the benzothiazole core with various heterocyclics (**11-13**),<sup>[43,44]</sup> replacement with naphthol derivatives (**14-15**)<sup>[45]</sup> or extended  $\pi$ -conjugation systems (**16-19**)<sup>[43,46]</sup> are shown in Figure 1.3.

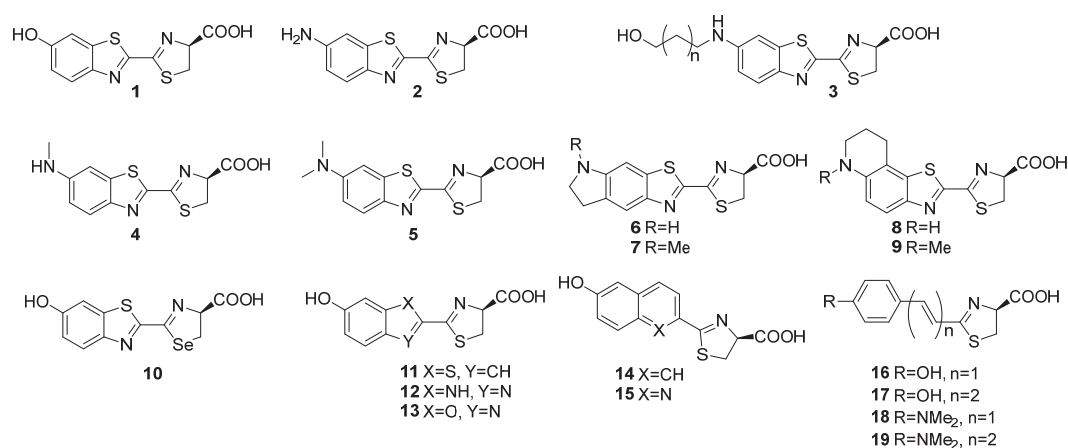


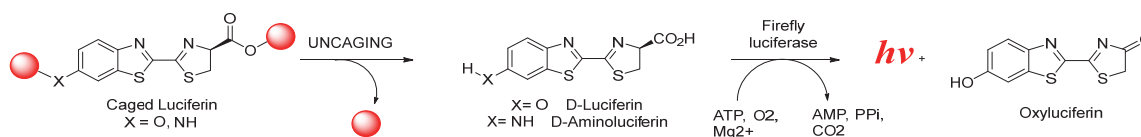
Figure 1.3: Examples of synthetic D-luciferin analogues as substrates for firefly luciferase.

Although strategies to synthesize novel D-luciferin derivatives that emit light at different wavelengths with a high quantum yield are still of high interest, D-luciferin and D-aminoluciferin are still the most frequently used substrates in BLI applications *in vivo*.<sup>[47]</sup> Both D-luciferin and its amino analogue are commercially available and have already been validated for *in vivo* application.<sup>[48]</sup>

## 1.4 Caged luciferins for sensing molecular changes *in vivo*

As mentioned earlier, modifications on the 6'-hydroxyl group of D-luciferin or 6'-amino group of aminoluciferin often restrict the recognition by the FLuc enzyme and thus prohibit the production of light. On the other hand, this restriction permits the development of caged-luciferin derivatives which are modified (i.e. caged) with groups that are sensitive to a biological process and luminescence is emitted only in the presence of the biological process of interest.<sup>[47,49]</sup> These caged-luciferin probes have been used to monitor various biological processes such as enzymatic activity, real-time imaging of small molecule uptake, cell surface modifications, metabolite production, as well as to study the efficiency of delivery, linker release, and biodistribution of cell-penetrating peptide conjugates.<sup>[50]</sup> The strategy of caging involves the 6'-hydroxy, 6'-amino or carboxyl group of D-luciferin (or aminoluciferin) to be modified with a cleavable functional group (**Scheme 1.4**). The presence of a bulky side group

causes steric hindrance and prevents the access to the luciferase active site. Upon removal of the caging group, D-luciferin molecule is released and can be oxidized by luciferase. Therefore, the amount of emitted signal is proportional to the quantity of free luciferin released. In other words, the light emission is correlated to the efficiency of uncaging and thus to the activity of the enzyme or the biomolecule of interest.

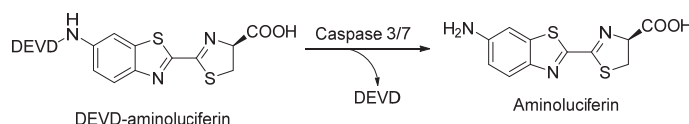


Scheme 1.4: Caged-luciferin strategy. The luciferins can be modified with a caging group on the phenolic hydroxyl, amino or carboxyl group that would prohibit the interaction with FLuc until the caging group is removed.

BLI has been widely used for longitudinal imaging of enzymatic activity.<sup>[51]</sup> While there are a number of luciferin derivatives validated for *in vitro* assays, only a few of them have been validated for real-time imaging *in vivo*, examples of which are described below.

#### 1.4.1 Bioluminescence imaging of protease activity

Apoptosis, or programmed cell death, is a highly regulated process, essential for the removal of damaged cells in multicellular organisms. Cytosolic caspases play central roles in mediating the initiation and propagation of the apoptotic cascade. Activation of both caspase 3 and caspase 7 is critical in the apoptotic pathway,<sup>[52,53]</sup> and is also linked to pathologies such as cancer and neurodegenerative disease.<sup>[54-56]</sup> A bioluminescent probe, DEVD-aminoluciferin, was developed to image caspase 3 activation *in vitro* and *in vivo* (**Scheme 1.5**), where the aminoluciferin derivative carries an Asp-Glu-Val-Asp (DEVD) peptide that is known to be a selective sequence for caspase 3 and to a lesser extent for caspase 7. The cleavage occurs at the C-terminal of the second aspartic acid (Asp) residue that yields the aminoluciferin release, which is used to quantify the caspase 3/7 activity. The use of this probe was shown to be beneficial for monitoring caspase 3/7 activity *in vitro*, screening caspase inhibitors and monitoring apoptotic effect of chemotherapeutics in cells.<sup>[57,58]</sup> The probe also provides a unique tool to evaluate the efficacy of therapeutic agents as well as to study the role of apoptosis in several disease models *in vivo* non-invasively.<sup>[59]</sup>



Scheme 1.5: DEVD-aminoluciferin probe for imaging Caspase 3/7 activity. DEVD peptide is selectively cleaved-off by caspase 3/7, releasing bioluminescent D-aminoluciferin molecule.

Using DEVD-aminoluciferin, Shah *et al.* demonstrated real-time imaging of caspase 3 mediated



apoptosis in living mice that were subcutaneously implanted with FLuc transfected glioma cells.<sup>[59]</sup> Another example of *in vivo* caspase 3/7 imaging using DEVD-aminoluciferin probe is monitoring apoptosis in living mice upon chemotherapeutic treatment, where apoptotic effect of docetaxel was evaluated on subcutaneous ovarian and mammary xenograft models.<sup>[60]</sup> Similar experiments were reported for monitoring induction of apoptosis and inhibition of tumor growth upon camptothecin and temozolomide treatment in different mouse xenografts models.<sup>[61]</sup> Moreover, DEVD-aminoluciferin was also used for measuring caspase 3/7 activity in a mouse liver failure model.<sup>[62]</sup>

Probes similar to DEVD-aminoluciferin have been developed and used for monitoring activity of other caspases such as caspases 8 and 9.<sup>[63]</sup> However, to date, these probes have only been evaluated in cells and zebrafish embryos but not validated in living mice.

Another example of protease imaging with caged-luciferin probes is imaging furin protease activity. Furin enzyme, ubiquitously expressed in mammalian cells, is a member of pro-protein convertase family which activates a number of precursor proteins upon cleavage.<sup>[64]</sup> Recent research has shown that furin is overexpressed in head and neck cancer, breast tumor, lung cancer and following viral-induced inflammatory conditions, such as HIV, influenza and dengue fever.<sup>[64-66]</sup> Inhibition of the furin enzyme has been shown to reduce the invasiveness and tumorigenicity of several human cancer cells lines *in vitro* and *in vivo*.<sup>[67,68]</sup> Furin cleaves at the C-terminus of a four-residue motif (Arg-X-Lys/Arg-Arg) where X is any amino acid<sup>[69]</sup> and this sequence is critical for binding the active furin.<sup>[70]</sup> In an aim to monitor furin activity *in vivo*, three tetrapeptides were conjugated to aminoluciferin (**Figure 1.4**); Ac-RYKR-aminoluciferin, Ac-RVRR-aminoluciferin, both of which are recognized by furin, and a control probe Ac-RRKY-aminoluciferin that is not recognizable by furin.<sup>[71]</sup> The first two probes demonstrated high specificity for furin cleavage in cell-free enzymatic assays, as well as in cells with high levels of furin expression. The control probe, Ac-RRKY-aminoluciferin, could not be hydrolyzed by furin, and therefore this probe was not bioluminescent. The Ac-RVRR-aminoluciferin probe, which generated higher bioluminescence signal *in vitro* compared to Ac-RYKR-aminoluciferin, was further validated in a mouse xenograft model.

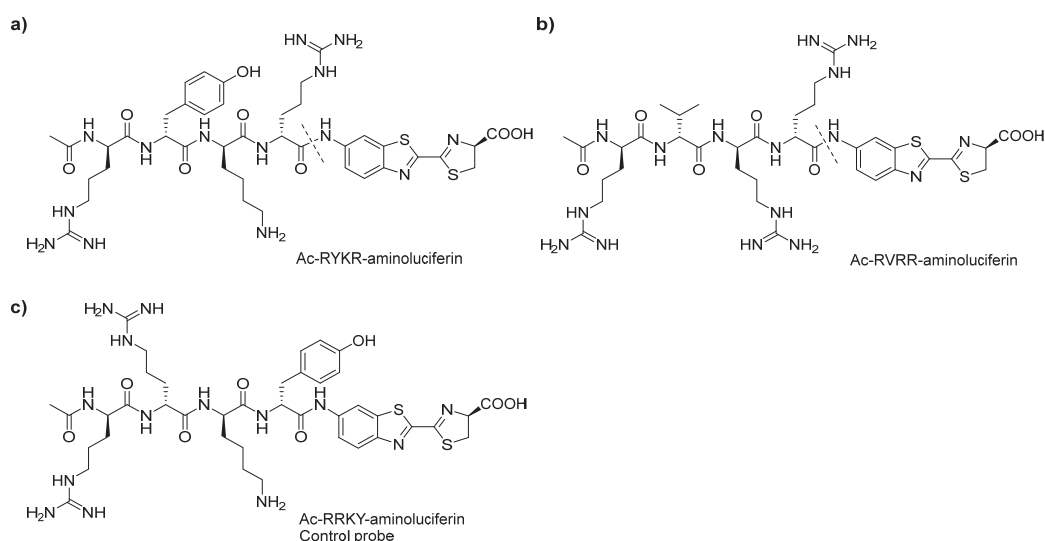


Figure 1.4: Structures of caged-luciferin probes for imaging furin activity. (a) Ac-RYKR-aminoluciferin, (b) Ac-RVRR-aminoluciferin and (c) the control probe Ac-RRKY-aminoluciferin.<sup>[74]</sup>

Carboxypeptidases (CPs) are a protease family of enzymes that hydrolyze polypeptides and proteins at the C-terminal end, performing diverse roles in normal biological processes and diseases.<sup>[72]</sup> Two probes for bioluminescence imaging of Carboxypeptidase A (CPA) and Carboxypeptidase G (CPG) activities were reported in the literature.<sup>[73]</sup> Quinolyl-D-luciferin (QLuc) and D-luciferin were modified on the carboxylic acid of the thiazoline ring with respectively a tyrosine (QLuc-Tyr) and a glutamic acid (Luc-Glu) as shown in Figure 1.5. These probes were shown to be cleaved specifically by CPA and CPG releasing free QLuc and Luc. To our knowledge, these probes were only tested in cell-free assays *in vitro*.

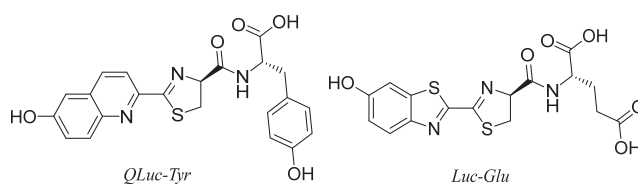


Figure 1.5: Caged substrates for imaging carboxypeptidases activity. QLuc-Tyr and Luc-Glu probes for carboxypeptidase G and carboxypeptidase A imaging respectively.<sup>[73]</sup>

Among other proteases, only the caged probes to assay caspase 3/7 and furin activity have been validated *in vivo*. However, this methodology could theoretically be used to image the activity of a number of proteases that cleave after specific peptide sequences without requirement of fixed amino acids after the cleavage site. The examples of such proteases and their specific amino acid sequences include caspase 2 (VDVAD),<sup>[74]</sup> caspase 6 (VEID),<sup>[74]</sup> caspase 8 (LETD) and caspase 9 (LEHD),<sup>[63]</sup> caspase 12 (ATAD),<sup>[75]</sup> thrombin (GGR),<sup>[76]</sup> dipeptidyl peptidase 4 (GP, AP or VP),<sup>[77,78]</sup> and tryptase (PRNK).<sup>[77,79]</sup> Additionally, this method could also be applied for a wide variety of bacterial, viral and

parasite proteases that are essential for infectious diseases.<sup>[80]</sup> Examples of these proteases and their specific amino acid sequences include SARS protease (TSAVLQ),<sup>[81,82]</sup> caspase-like (nLPnLD)<sup>[83]</sup> and trypsin-like (LRR) proteases.<sup>[77]</sup>

#### 1.4.2 Caged-luciferin probes for imaging biological processes

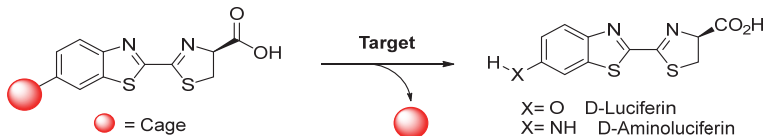


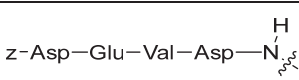

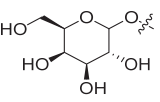
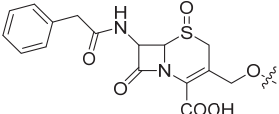
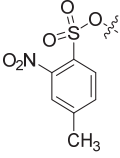
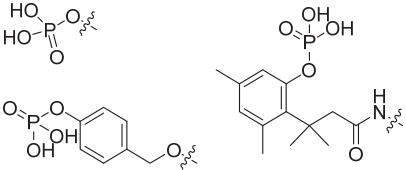
Apart from proteases, caged-luciferin probes for imaging a wide variety of enzymes and biological processes were also reported in the literature. Covering all the examples in detail is beyond the scope of this introduction, however a brief overview will be provided. Probes developed via functionalization of the 6'-position on the luciferin scaffold are shown in Table 1.2. These caged-luciferins were modified on the phenyl oxygen or 6'-nitrogen atom by conjugation with a specific substrate of the enzyme of interest. For example, a probe for imaging  $\beta$ -galactosidase was developed via conjugating the phenolic oxygen of D-luciferin to a galactoside moiety. The resulting probe, a D-luciferin-*O*- $\beta$ -galactoside, also named Lugal, has been validated for sensing galactosidase activity in numerous examples and is now commercially available (**Table 1.2**, entry **3**). Lugal reacts specifically with the  $\beta$ -galactosidase enzyme to release D-luciferin *in vivo*.<sup>[46,84]</sup> Similarly, caged-luciferin probes for  $\beta$ -lactamases,<sup>[85]</sup> glutathione S-transferase,<sup>[86]</sup> alkaline phosphatase<sup>[87]</sup> and sulfatase<sup>[88]</sup> were reported for imaging in different experimental setups, ranging from *in vitro* cell-free assays to *in vivo* experiments (**Table 1.2**, entries **4-7**).

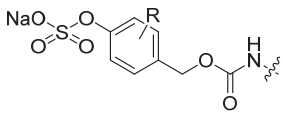
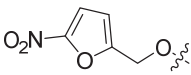
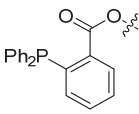
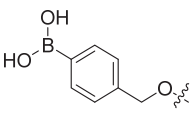
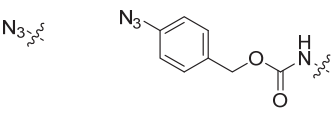
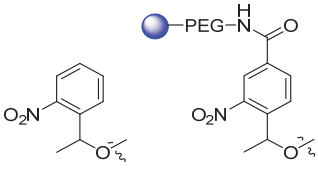
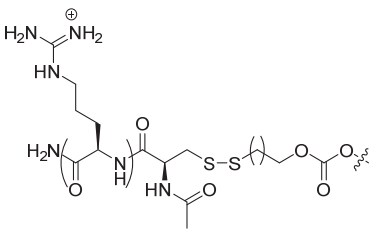
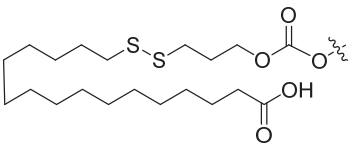
Our laboratory recently reported a caged luciferin probe for imaging nitroreductase (NTR) enzyme in living animals.<sup>[89]</sup> D-luciferin scaffold was modified on the phenolic oxygen with a nitrofuryl moiety (**Table 1.2**, entry **8**). The reduction of the nitro group by NTRs results in an electron-donating amino group which promotes the cleavage of the C-O bond leading to subsequent release of D-luciferin. This probe was validated for imaging NTRs in living bacteria, mammalian cells as well as in mouse models of cancer and bacterial infection.<sup>[89]</sup> This new probe should significantly simplify the screening of prodrugs *in vivo* and accelerate the process to develop enzyme-activatable therapeutics.

As described earlier, BLI is a powerful imaging modality to quantify enzymatic activities in real time with specific caged-luciferin derivatives, and not surprisingly, this method has also been used to study metabolites *in vivo*. Metabolites are small molecules that play essential roles in diverse biological processes such as energy production, protein synthesis and signaling. The ability to image real time metabolite uptake, spatial localization of transport and absorption, or concentration variation during a biological process is of high importance. Cohen *et al.* developed a bioluminescent assay to measure level of glycosylation on the cellular membrane using the caged-luciferin approach.<sup>[90]</sup> In this study, the probe had D-luciferin conjugated to a triphenylphosphine that, upon reaction with azido groups on the

targeted azido-modified glycans, released free D-luciferin via bioorthogonal Staudinger ligation (**Table 1.2**, entry **9**). This approach could potentially be applied to any metabolite or molecule of biological interest that can be modified with an azido group.

Table 1.2: List of reported caged-luciferin probe for imaging processes of interest (target). The cage molecular structures on the 6'-position of D-luciferin for specific targets are depicted as well as the scope of the reported application.

Cage Structure(s)		Target(s)	Validated Application Scopes	Ref.
  = Cage		 X= O D-Luciferin X= NH D-Aminoluciferin		
1	 <i>z-DEVD-aminoluciferin</i>	Caspase-3/7	<i>In vivo</i>	57-62
2	 <i>Ac-RVRR-aminoluciferin</i>	Furin	<i>In vivo</i>	71
3	 <i>Lugal</i>	$\beta$ -galactosidase	<i>In vivo</i>	46,84,91
4	 <i>Bluco</i>	$\beta$ -Lactamases	<i>In vivo</i>	85
5		glutathione S-transferase	<i>In vitro</i> cell-free	86
6		Alkaline phosphatase	<i>In vitro</i> cell-free	87

7	 <p>R=H, or R=2,6-F, or R=3,5-F</p>	Sulfatase	<i>In vitro</i> cell lysate and live cell	88
8	 <p>nitrofuryl caged-luciferin</p>	Nitroreductase	<i>In vivo</i>	89
9	 <p>triphenylphosphine caged-luciferin</p>	Glycosylation (azido-modified sugars)	<i>In vitro</i> cell-based	90
10	 <p>PCL-1</p>	Hydrogen peroxide	<i>In vivo</i>	92
11		Hydrogen sulfide	<i>In vivo</i>	93,94
12	 <p>● = Nanoparticle</p> <p>Photocaged-luciferin</p>	Light irradiation	<i>In vivo</i>	95,96
13		Cellular uptake (probe reduction by Glutathione)	<i>In Vivo</i>	97,98
14	 <p>FFA-SS-Luc probe</p>	Cellular uptake of fatty acid (probe reduction by Glutathione)	<i>In vivo</i>	99

In the same way, a caged-luciferin probe, PCL-1, was developed for imaging H<sub>2</sub>O<sub>2</sub> production in living systems (**Table 1.2**, entry **10**).<sup>[92]</sup> Based on a similar approach, caged-luciferin probes for detection and imaging of H<sub>2</sub>S were developed,<sup>[93,94]</sup> as well as photocaged-luciferins (**Table 1.2**, entry **11**) where the uncaging process occurs via photolysis at specific wavelength.<sup>[95,96]</sup>

Another application of caged-luciferin approach is monitoring cellular uptake of molecules in cells. Methods to monitor cellular uptake of a target molecule is highly beneficial to understand the mechanism of uptake, quantify the uptake's efficiency or adapt the dose treatment. The most commonly used method to study cellular uptake of drug molecules and biomolecules is to couple the molecule of interest with a fluorophore (e.g. FITC, TAMRA) and then measure the fluorescence of the treated cells with fluorescence spectroscopy or FACS.<sup>[100]</sup> These methods may however suffer from a non-specific signal coming from molecules bound to the cell surface that cannot be discriminated from the internalized signal.<sup>[101]</sup> Moreover, hydrophobic and large fluorescent probes could significantly alter the properties and behavior of the molecule of interest.<sup>[102-104]</sup> To date, only few examples describing the application of BLI to monitor cellular uptake of molecules were reported. This methodology is based on the fact that, for mammalian cells expression, FLuc enzyme is a cytosolic enzyme, and therefore, light is emitted only when the molecule of interest had already crossed the membrane barrier. Caged-luciferin molecules designed to monitor cytosolic uptake would facilitate the evaluation of internalization mechanisms and kinetics in living systems.

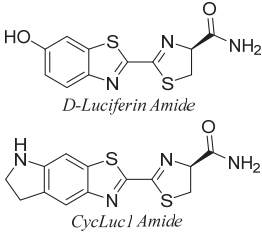
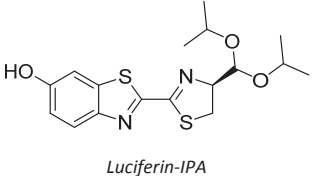
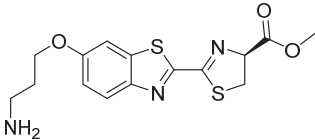
Examples of caged-luciferin molecules to study cellular uptake includes cell-penetrating peptides coupled to D-luciferin via a disulfide linker, which is selectively cleaved upon cellular entry where high concentration of glutathione is present (**Table 1.2**, entry **13**). The intermediate thiol then undergoes an intramolecular cyclization reaction to release D-luciferin, which would subsequently emit light in the presence of FLuc enzyme.<sup>[97]</sup> These probes were validated *in vivo* for real-time quantification of cell permeable peptides uptake.<sup>[98]</sup> A similar strategy was adapted to investigate fatty acid uptake *in vivo*. The caged probe consists of a long-chain fatty acid conjugated to D-luciferin via an intracellular releasable linker (**Table 1.2**, entry **14**).<sup>[99]</sup>

All the bioluminescent probes covered so far were developed via "caging" the D-luciferin (or amino analogue) through acylation or alkylation of the 6'-substituent, the phenyl-oxygen or nitrogen atom. Another possibility to cage luciferins is to modify the thiazoline carboxylic acid. Such examples were reported in the literature as probes to image fatty acid amide hydrolase activity, in which the carboxyl group of D-luciferin (or derivatives) were replaced with an carboxamide moiety (**Table 1.3**,

entry **1**), or Luciferin-IPA, an isopropyl acetal of D-luciferin, to image Cytochrome P450 3A4 isoform activity (**Table 1.3**, entry **2**). Luciferin-IPA probe is initially processed by CYP3A4, yielding a D-luciferin ester that further need to be hydrolyzed by esterases for the generation of free D-luciferin.<sup>[105-107]</sup> Both probes were validated in living mice for imaging of their respective targets.

In addition to caging through either hydroxyl/amino or carboxyl groups, a dual caged luciferin probe was developed for imaging monoamine oxidase (MAO) activity. This probe consists of a D-luciferin scaffold, caged on the phenolic oxygen with an aminopropyl group and on the carboxylic acid with a methyl group (**Table 1.3**, entry **3**). MAO enzyme converts the amine group to imine that will undergo non-enzymatic reactions to yield D-luciferin methyl ester. Then, esterase function is necessary to release the bioluminescent D-luciferin molecule.<sup>[108]</sup>

Table 1.3: Reported probes caged on the carboxylic acid of luciferin scaffold. The probe structures for specific targets are depicted as well as the scope of the reported application.

Caged-luciferin Structure(s)	Target(s)	Application Scope	Ref.
<b>1</b>  <i>D-Luciferin Amide</i> <i>CycLuc1 Amide</i>	Fatty acid amide hydrolase	<i>In vivo</i>	105
<b>2</b>  <i>Luciferin-IPA</i>	Cytochrome P450	<i>In vivo</i>	106,107
<b>3</b> 	Monoamine oxidases (isozymes A and B)	<i>In vitro</i> cell-free and cell lysate	108,109

Development of caged-luciferin derivatives extended the use of BLI *in vitro* and *in vivo*. These modified luciferins allowed imaging of multiple biological events non-invasively in real time. Number of caged-luciferin probes were validated for imaging and quantifying enzymatic activities, monitoring metabolite production, cellular uptake or cargo delivery as well as detecting cellular proximity. The variety of probes based on D-luciferin or derived scaffold demonstrates the versatility of modifications that can be realized, broadening the scope of BLI applications.

Compared to other *in vitro* and *in vivo* optical imaging techniques, BLI has the advantage of high sensitivity, convenience and ease of use. Unlike fluorescence, BLI does not demand an excitation light source, resulting in no background signal from naturally occurring fluorophores or induced phototoxicity.<sup>[110]</sup> Consequently, BLI is highly sensitive and yields superior signal-to-background ratio, making it advantageous over fluorescence imaging especially for *in vivo* applications.<sup>[5]</sup> On the other hand, fluorescent probes are usually brighter compared to bioluminescent reporters as they can be used with powerful excitation sources.<sup>[20]</sup> Moreover, available emission wavelengths of fluorescent probes cover almost all the light spectrum, offering a straightforward possibility of multicolor imaging. These properties render fluorescence imaging a preferred solution for *in vitro* applications such as fluorescence microscopy, which provides subcellular information.<sup>[6]</sup>

BLI has found considerable use in monitoring biological processes such as tumor growth,<sup>[111,112]</sup> gene expression,<sup>[113]</sup> pathogen detection and therapy evaluation,<sup>[114,115]</sup> protein-protein interactions<sup>[116]</sup> as well as ADMET (absorption, distribution, metabolism, excretion and toxicity) studies.<sup>[6]</sup> Moreover, BLI is a non-invasive imaging technique which, when coupled with the low toxicity of the substrate D-luciferin *in vivo*, allows multiple imaging on the same subject over a prolonged period of time, facilitating the tracking of molecular changes longitudinally. BLI probes are ideal for *in vivo* applications, providing good sensitivity with low toxicity. Excitation light is not required in BLI, thus overcoming related drawbacks of traditional fluorescent probes. The main limitation of the D-luciferin/FLuc system is the dependence on the luciferase enzyme which limits BLI applications to biological systems expressing this enzyme (e.g. engineered cells or genetically-modified animals). Another limitation of BLI is the sub-optimal tissue penetration of the produced light. Recent developments on the red-shifted and brighter D-luciferin derivatives however, address the low tissue penetration of light with BL.<sup>[41-43,45,117]</sup> These novel molecules show great promise to enhance the detection sensitivity and therefore offer the possibility to monitor biological events occurring in deep tissues. The progress on the development of red-shifted luciferase mutants,<sup>[16,118-121]</sup> coupled with increased selectivity of new luciferin scaffolds will allow BLI with better sensitivity. This is promising for imaging fewer cells *in vivo* and will provide new opportunities for multiplexing imaging, where different luciferin/luciferase pairs could be used and measured simultaneously at different wavelength.<sup>[40]</sup>

## 1.5 Bioorthogonal click reactions

The discovery of green fluorescent protein (GFP) greatly enhanced the field of protein imaging in living environment.<sup>[122]</sup> Fusion proteins with GFP or other fluorescent protein variants have proven to be a very efficient tools to study and visualize proteins in their native environment. Other genetically



encoded tags were also developed for covalent labelling of proteins with fluorescence imaging agents.<sup>[123]</sup> These methods include self-labelling enzymes (e.g. SNAP or CLIP tags),<sup>[124-126]</sup> peptide-based post-translational labeling<sup>[127,128]</sup> and enzymatic labelling of proteins (e.g. probe incorporation mediated by enzyme, PRIME).<sup>[129,130]</sup> However, non-proteinaceous biomolecules such as nucleic acids, glycans, lipids as well as post-translational modifications on proteins cannot be monitored using the genetic-encoded tags. In order to image these biomolecules in their native environment, further chemical modifications are necessary. To overcome this question, bioorthogonal ligation reactions were employed. In a first step, a small tag – the chemical reporter – is introduced in the biomolecules of interest using metabolic or enzymatic labelling.<sup>[130,131]</sup> In a second step, the biomolecule of interest is conjugated to a molecular probe bearing a functionality complementary to the chemical reporter.<sup>[132,133]</sup> In order to perform this conjugation reaction, selective and efficient ligation reactions are necessary. Bioorthogonal ligation reaction (or biocompatible click reactions), do not interfere with chemical functionalities found in living system (**Figure 1.6**).<sup>[131,133]</sup> They fulfill all the requirements to be used in complex and molecularly diverse environments as biological systems. The reaction needs to be very selective to minimize the background, have a fast reaction rate at physiological temperature and be compatible with physiological conditions such as the presence of water and oxygen. Moreover, the ligation product needs to be stable and non-toxic. Apart from application in living system, functionalization of targeting molecules (e.g. antibodies, proteins) is also simplified with bioorthogonal chemistry, allowing easy and selective conjugation with simpler purification steps.

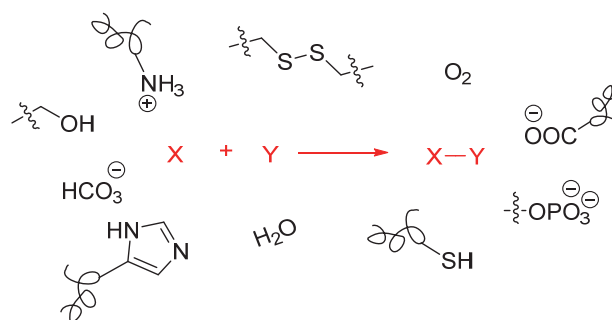


Figure 1.6: Bioorthogonal reactions: The reaction between compounds X and Y occurs efficiently and selectively to form the ligation product without interfering with the functionalities naturally found within biological environment (Figure adapted from [133]).

Bioorthogonal reactions have gained in popularity in the previous decades.<sup>[133]</sup> While a number of biocompatible ligation reactions have been used to study biological molecules, only a fraction of them possess the requirements necessary for application in living cells. Even though studies with live cells have tremendously advanced our understanding in many human pathologies, their great complexity requires tools to study on the level of the whole organism. Since multiple animal models of

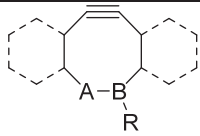
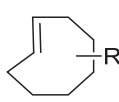
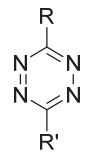
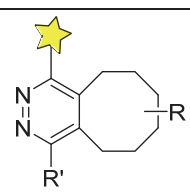
various human pathologies have been successfully established,<sup>[134-139]</sup> development of new biocompatible reactions applicable to the whole animal could play crucial role in biology and medical research.

The complexity of the system increases when moved from cellular to living animal environment, and therefore the requirements for the chemistry increase to be more efficient and selective. The two components now have to react with each other in the presence of a much more complex biological environment with many other additional active substances. Moreover, a living animal represents a dynamic system, where the reagents could be quickly metabolized or simply cleared from the circulation before they are able to react. Parameters such as toxicity, bio-distribution and half-life of the reagents are crucial for the success of this methodology *in vivo*. Regarding all these restricting requirements, only a few biocompatible reactions have been validated in living organisms and animals. These *in vivo* bioorthogonal reactions encompass the strain-promoted azide-alkyne cycloaddition (SPAAC),<sup>[140-145]</sup> the Staudinger ligation (SL)<sup>[146-154]</sup> and the inverse electron demand Diels-Alder reaction (IED DA) (Table 1.4).<sup>[155-161]</sup>

Azides are one of the most widely used bioorthogonal reactive partners in bioligation and labelling applications. Due to their small size, azides can be incorporated into biomolecules without significantly affecting the molecular characteristics or interaction of the biomolecule within the natural environment. Azide functional group is not endogenously available and is inert in biological conditions. They can react efficiently and selectively with different various bioorthogonal reagents such as SL reagents or alkynes via SPAAC (Table 1.4).

Table 1.4: Bioorthogonal ligation reactions for *in vivo* applications. The chemical reporter (Reagent X) on the biomolecule of interest is conjugated with a molecular probe (Reagent Y) bearing the complementary bioorthogonal functionality. The yellow star represents the imaging reporter (e.g. fluorophore, radiolabel).

	Reaction	Reagent X	Reagent Y	Ligation product	Ref.*
1	Staudinger Ligation (SL)	R-N <sub>3</sub>			90,143,149,150,162-164
2	Strain-Promoted Azide-Alkyne Cycloaddition (SPAAC)		<p>A = H, F</p>		165-170

3			 <p>A = CH<sub>2</sub>, C=O B = CH, N</p>		163,169
4	Inverse Electron Demand Diels-Alder reaction (IED DA)				156,163,171-175

\* Examples for *in vivo* applications of the bioorthogonal reaction.

The SL is a modified type of Staudinger Reaction where an electrophilic intramolecular trap is introduced on the triarylphosphine, leading to formation of a covalent bond, enabling the conjugation (**Table 1.4**, entry 1).<sup>[147]</sup> SL is particularly advantageous as it occurs under physiological conditions without a catalysts.<sup>[176]</sup> However, SL has disadvantages such as poor shelf life of the SL reagent due to sensitivity of phosphine to oxidation and relatively slow reaction kinetics ( $k = 2.5 \times 10^{-3} \text{ M}^{-1} \text{ s}^{-1}$ )<sup>[146]</sup> compared to other bioorthogonal reactions.<sup>[177]</sup>

The SL has extensively been used for fluorescent labelling in living cells.<sup>[152,153,178-180]</sup> Due to favorable pharmacokinetic properties and low toxicity, the SL has also been shown to work efficiently in living mice, avoiding non-specific binding to other biomolecules. Beside its applications in cells, SL was reported for labelling and imaging cell surface glycans in living mice,<sup>[90,143,145,149,150]</sup> including radionuclide and fluorescent labelling in a mouse subcutaneous xenograft model.<sup>[162]</sup>

SPAAC reaction consist of a 1,3-dipolar cycloaddition between a cyclic alkyne and an azide to yield a substituted triazole. Functionalized activated cyclooctynes were developed as bioorthogonal reagents and many derivatives were reported for biological applications.<sup>[177]</sup> In order to activate the alkynes in cyclooctynes, different strategies were applied, such as the introduction of electron withdrawing groups on the alpha position of the triple bond (e.g. difluorinated cyclooctyne (DIFO)) (**Table 1.4**, entry 2),<sup>[181]</sup> or increasing the ring strain by introduction of unsaturation on the cyclic octyne (e.g. dibenzocyclooctyne (DIBO)) (**Table 1.4**, entry 3).<sup>[144]</sup> Different cyclooctyne derivatives combining these two activation approaches were reported,<sup>[141,142,182]</sup> with reaction kinetics ranging from  $10 \times 10^{-3}$  to  $400 \times 10^{-3} \text{ M}^{-1} \text{ s}^{-1}$ .<sup>[183]</sup> Therefore, SPAAC reagents such as DIFO or DIBO that induce fast reactions with no toxicity have been shown to be better alternatives for live cell applications compared to SL. On the other hand, cyclooctyne-based probes seem to be less attractive than Staudinger reagents for *in vivo*

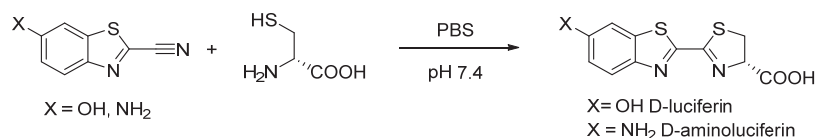
applications in rodents, probably because of unfavorable bioavailability.<sup>[90,143,149,169]</sup> Using a DIFO-fluorophore conjugate, non-invasive imaging of cell-surface glycans in zebrafish embryos was performed upon metabolic labelling with an azido-modified sugar, allowing the spatiotemporal study of cell-surface glycan expression with multicolor fluorescence microscopy.<sup>[166,168]</sup> Using a similar approach, the distribution and dynamics of glycans biosynthesis was studied in *Caenorhabditis elegans* (*C. elegans*).<sup>[167]</sup> In mice, Azido labelled splenocytes were modified *in vivo* using SPAAC, further revealed with a fluorescent probe *ex vivo* and analyzed by flow cytometry.<sup>[165]</sup> Another example of SPAAC use *in vivo* is the fluorescent imaging of azido labelled glycans in a subcutaneous mouse model.<sup>[163]</sup>

Tetrazines can react selectively with *trans*-cyclooctenes (TCO) *via* an IED DA reaction (**Table 1.4**, entry **4**), followed by a retro-[4 + 2] cycloaddition, yielding the ligation product with N<sub>2</sub> release.<sup>[159,184]</sup> Different TCO or tetrazines derivatives were reported, resulting in different reaction rates (*k* ranging from 10<sup>3</sup> to 10<sup>4</sup> M<sup>-1</sup>s<sup>-1</sup>).<sup>[159,173,185-187]</sup> IED DA reactions between tetrazines derivatives and TCO conjugates were used as bioorthogonal reactions for fluorescent labelling on cell surface and intracellular targets.<sup>[188-191]</sup> Using a pre-targeting approach with a TCO labelled antibody, fluorescent labelling of cancer epitopes was performed by subsequent reaction with tetrazines-polymer conjugate in a tumor xenograft mouse model. The polymer was functionalized with fluorophores or a positron emission tomography (PET) tracer, allowing *in vitro* and *in vivo* microscopy as well as PET analysis in living mice.<sup>[156]</sup> Other reports of the IED DA reaction for imaging application include fluorescent labelling,<sup>[163]</sup> PET analysis in murine cancer models<sup>[171,172]</sup> and single-photon emission computed tomography (SPECT) applications<sup>[173-175]</sup>

## 1.6 Condensation reaction between 2-cyanobenzothiazole (CBT) and 1,2-aminothiols

Bioorthogonal reactions have been extensively used for multiple biochemical or imaging applications. Such chemistries revealed to be convenient, reliable and versatile as ligation reactions, both *in vitro* and in biological systems. Nevertheless, there is still a need for new biocompatible ligation reactions as supplementary tools that can potentially be more efficient and/or be used in conjugation with other bioorthogonal reactions. There has been a recent interest in 2-cyanobenzothiazole (CBT)-based ligation reaction for bioconjugation applications. This reaction is a condensation reaction between CBT derivatives (e.g. 6-hydroxy-CBT (HO-CBT) or 6-amino-CBT (H<sub>2</sub>N-CBT) conjugates) and a 1,2-aminothiol group. When the aminothiol moiety is a D-cysteine molecule, the reaction is called *split luciferin reaction* (**Scheme 1.6**), which was first reported in 1963 as the final step in the synthesis of D-

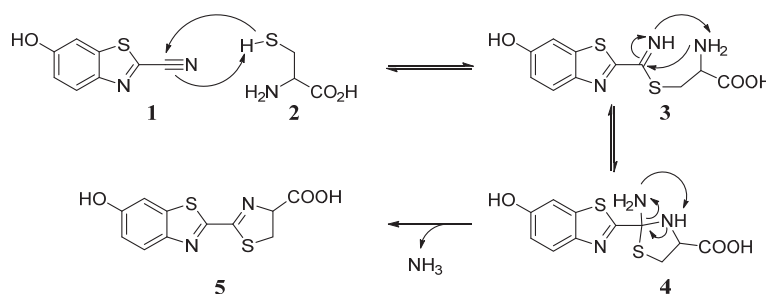
luciferin.<sup>[192]</sup> As split luciferin reaction potentially occurs naturally and efficiently in fireflies, it is bio-compatible and therefore can be used as ligation reaction in biological environments.



Scheme 1.6: Condensation reaction between 6-hydroxy-2-cyanobenzothiazole or 6-amino-2-cyanobenzothiazole with D-cysteine yielding D-luciferin or D-aminoluciferin, respectively.

The CBT condensation reaction with 1,2-aminothiols is particularly appealing for bioconjugation applications, because it can be conducted at ambient temperature under physiological (i.e. aqueous) conditions and shows high selectivity toward aminothiols over any other biological nucleophiles. Moreover, the reaction is highly rapid: second-order rate constant for the reaction of cysteine with a CBT derivative (*N*-(2-cyano-benzothiazol-6-yl)-succinamic acid) is  $9.19 \text{ M}^{-1}\text{s}^{-1}$ .<sup>[193]</sup> This second order reaction rate is significantly higher than other well established bioorthogonal reactions such as the reaction of azides with cyclic-oxyenes (SPAAC) or phosphines (SL), respectively two and three order of magnitude higher (i.e. DIFO:  $k = 7.6 \times 10^{-2} \text{ M}^{-1}\text{s}^{-1}$ <sup>[165]</sup>; substituted triphenylphosphine  $k = 2.0 \times 10^{-3} \text{ M}^{-1}\text{s}^{-1}$ <sup>[146]</sup>). Moreover, split luciferin reaction is highly efficient, resulting in high yields, with chromatographic purification not systematically necessary.<sup>[194-198]</sup>

Condensation of cysteine with electrophilic nitriles occurs in three steps, optimally at slightly basic pH (**Scheme 1.7**): reversible attack of the cysteine (**2**) thiol to the nitrile (**1**) to form a thioimide intermediate (**3**); intramolecular attack of vicinal amine to the thioimide forming the thiazolidine (**4**); and loss of ammonia to form the thiazoline product (**5**).

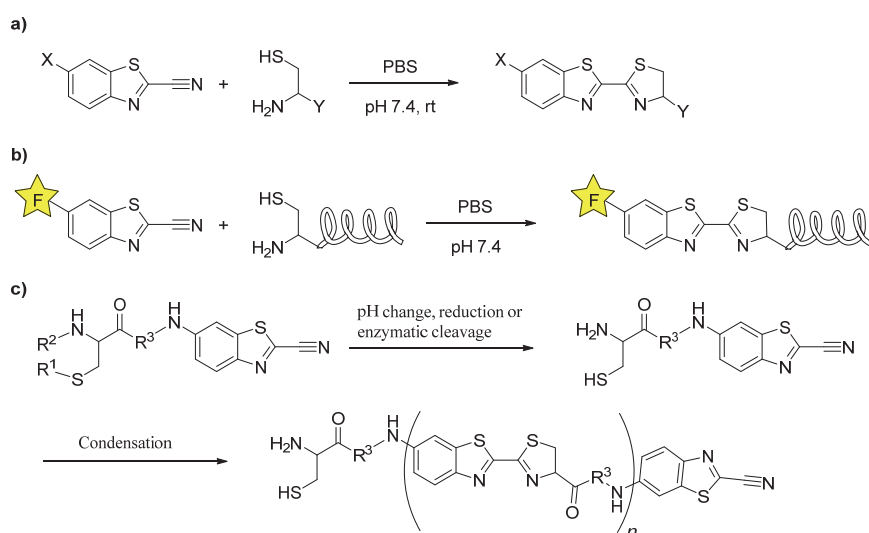


Scheme 1.7: Reaction mechanism between 6-hydroxy-2-cyanobenzothiazole (HO-CBT) and cysteine.

The bimolecular interaction between cysteine and the nitrile in the first step is the rate-limiting step (**Scheme 1.7**). The second and third reaction steps are rapid intramolecular processes that lead to the formation of thiazoline product. Reaction of electrophilic nitriles with thiols that lack the vicinal amino group stops at the first step to yield thioimides (**3**). Accordingly, simultaneous treatment of

electrophilic nitriles with aminothiols and simple thiols results in the formation of thiazoline products derived from the aminothiols. This suggests that aminothiols can react with the thioimides of simple thiols or that the reversibility of the thioimide reaction with simple thiols allows formation of the stable thiazoline product to predominate.<sup>[193]</sup> Aminothiols are thus selective coupling partners even in the presence of simple thiols (e.g., *N*-terminal cysteines in peptides and proteins can form stable products in the presence of internal cysteines).

The CBT-condensation reaction with 1,2-aminothiols was employed for several bioconjugation applications (**Scheme 1.8a**). The split luciferin reaction can be blocked (caged) via chemical modification of the 1,2-aminothiol moiety. When the amine, the thiol or both are functionalized, the condensation reaction with CBT is blocked. Therefore, addition of specific molecular patterns on these positions opens up the possibility to control the reaction by specific stimuli. This concept has generated multiple applications where the CBT-based ligation reaction is only occurring under specific conditions.



Scheme 1.8: 2-cyanobenzothiazole (CBT) condensation reaction with 1,2-aminothiols. a) Ligation reaction between the nitrile of CBT and 1,2-aminothiol. X moiety on the CBT molecule or Y moiety on the 1,2-aminothiol can be modified for particular applications. b) Site specific fluorescent labelling of proteins containing *N*-terminal cysteine.<sup>[193]</sup> c) Polymeric condensation reaction controlled by pH, disulfide reduction or enzymatic cleavage depending on the nature of R<sup>1</sup> and R<sup>2</sup> groups. R<sup>3</sup> can be used for functionalization with a fluorophore or a tag (e.g. biotin).<sup>[194]</sup>

Selective functionalization of proteins at *N*-terminal cysteine residue with a fluorophore was performed using the CBT-based ligation reaction in living cells (**Scheme 1.8b**).<sup>[193]</sup> In this study, a fluorophore-CBT conjugate was used for imaging a cell-membrane protein, engineered to have an *N*-terminal cysteine residue. Importantly, the CBT fluorescent conjugate selectively reacts with the *N*-terminal cysteine but not with thiols from cysteine residues present in the middle of the sequence. Using a similar CBT molecule conjugated to a fluorescent probe, site specific labelling of proteins was achieved

by the use of a genetically encoded 1,2-aminothiol.<sup>[199,200]</sup> The reverse strategy was applied with a CBT-modified nucleotide in combination with a 1,2-aminothiol fluorophore construct and employed for site-specific modification of DNA.<sup>[201]</sup> Moreover, site-specific immobilization of proteins and biomolecules containing terminal 1,2-aminothiols were performed using the CBT-based ligation reaction.<sup>[202,203]</sup> A controlled assembly of polymer and nanostructure in living cells was achieved by creative design of a monomer, a CBT molecule conjugated to functionalized-1,2-aminothiol (**Scheme 1.8c**).<sup>[194]</sup> The triggering process of the condensation reaction is the removal of the molecular masks on the aminothiol function, revealing free 1,2-aminothiol that could then react with the nitrile of another monomer. The condensation reaction can be directed by pH, disulfide reduction or protease cleavage. Moreover, the structure of the monomer can tune the size of the assembled structure properties. Protease imaging by controlled macro-cyclization was performed using a comparable approach.<sup>[195]</sup>

Liang and coworker have used the potential of split luciferin reaction for multiple applications. They used the CBT-based ligation reaction for the preparation of nanostructures. For example, multi-functional small monomers containing both the 1,2-aminothiols and CBT nitrile functionalities were designed to produce a controllable and reversible polymerization process to prepare oligomeric nanoparticles.<sup>[196]</sup> Similarly, glutathione (GSH) dependent self-assembly of nanorings was used for *in vitro* detection of GSH,<sup>[198]</sup> as well as a caspase-3 dependent condensation reaction for self-assembling biotinylated nanoparticles that can capture and subsequently turn on the fluorescence signal of FITC-labelled streptavidin.<sup>[204]</sup>

The CBT-based ligation reaction was also applied to various imaging modalities. Miao *et al.* used a furin-controlled intracellular formation of nano-structure formed by the CBT-based condensation reaction of radiolabeled-monomers. This could help retaining the radionuclides in cancer cells and thus could be promising for potential nuclear medicine applications.<sup>[205]</sup> Moreover, the condensation reaction between CBT and 1,2-aminothiols was reported for the assembly of Gadolinium labelled nanoparticles that process an enhanced relaxivity *in vitro* and in living cells compared to the precursors.<sup>[206]</sup> Using an <sup>18</sup>F-modified CBT, Jeon *et al.* reported radio-labelling of a dimeric cRGD peptide bearing 1,2-aminothiol functionality and its subsequent use for *in vivo* tumor imaging using PET. Site specific <sup>18</sup>F-labelling of a protein was also shown using the same chemistry,<sup>[207]</sup> as well as <sup>18</sup>F-labelling of cyclo-(RGDfK) targeting moiety (**Figure 1.7**).<sup>[208]</sup>

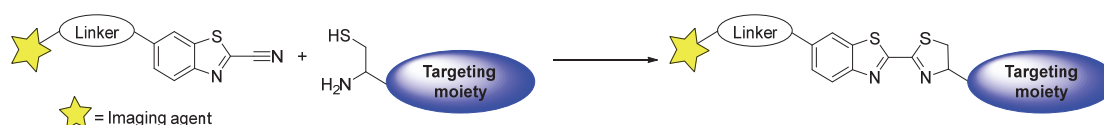


Figure 1.7: Functionalization of targeting moieties with imaging reporters via the CBT-based ligation reaction.

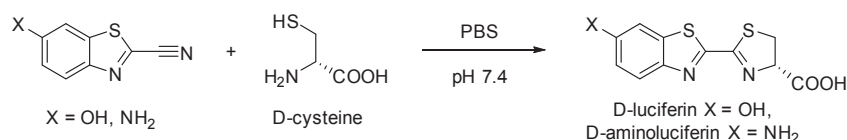
Any targeting moieties, such as peptides, proteins, antibodies or small molecules, could potentially benefit from the CBT-based ligation reaction for functionalization with imaging probes. CBT could be conjugated to an imaging reporter such as a fluorophore, radionuclide or chelating agent (e.g. DOTA, NOTA) and thus could be used for the development of targeted probes for imaging. Moreover, as the 1,2-aminothiol can be easily introduced in proteins or peptides as *N*-terminal cysteine, it simplifies greatly the introduction of a chemical handle for functionalization on proteinaceous molecules.



# Chapter 2 Bioluminescence Imaging Using Biocompatible Split Luciferin Reaction

Studies on the level of living cells have tremendously advanced our understanding of pathologies. However, the great complexity of diseases requires animal models of human pathologies<sup>[134-139]</sup> and thus tools that allow imaging on the level of whole organism (*in vivo*) are necessary. Accordingly, development of new biocompatible ligation reactions applicable for studies of biological processes *in vivo* can play a crucial role in biology and medical research. When the complexity of the system increases from cells to animals, more requirements come into play for a successful ligation reaction. In the past decade many biocompatible ligation reactions have been developed to study various biological processes in cells.<sup>[133]</sup> However, only a fraction of these reactions can be used in living animals. These *in vivo* bioorthogonal reactions comprise the strain-promoted azide-alkyne cycloaddition (SPAAC),<sup>[140-145]</sup> the Staudinger ligation (SL)<sup>[146-154]</sup> and the inverse electron demand Diels-Alder reaction (IED DA) (**Table 1.4**, chapter 1).<sup>[155-161]</sup>

Considering all this, novel *in vivo* compatible bioorthogonal reactions are needed in order to expand the application scope of imaging and functionalization methodology. One reaction of interest is the *split luciferin reaction* between D-cysteine and 6-hydroxy-2-cyanobenzothiazole (HO-CBT) that was first reported half a century ago as the final step in the synthesis of D-luciferin (**Scheme 2.1**).<sup>[192]</sup> More recently, other groups have reported applications of this reaction for selective labeling of proteins on *N*-terminal cysteines<sup>[193,199]</sup> as well as for controlled assembly of polymers in physiological solutions and living cells.<sup>[194,195]</sup> Notably, the rate of split luciferin reaction has been reported to be three orders of magnitude faster than that of Staudinger ligation.<sup>[193]</sup>



Scheme 2.1: Split luciferin reaction. Condensation reaction between HO-CBT or H<sub>2</sub>N-CBT with D-cysteine resulting in the formation of respectively D-luciferin or D-aminoluciferin.

The reaction between D-cysteine and HO-CBT or 6-amino-2-cyanobenzothiazole ( $\text{H}_2\text{N-CBT}$ ) can yield substrates for firefly luciferase (FLuc), and thus has great potential for use in bioluminescence imaging (BLI).<sup>[6,114,209]</sup> In this chapter, the evaluation and validation of the split luciferin reaction for BLI application is reported. The bioluminescence emission resulting from the administration of HO-CBT or  $\text{H}_2\text{N-CBT}$  and D-cysteine were compared with that from corresponding luciferins, in enzymatic, cells and animals assays. Until the current study, the split luciferin reaction has neither been employed *in vivo*, nor for BLI applications. We demonstrated that D-cysteine and HO-CBT or  $\text{H}_2\text{N-CBT}$  can efficiently generate luciferins in biological environment such as living cells and living mice. This split luciferin ligation reaction is therefore highly valuable for *in vivo* imaging applications and could be of interest for *in vivo* biocompatible labeling.

## 2.1 *In vitro* formation of D-luciferin and D-aminoluciferin in physiological solutions

Since the previously reported reactions between HO-CBT or  $\text{H}_2\text{N-CBT}$  and cysteine derivatives produce luciferin-like structures,<sup>[193-195,199]</sup> whether HO-CBT and  $\text{H}_2\text{N-CBT}$  could form their respective luciferins directly in a physiological environment and could be detected by BLI was initially investigated (Figure 2.1).

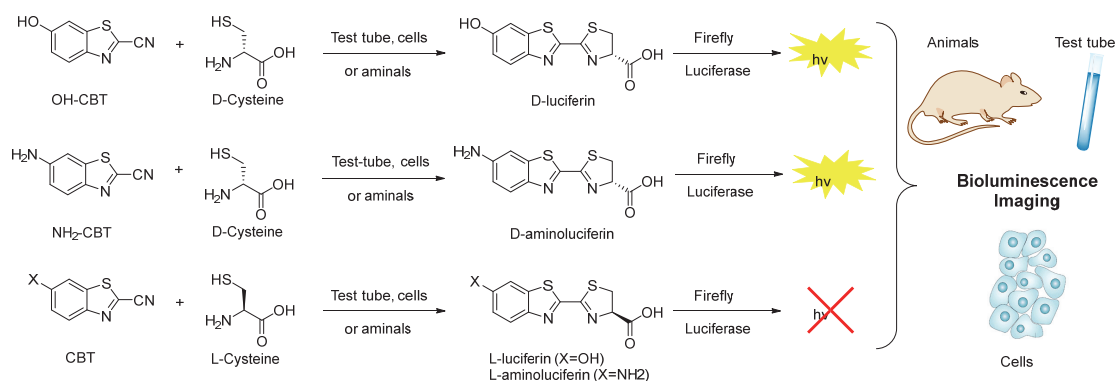


Figure 2.1: Overall schematic of the split luciferin ligation reaction between D- or L-cysteine and hydroxy- or amino-cyanobenzothiazole derivatives (HO-CBT and  $\text{H}_2\text{N-CBT}$ ) in various biological environments.

$\text{H}_2\text{N-CBT}$  or HO-CBT were incubated with either D- or L-cysteine in buffer containing FLuc enzyme (Figure 2.2) the BL emission was acquired. Importantly, the signal produced from the sample that had both  $\text{H}_2\text{N-CBT}$  and D-cysteine was 1000-folds higher than the signals obtained from the sample containing  $\text{H}_2\text{N-CBT}$  alone.  $\text{H}_2\text{N-CBT}$  plus L-cysteine generated 50-folds higher light emission than CBT alone (Figure 2.2a). Similar results were obtained with HO-CBT and D-cysteine, with 1200-folds and

20-folds increase compared to respectively HO-CBT/D-cysteine and HO-CBT alone or HO-CBT/L-cysteine and HO-CBT alone (**Figure 2.2b**).

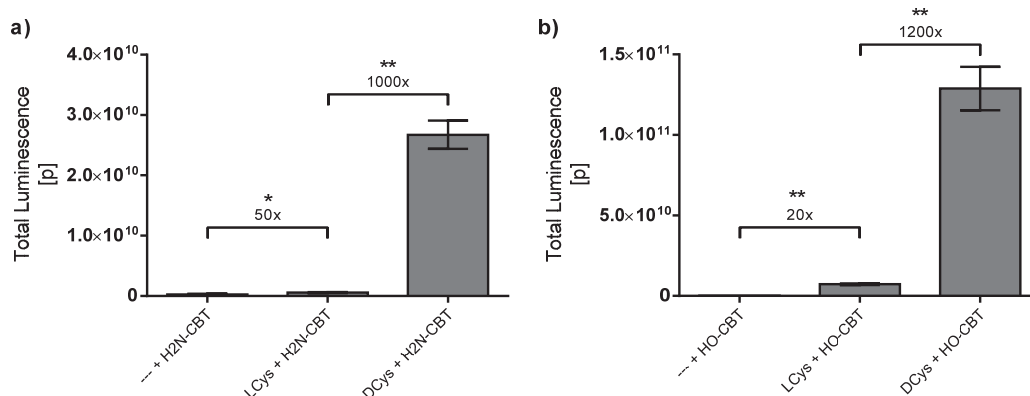


Figure 2.2: Formation of D-luciferin *in vitro*. (a) Total bioluminescent signal integrated over 30min observed from incubation of H<sub>2</sub>N-CBT (10 μM) with D-cysteine (10 μM), L-cysteine (10 μM) or vehicle in PBS solution, followed by addition of a FLuc solution and imaging. Error bars are ± SD for three independent measurements. (b) Total bioluminescent signal integrated over 30min observed from incubation of HO-CBT (10 μM) with D-cysteine (10 μM), L-cysteine (10 μM) or vehicle in PBS solution, followed by addition of a FLuc solution and imaging. Error bars are ± SD for three independent measurements. Statistical analyses were performed with a two-tailed Student's t test. \*\*P < 0.001, \*P < 0.05.

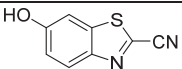
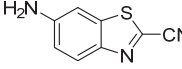
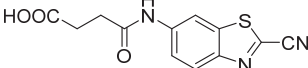
Next, formation of corresponding D-luciferin and D-aminoluciferin was confirmed using high performance liquid chromatography (HPLC) and high resolution mass spectrometry (HRMS). H<sub>2</sub>N-CBT or HO-CBT was incubated with D-cysteine in PBS buffer and the samples were analyzed (**Figure S2.1**). The results demonstrate efficient formation of luciferin analogs in PBS, that could directly produce photons of light in the presence of FLuc enzyme, confirming that the BL emission observed in the enzymatic assay (**Figure 2.2**) correlates with D-luciferin or amino analogue formation.

### 2.1.1 Kinetic studies of the reaction between CBT derivatives and L-cysteine

We next studied the rate of the reaction between CBT derivatives and L-cysteine under pseudo-first order conditions, using a standard HPLC assay.<sup>[195]</sup> The rate constants for the reactions of HO-CBT and H<sub>2</sub>N-CBT with L-cysteine were 3.2 and 2.6 M<sup>-1</sup>s<sup>-1</sup> respectively, which is three orders of magnitude faster than those reported for the Staudinger ligation.<sup>[146,148,151,152]</sup> We further compared these reaction rates to that of a previously reported N-succinamidyl CBT derivative<sup>[193]</sup> (compound **3**, **Table 2.1**, **Figure S2.2**, **Figure S2.3**, **Figure S2.4**). The rate constant for this compound was found to be 7.1 M<sup>-1</sup>s<sup>-1</sup> that is in agreement with the previously published value of 9.1 M<sup>-1</sup>s<sup>-1</sup>.<sup>[193]</sup> The lower reaction rate of H<sub>2</sub>N-CBT compared to its less electron-donating succinamide derivative is consistent with mesomeric effects on the reactivity of the nitrile. Thus, the rate of this reaction with CBT derivatives could

be further modulated by the introduction of electron-donating or electron-withdrawing ring substituents, and other electrophilic nitriles could be suitable reaction partners for cysteine.<sup>[210]</sup>

Table 2.1: Reaction rate constants between 2-cyanobenzothiazoles derivatives and L-cysteine.

	Compound	Structure	Rate constant [M <sup>-1</sup> s <sup>-1</sup> ]	[M+H] <sup>+</sup> of product (found)	[M+H] <sup>+</sup> of product (calculated)
1	HO-CBT		3.24 ± 0.117	280.9991	281.0055
2	H <sub>2</sub> N-CBT		2.63 ± 0.264	280.0200	280.0209
3	N-succinamidyl-CBT		7.10 ± 0.106	380.0372	380.0369

## 2.2 Real time non-invasive imaging and quantification of the split luciferin ligation reaction in living cells

Next, whether HO-CBT and H<sub>2</sub>N-CBT could form their respective luciferins directly in live cells was investigated (**Figure 2.1**). Ovarian and breast cancer cells, stably expressing FLuc (SKOV3-luc-D3 and MDA-MB-231-luc-D3H2LN), were treated with HO-CBT or H<sub>2</sub>N-CBT only, followed by imaging with a cooled CCD camera. Consistent with the *in vitro* cell-free results, treatment with either CBT derivative or D-cysteine alone produced only a low level of signal. L-luciferin was reported to produce light under certain conditions, but is also behave as a competitive inhibitor with respect to D-luciferin.<sup>[30,35]</sup> L-luciferin formed upon HO-CBT reaction with endogenous L-cysteine could have affected the results either by generating background light emission upon administration of CBT only or lowering light emission upon CBT derivatives and D-cysteine treatment and could have resulted in high background upon administration of CBT only or diminished light emission upon CBT derivatives and D-cysteine treatment by FLuc inhibitory effect. The BL signal from cells treated with HO-CBT only is approximately 23 times higher than the one without CBT, but remains very low compared to HO-CBT plus D-cysteine light emission. Signal measured from cells treated with HO-CBT only is more than 200 times lower than the light emitted from cells administered with HO-CBT and D-cysteine (**Figure 2.3**, **Figure 2.4**, **Figure 2.5**). Similarly, cells treated with equimolar amounts of both HO-CBT and L-cysteine produced a background signal close to the light emission of cells treated with HO-CBT alone. Similar results were observed with H<sub>2</sub>N-CBT instead of the hydroxyl analogue. It can be concluded that endogenous or supplemented L-cysteine produce only a negligible light production after reaction with both HO-CBT or H<sub>2</sub>N-CBT compared to similar experiments with D-cysteine. In contrast, cells treated with either D-luciferin or D-

aminoluciferin produced robust signal that was significantly higher than background (**Figure 2.3, Figure 2.4, Figure 2.5**).

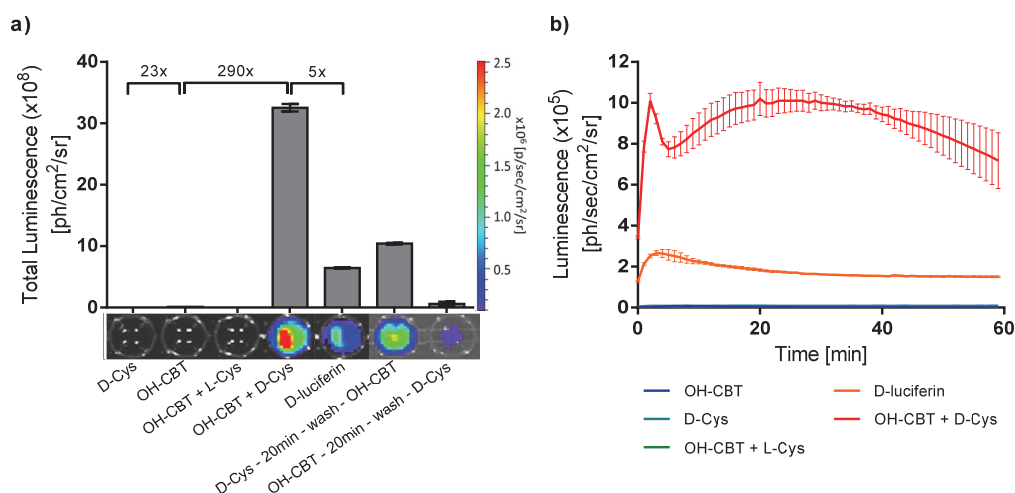


Figure 2.3: Light emission resulting from the split luciferin reaction in living cells. (a) Total luminescence produced in 1 h from live SKOV3-Luc-D3 cells incubated with corresponding reagents, calculated by integrating the area under corresponding kinetic curves in Figure 2.3b. SKOV3-Luc-D3 cells were incubated for 1 h with either D-cysteine; HO-CBT; HO-CBT and L-cysteine (added simultaneously); D-luciferin, or HO-CBT and D-cysteine (added simultaneously) at 75  $\mu$ M in PBS (wells 1-5). Cell first pretreated with D-cysteine for 20 min, followed by washing and 1 h incubation with HO-CBT and cell first pretreated with HO-CBT for 20 min, followed by washing and 1 h incubation with D-cysteine (all at 75  $\mu$ M in PBS, wells 6-7). Error bars are  $\pm$  SD for three independent measurements. (b) Observed bioluminescence produced as a function of time from SKOV3-Luc-D3 live cells, incubated with following reagents: D-cysteine; HO-CBT; HO-CBT plus L-cysteine; HO-CBT plus D-cysteine; and D-luciferin (all at 75  $\mu$ M in PBS pH=7.4). Error bars are  $\pm$  SD for three independent measurements.

When the cells were incubated with equimolar concentrations of HO-CBT in the presence of D-cysteine, the amount of light produced by the cells treated with D-cysteine and HO-CBT exceeded the signal from an equivalent amount of D-luciferin by more than a factor of 5 (**Figure 2.3, Figure 2.5a**). Incubation of live ovarian cancer cells with a 1:1 ratio of HO-CBT and D-cysteine produced 5-fold more light than incubation with an equimolar amount of D-luciferin (**Figure 2.3**). Similarly, a 6.5-fold enhancement was obtained when the same experiment was repeated in live breast cancer cells (**Figure 2.5a**). An increase in light emission was also observed when cells were incubated with equimolar concentrations of H<sub>2</sub>N-CBT in the presence of D-cysteine compared to the resulting light emission after D-aminoluciferin treatment (**Figure 2.4, Figure 2.5b**). The signal produced from the two luciferin precursors was concentration dependent in both cell lines. A higher BL signal was observed with increasing concentrations of HO-CBT or H<sub>2</sub>N-CBT and D-cysteine (**Figure S2.5, Figure S2.6**). The higher signal with HO-CBT or H<sub>2</sub>N-CBT and D-cysteine compared to the corresponding luciferins could be explained by

differences in their cell permeability. HO-CBT or H<sub>2</sub>N-CBT and D-cysteine may have better cell permeability than the D-luciferin itself. It was previously reported that D-luciferins have sub-optimal penetration properties, which can be improved by making their structures more lipophilic.<sup>[38,40]</sup>

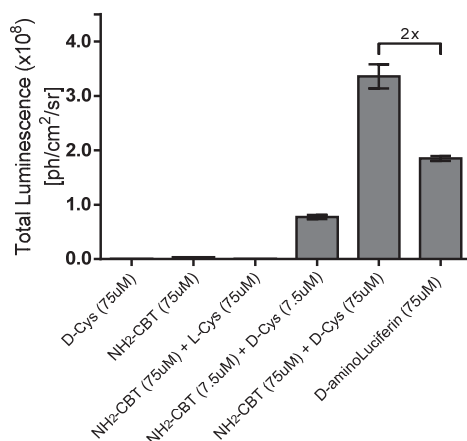


Figure 2.4: Split luciferin ligation reaction in living SKOV3-Luc-D3 cells. (a) Total bioluminescence signal observed over a period of 1 h (AUC) with SKOV3-Luc-D3 cells. Cells were first incubated 5 min with D-cysteine (7.5 or 75 μM), L-cysteine (75 μM) or PBS, followed by addition of H<sub>2</sub>N-CBT (7.5 or 75 μM) or D-aminoluciferin (75 μM) just before imaging. Error bars are ± SD for three measurements.

We speculated that if the hypothesis that the luciferin precursors possess higher cell penetration abilities is true, a big portion of the reaction should be happening inside the cell. In order to see whether this is the case, the cells were pre-incubated with one of the reagents, followed by washing. Light emission was observed in both cases, with higher signal being produced when the cells were pre-incubated with D-cysteine, followed by extensive washing and subsequent addition of CBT (**Figure 2.3a, Figure S2.5a, Figure S2.6a**). In fact, only 20 min exposure of the cells to D-cysteine followed by a wash and subsequent addition of HO-CBT, resulted in 30% and 60% of the overall signal produced in SKOV3-Luc D3 and MDA-MB-231-Luc-D3H2LN cells respectively, compared to incubation with equimolar concentrations of both of the reagents simultaneously for the same period of time (**Figure 2.3a, Figure S2.5a, Figure S2.6a**). In addition, these signals are respectively 20% and 400% higher than the signal observed from the SKOV-Luc D3 and MDA-MB-231-Luc-D3H2LN cells, treated with equimolar concentration of D-luciferin control (**Figure 2.3a, Figure S2.5a, Figure S2.6a**).

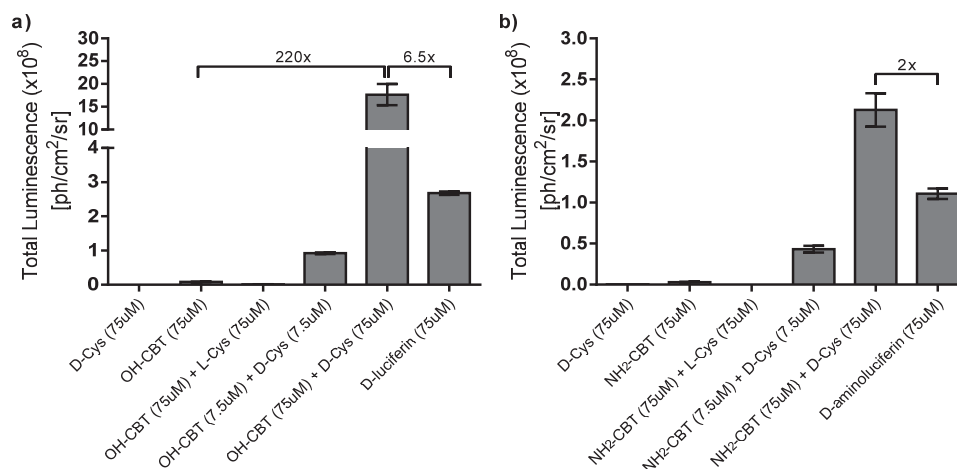


Figure 2.5: Split luciferin ligation reaction in living MDA-MB-231-Luc-D3H2LN cells. (a) Total bioluminescence signal observed over a period of 1 h (AUC) with MDA-MB-231-Luc-D3H2LN cells. Cells were first incubated 5 min with D-cysteine (7.5 or 75 μM), L-cysteine (75 μM) or PBS, followed by addition of HO-CBT (7.5 or 75 μM) or D-luciferin (75 μM) just before imaging. (b) Total bioluminescence signal observed over a period of 1 h (AUC) with MDA-MB-231-Luc-D3H2LN cells. Cells were first incubated 5 min with D-cysteine (7.5 or 75 μM), L-cysteine (75 μM) or PBS, followed by addition of H<sub>2</sub>N-CBT (7.5 or 75 μM) or D-aminoluciferin (75 μM) just before imaging. Error bars are ± SD for three measurements.

However, when the same experiment was repeated where the sequence of addition of the reagents was reversed (pre-incubated with HO-CBT for 20 min, then washed and treated with D-cysteine), less than 10% of overall signal was observed in comparison to the signal resulted from simultaneous addition of both CBT and D-cysteine reagents in both cell lines (**Figure 2.3b**, **Figure S2.5a**, **Figure S2.6a**). The light emission from the experiments where SKOV-3 cells were first incubated with D-cysteine, washed and incubated with HO-CBT is 20 times higher (40 times for MDA-MB-231 cells) than the same experiments where HO-CBT is incubated first (**Figure S2.5a**, **Figure S2.6a**). This suggest that D-cysteine remains available for reaction with HO-CBT after 20 min incubation and washing. On the other hand, it seems not to be the case for HO-CBT and a possible explanation would be a poorer cell permeability of CBT compared to D-cysteine. This might also be explained by reaction of HO-CBT with intra- or extra-cellular nucleophiles, reducing the CBT molecules available to react with D-cysteine. The reversible reaction of CBTs with free thiols was reported before, although the reaction remains selective for 1,2-aminothiols over free thiol moieties.<sup>[193]</sup> Cell permeability of luciferin precursors and luciferins could have been investigated in more detail by incubation of non-luciferase expressing cells with or without D-cysteine and HO-CBT or H<sub>2</sub>N-CBT, followed by cell lysis after incubation. Addition of Fluc to cell lysate and subsequent BL acquisition would have been gainful to determine and compare cell permeability of different luciferin precursors and corresponding luciferin analogues.

Lastly, a robust concentration-dependent increase in signal was observed when the cells were treated with increasing amounts of D-cysteine, while the concentration of HO-CBT or H<sub>2</sub>N-CBT was kept constant (**Figure S2.5, Figure S2.6**). Importantly, this increase was not due to changes in FLuc activity as no increase in signal production was observed when the control cells were incubated with D-luciferin and increasing concentrations of D-cysteine (**Figure 2.6**).

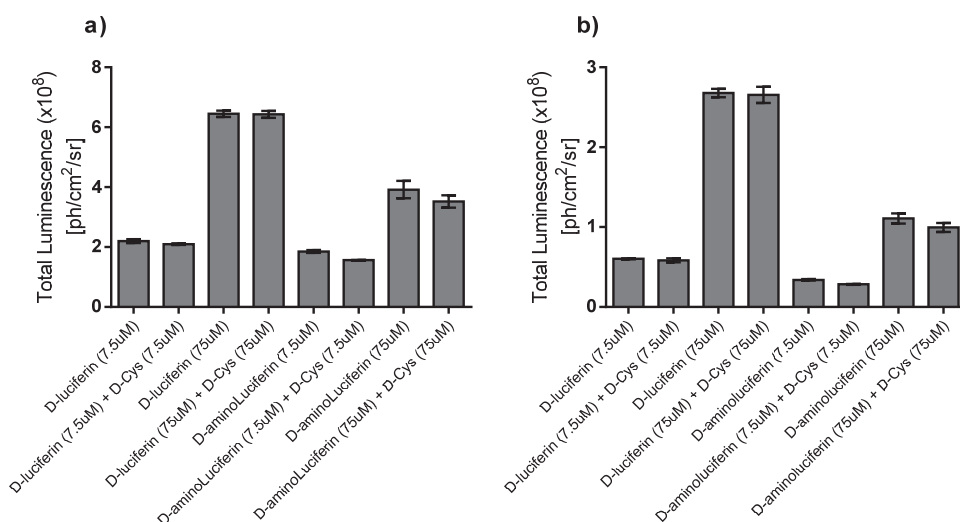


Figure 2.6: Effect of high D-cysteine concentrations on bioluminescence emission in SKOV3-Luc-D3 (a) and MDA-MB-231-luc-D3H2LN (b) living cells. Total bioluminescence signal integrated over 1 h. Cells were incubated with D-cysteine (7.5 or 75 μM) or PBS together with either D-luciferin (7.5 or 75 μM) or D-aminoluciferin (7.5 or 75 μM). The cells were imaged immediately after addition of the last compound. Error bars are ± SD for three measurements.

Taken all together, these data suggest that both reagents might have much higher permeability than D-luciferin alone or higher stability in biological environment, which is supported by a significant increase in signal after equimolar addition of the two precursors in comparison to full luciferin controls (**Figure 2.3, Figure S2.5, Figure S2.6**). Indeed, HO-CBT or H<sub>2</sub>N-CBT are more hydrophobic than luciferins due to lack of carboxylic acid moiety, which could explain their better diffusion through the cell membranes. Moreover, while no specific transporters are known to facilitate penetration of luciferins, D-cysteine could still be a substrate for cysteine transporters, responsible for the uptake of L-cysteine by mammalian cells.<sup>[211-214]</sup> In addition, better stability and longer life time of the split luciferin ligation reagents in comparison to luciferins<sup>[25,37,58,97,215,216]</sup> may also play a significant role in the increased light output from live cells.

Such excellent signal to background ratio and low contribution of endogenous L-cysteine makes split luciferin reaction ideal for bioluminescence imaging applications.<sup>[6,114,194]</sup> Moreover, the



significantly higher light observed from the addition of luciferin precursors in comparison to its corresponding luciferin analogue presents an opportunity for much higher sensitive imaging of biological processes in live cells.

### 2.3 Real time non-invasive imaging and quantification of split luciferin ligation reaction in living animals

Inspired by the exciting data from live cell assays, whether both of the luciferin precursors, HO-CBT or H<sub>2</sub>N-CBT and D-cysteine, can react directly in living animals to form their respective luciferins was investigated (**Figure 2.7**). In order to visualize the luciferin formation non-invasively in real-time, transgenic animals that ubiquitously express luciferase in every cell under the control of the beta-actin promoter (FVB-luc+ mice) were used.<sup>[217,218]</sup>

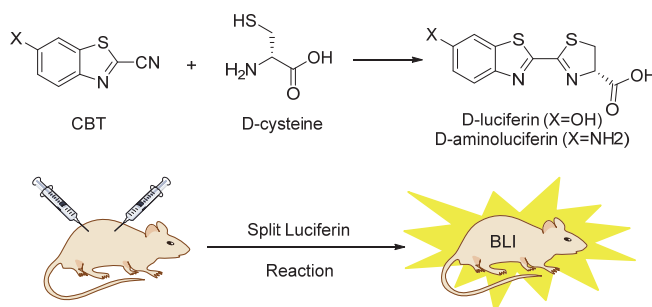


Figure 2.7: Imaging split luciferin reaction in living mice. Overall schematic of in situ formation of D-luciferin or D-aminoluciferin in living transgenic reporter animals.

First, the mice were injected with either HO-CBT or H<sub>2</sub>N-CBT alone and the resulting luminescence emission was measured. Similarly to the results obtained in living cells, only background signals were observed (**Figure 2.7, Figure 2.8**) with the HO-CBT or H<sub>2</sub>N-CBT compared to luciferins signals. When these experiments were repeated with addition of an equimolar amount of D-cysteine 3 min before injection of HO-CBT or H<sub>2</sub>N-CBT, a robust signal was obtained only a few minutes after injection, suggesting the relatively fast rate of conversion of the reagents to full D-luciferin scaffold *in vivo* (**Figure 2.9**).

Notably, the signal produced from the animals injected with D-cysteine and H<sub>2</sub>N-CBT was 2.4 times higher, but not significantly, than the signal from HO-CBT and D-cysteine ( $P = 0.0883$ , **Figure 2.8a**), which is consistent with previously reported data for relative light output between D-aminoluciferin and D-luciferin, being very close.<sup>[36,40]</sup> The split luciferin ligation reagents appear to possess desirable pharmacokinetic properties, supported by the fact that robust signal is observed throughout the body of the living animal shortly after injection of both reagents (**Figure 2.8b**).

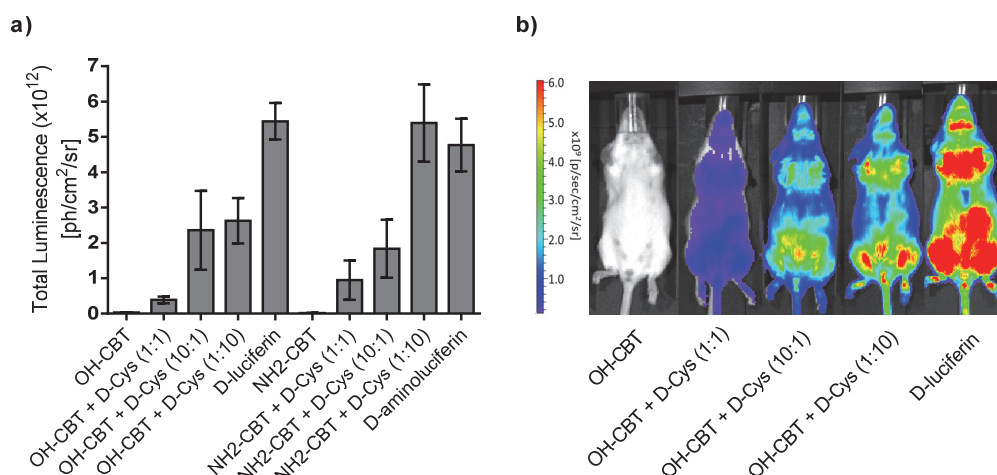


Figure 2.8: Split luciferin ligation reaction in living mice. (a) Total luminescence over 50 min from resulting bioluminescent signal from luciferase transgenic mice after IP injection of HO-CBT; D-cysteine and HO-CBT in equimolar concentrations (1:1); D-cysteine and HO-CBT in 1:10 ratio; and D-luciferin (1 equivalent represent a dose of  $0.268 \text{ mmol}\cdot\text{kg}^{-1}$  in  $100 \mu\text{L}$  of PBS). Error bars are  $\pm$  SD for five measurements. Statistical analyses were performed with a two-tailed Student's *t* test. (b) Representative image of mice 15 min post-injection of HO-CBT, HO-CBT + D-cysteine (equimolar concentration), HO-CBT + D-cysteine (10:1 respective concentration ratio), HO-CBT + D-cysteine (1:10 respective concentration ratio) and D-luciferin (1 equivalent represent a dose of  $0.268 \text{ mmol}\cdot\text{kg}^{-1}$  in  $100 \mu\text{L}$  of PBS).

### 2.3.1 Optimization studies of split luciferin ligation reaction in living mice

The total light output produced in the mice injected with D-cysteine and equimolar amounts of HO-CBT or H<sub>2</sub>N-CBT were approximately 10 and 20 % of the overall signal obtained from D-luciferin or D-aminoluciferin injected groups, respectively (**Figure 2.8a**). The opposite trend was observed in cells where the split luciferin reagents produced several fold higher light emission than the corresponding luciferin derivatives (**Figure 2.3**, **Figure 2.4**, **Figure 2.5**). This difference in the ratio of signal production between live animals and tissue culture cells could be explained by the fact that, in mice, the reaction is taking place in a large and complex environment. Reaction of CBT derivative with free endogenous L-cysteine, binding to serum proteins, or metabolism of CBT in the liver could influence the yield of reaction and thus the resulting light emission.

Since increased concentration of D-cysteine led to a significant increase in the overall signal production in cells (**Figure 2.3**, **Figure S2.5**, **Figure S2.6**), the FVB luc<sup>+</sup> mice were injected with 10 equivalents of D-cysteine, followed by one equivalent of HO-CBT or H<sub>2</sub>N-CBT administration. The resulting signal increased by 7- and 6- fold for HO-CBT and H<sub>2</sub>N-CBT respectively, compared to the light output from injection of 1:1 ratio of both reagents (**Figure 2.8**). Substantially, the total light output from the mice injected with a 1:10 ratio of HO-CBT and D-cysteine produced half of the signal obtained from D-

luciferin control group. Moreover, animals injected with a 1:10 ratio of H<sub>2</sub>N-CBT and D-cysteine produced an equivalent amount of light to the mice injected with the D-luciferin or D-aminoluciferin (**Figure 2.8**). This significant signal enhancement *in vivo* with increased concentration of D-cysteine is consistent with the cell culture experiments (**Figure 2.3**, **Figure S2.5**, **Figure S2.6**). When the animals were injected with 1 equivalent of D-Cysteine and 10 equivalents of either HO-CBT or H<sub>2</sub>N-CBT, significant light enhancement was observed only in case of HO-CBT when compared to equimolar amounts of both the reagents. This observation might be explained by the fact that HO-CBT or H<sub>2</sub>N-CBT compounds might have different pharmacokinetic properties in living animals. But, it is important to keep in mind that the background generated by 10 equivalent of CBT derivatives alone would probably contribute to the enhanced signal. Further experiments would be necessary, to estimate the background generated by 10 equivalents of HO-CBT and H<sub>2</sub>N-CBT.

### 2.3.2 *In vivo* comparative studies of signal stability of split luciferin ligation reaction with D-luciferin

D-luciferin, when injected IP, typically produces a sharp peak reaching maximum at around 15 min post-injection with about 3- to 4-fold increase in intensity of the signal, followed by the sudden drop.<sup>[36,113]</sup> This rapid change in the intensity of the signal with D-luciferin injection in animals has been recognized as a critical disadvantage in BLI.<sup>[113,219,220]</sup> For example, BLI has been widely used to quantify the size of the tumor in xenograft models where the animals are injected with luciferase-transfected human cancer cells.<sup>[221,222]</sup> This model, in combination with BLI, has been one of the major tools in drug discovery for testing anticancer drugs in animals.<sup>[223,224]</sup> However, since the BL signal from injected D-luciferin changes significantly over time,<sup>[36,219,220]</sup> it could be difficult to assess the tumor size accurately. Currently, methods to stabilize the D-luciferin signal is even more urgent as new 3D BLI technologies have become routine and require longer imaging times.<sup>[225,226]</sup>

Table 2.2: Signal variability of D-luciferin and its derivatives upon I.P. injection in living mice.

Compounds	Signal peak [min]	% of increase before signal peak	% of decrease after signal peak	Decrease in intensity compared to unmodified luciferin	Synthetic modification / commercial availability
Amino-D-luciferin <sup>a)</sup>	10	300	75 in 50 min		No / Yes
D-luciferin <sup>a)</sup>	5	200	67 in 50 min		No / Yes
D-luciferin <sup>b)</sup>	15	200	60 in 1 h		No / Yes
Glycine-D-aminoluciferin <sup>a)</sup>	20	<sup>c)</sup>	30 in 1 h	20-30 x	Yes / No
PEG-D-aminoluciferin <sup>d)</sup>	240	150	60 in 8 h	1.2 x	Yes / No
HO-CBT + D-Cysteine <sup>b)</sup>	15	30	40 in 1 h	10 x	No / Yes

<sup>a)</sup> Reference 36, <sup>b)</sup>Figure 2.9, <sup>c)</sup> the bioluminescence emission from Glycine-D-luciferin starts at 0 Total photon/sec and increase to approximately 2.5 Total photon/sec in 20 min.<sup>[36]</sup>, <sup>d)</sup> Reference [220].

Several attempts have been reported to address the D-luciferin signal variability *in vivo* including usage of costly implantable osmotic pumps<sup>[219]</sup> and repeated substrate injections.<sup>[36]</sup> However,

suboptimal results were obtained in both cases leading to development of new chemically modified luciferins, which allow stabilization of the signal. Shinde *et al.* reported a glycine-D-aminoluciferin analog, which produced much more stable signal in comparison to D-luciferin alone, although the intensity of the signal was 20-30 times lower than that of D-luciferin or D-aminoluciferin.<sup>[36]</sup> Similarly, the Denmeade group reported PEGylated luciferin derivatives that yield more stable and prolonged light production compared to D-Luciferin, albeit with a significant reduction in overall light output (**Table 2.2**).<sup>[220]</sup>

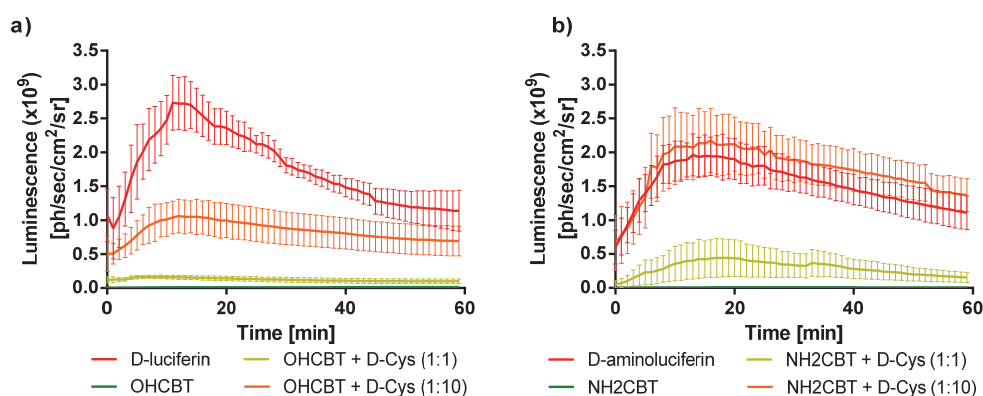


Figure 2.9: Split luciferin ligation reaction in living mice. (a) Observed luminescence as a function of time after i.p. injection of HO-CBT; D-cysteine and HO-CBT in equimolar concentrations (1:1); D-cysteine and HO-CBT in 1:10 ratio; and D-luciferin (1 equivalent represent a dose of 0.268 mmol·kg<sup>-1</sup> in 100 μL of PBS). Error bars are ± SD for five measurements. (b) Observed luminescence as a function of time after IP injection of H<sub>2</sub>N-CBT; D-cysteine and H<sub>2</sub>N-CBT in equimolar concentrations (1:1); D-cysteine and H<sub>2</sub>N-CBT in 1:10 ratio; and D-aminoluciferin (1 equivalent represent a dose of 0.268 mmol·kg<sup>-1</sup> in 100 μL of PBS). Error bars are ± SD for five measurements.

Figure 2.9a shows the kinetics of light production with D-luciferin in FVB-Luc+ mice in comparison to equimolar injections of two luciferin ligation precursors (HO-CBT and D-cysteine). The signal from D-luciferin increased 200% in the first 15 minutes, reaching the maximum value, followed by 60% decrease from the peak by 60 min post injection, representing a significant change in a short period of time (**Figure 2.9a**, red line). However, the signal from HO-CBT and D-cysteine increased by only 30% in the first 15 minutes followed by 40% decrease from the peak by 60 min post injection, producing much smaller variability in overall signal. In addition, the light output could be dramatically enhanced by injection of increased amounts of D-cysteine or HO-CBT without significant loss in signal stability (**Figure 2.9a**, orange and yellow lines). Therefore, the new *in vivo* ligation reaction between HO-CBT and D-cysteine achieved remarkable stabilization of the signal without any synthetic manipulation (**Table 2.2**). Since HO-CBT and D-cysteine are commercially available and are several times cheaper than unmodified D-luciferin, this technology offers a simple and powerful tool to overcome signal variability of D-luciferins and have high potential in 3D imaging applications. On the other hand, H<sub>2</sub>N-CBT and D-

cysteine did not produce a stable the light emission over time, unlike HO-CBT and D-cysteine. Differences in biodistribution or pharmacokinetics could be part of the explanation. This observation suggests that HO-CBT and D-cysteine would be the imaging reagents of choice for BLI application where having a stable signal over time is important.

## 2.4 Conclusion

In this chapter the study of split luciferin reaction in enzymatic assay, living cells and animals, was presented. Current study shows that D-cysteine and HO-CBT or its amino analogue can efficiently react with each other in physiological environment, and therefore, the split luciferin approach is appropriate for bioluminescence imaging of biological systems.

In cells, the bioluminescent signal with the split luciferin reaction was higher than with the already formed D-luciferin or its amino analogue, suggesting that the luciferin precursors benefit from higher cellular permeability. A strong light emission was also observed in luciferase expressing animals after sequential administration of HO-CBT or its amino analogue and D-cysteine. In addition, the intensity of the light output resulting from split luciferin ligation reaction increased significantly by injection of higher concentration of D-cysteine (**Figure 2.8**). The light emission was more stable over time than the emission generated by luciferins – an interesting property that might be useful for different applications requiring signal quantification or three dimensional imaging. Several-fold signal variation over a short period of time with D-luciferin causes significant errors in quantification of tumor size or transcriptional activation.<sup>[211,213,214]</sup> Split luciferin reaction in mice resulted in major signal stabilization compared to D-luciferin signal (30% vs 200% in signal variation in the first 15 min post-injection for equimolar concentrations) without use of any specially synthesized or expensive reagent, nor implanted osmotic pumps (**Figure 2.9**).<sup>[211,213,214]</sup>

L-luciferin, upon reaction with FLuc enzyme, was reported to be capable of light emission under certain condition.<sup>[30,31]</sup> As HO-CBT or H<sub>2</sub>N-CBT reacts with L-cysteine to form the corresponding L-luciferin or its amino analogue, the resulting emission background could have been problematic. With the concentrations of reagent used in the present study, the influence of endogenous L-cysteine on signal was found to be negligible in both living cells and animals.

Apart from bioluminescence imaging, the condensation reaction of CBT derivatives with 1,2-aminothiols could be used for conjugation applications. The condensation reaction between the luciferin precursors is selective and highly efficient with rate of reaction faster than many other efficient

biorthogonal reactions.<sup>[177,227,228]</sup> The reaction rates of the split luciferin reaction is three orders of magnitude higher than that of Staudinger ligation, opening wide range of opportunities for the use of this reaction to study fast biological processes where the use of the Staudinger ligation was not feasible (**Table 2.1**). The condensation reaction of CBT derivatives with 1,2-aminothiols could be used for conjugation in tandem with the known bioorthogonal reactions. The split luciferin chemistry is compatible with the chemistry of other classical bioorthogonal reactions, which involve either azide, alkyne, triphenylphosphine or tetrazine moieties.<sup>[133,140-153,155-159,161]</sup> This could be particularly useful *in vivo*, where applications of multiple biocompatible reactions have not been reported to study simultaneous events at the same time. It is worth mentioning that the SPAAC or SL reactions were employed in conjugation with tetrazine/trans-cyclooctene ligation reaction in the same experiments in living mice. Despite the fact that these double biorthogonal reactions were used for a two-steps labeling approach and not for imaging multiple biological process, it allowed use of lower reagent concentration for the second step due to higher reaction rate of the IED DA reaction.<sup>[163,229]</sup> These features make split luciferin reaction highly valuable to study complex biological processes.

Altogether, this study demonstrate that the split luciferin ligation reaction possesses several unique features which could make it very useful for a wide variety of biological applications, depicting high potential for the field of chemical biology and medical research. More applications of this technology for non-invasive imaging of biological process *in vivo* are currently being explored in our laboratories.

**Notes.** Simultaneously to this study, another research group has also investigated the use of the split luciferin reaction for bioluminescence applications. Our works were published during the same period.<sup>[230,231]</sup>

## 2.5 Experimental section

**General Material and Methods.** N-succinamidyl-CBT derivative (compound **3**, **Table 2.1**) was synthesized according to a reported procedure.<sup>[195]</sup> D-cysteine (Sigma-Aldrich) and H<sub>2</sub>N-CBT (Sigma-Aldrich), L-cysteine (Alfa Aesar), HO-CBT (ABCR GmbH), D-luciferin potassium salt (Biosynth AG), D-aminoluciferin (Assay biotechnology Company Inc.), Luciferase (Sigma-Aldrich prod. number L9506 or SRE0045), Adenosine 5'-triphosphate disodium salt (ATP, AppliChem GmbH), Phosphate Buffered Saline (PBS) (Life Technologies Corporation) were obtained from commercial sources and used without further purification. HPLC analysis was performed on Agilent Infinity 1260 HPLC system with either an Agilent Eclipse-XDB-C18 5  $\mu$ m 4.6 x 250 mm column or Agilent Poroshell 120 EC-C18 2.7  $\mu$ m 4.6 x 75 mm column using degassed HPLC gradient grade solvent (Fisher Chemicals) and Millipore water. The

products of the reaction were initially analyzed by Agilent 6120 Quadrupole LC/MS (Agilent). More detailed HR ESI-MS measurements were conducted at the EPFL ISIC Mass Spectrometry Service using Micro Mass QTOF Ultima (Waters Corp). Millipore water was used for sample preparation of all the *in vitro*, cellular, and animal assays. Luciferase buffer used to quantify the amount of luciferin formed during incubation was prepared as following: 60  $\mu\text{g mL}^{-1}$  firefly luciferase (Sigma-Aldrich) in 0.1M Tris-HCl pH=7.4, 2 mM ATP, and 5 mM  $\text{MgSO}_4$ . All *in vitro* and cellular studies were performed in clear bottom black 96 well plates (Becton Dickinson and Co.). Spectramax Gemini (Molecular Devices), IVIS 100 (Xenogen) or IVIS Spectrum (Xenogen) were used to measure the amount of BLI signal production.

**Split luciferin reaction - Cell-free experiments.** In a black 96-well plate, 98  $\mu\text{L}$  of PBS were added in the wells followed by the addition of 1  $\mu\text{L}$  of a D-cysteine solution (1 mM in PBS), L-cysteine solution (1 mM in PBS) or PBS. Then, 1  $\mu\text{L}$  of a HO-CBT solution (1 mM in DMSO),  $\text{H}_2\text{N}$ -CBT solution (1 mM in DMSO) or DMSO was added to the solutions. Finally, 50  $\mu\text{L}$  of a luciferase solution (120  $\mu\text{g/mL}$  luciferase enzyme in Tris-HCl pH 8, 4 mM ATP and 10 mM  $\text{MgSO}_4$ ) were added just before the imaging. The plate was imaged in an IVIS 100 imaging system for 30 min at 37 °C with one minute intervals under automatic settings. BLI signal was quantified using region-of-interest (ROI) analysis available on Living Image software 4.4 (Caliper Life Sciences).

**HPLC Assays.** 100  $\mu\text{L}$  solution of 0.01M of HO-CBT or  $\text{H}_2\text{N}$ -CBT was mixed with 50  $\mu\text{L}$  solution of 0.01M L-cysteine, and 5  $\mu\text{L}$  of the resulting solution was injected into LC-MS. The following conditions were used to separate the resulting products (**Figure S2.1 a-b**): Agilent Poroshell 120 EC-C18 2.7  $\mu\text{m}$  4.6x75mm column: 2 mL/min flow, 0-1 min 10% MeCN + 90 % water, containing 0.1%  $\text{HCOOH}$ , then from 1 to 5.5 min concentration of MeCN was linearly increased to 100%. After that the column was washed and pre-equilibrated with 10% MeCN + 90% water, containing 0.1%  $\text{HCOOH}$  for 2.5 min before the next injection.

**Split luciferin reaction – Kinetic experiments.** All the solvents were freshly degassed and the solutions of reagents (HO-CBT,  $\text{H}_2\text{N}$ -CBT or N-succinamidyl-CBT and L-cysteine) were freshly prepared prior to the experiments. The degree of conversion was determined by the intensity of UV absorbance at the corresponding characteristic wavelength of pure CBT derivative on HPLC data. The pseudo-first order constants were determined for each concentration of L-cysteine by linearization in  $\ln [\text{C}(\text{nitrile})]$  vs time coordinates (**Figure S2.2, Figure S2.3, Figure S2.4**). Second order constants were determined for each concentration of L-cysteine by dividing the pseudo-first order values to the corresponding cysteine concentration in the resulting reaction mixture. Procedure for rate constant determination for HO-CBT and  $\text{H}_2\text{N}$ -CBT and N-succinamidyl-CBT derivative<sup>[193]</sup> (respectively compound **1**, **2** and **3**,

**Table 2.1):** 20  $\mu$ L 0.01 M solution of the CBT derivative in MeCN was added to 950  $\mu$ L of PBS and mixed. To this mixture, a solution of 30  $\mu$ L 0.1, 0.125, 0.15 or 0.2 M of L-cysteine in PBS was added followed by extensive shaking. The resulting aliquots of 100  $\mu$ L of the reaction mixture was taken at 1-5 min time points and quenched with 200  $\mu$ L of 10% aqueous HCl to stop the reaction. Aliquots of 100  $\mu$ L of the quenched solution was directly injected into analytical LC-MS to determine the degree of conversion. The resulting products were initially analyzed by ESI-MS, followed by product isolation and further analysis by HRMS.

**Split luciferin reaction - Cellular Experiments.** IVIS Spectrum (Xenogen) was used for bioluminescent imaging in all cell experiments. SKOV-3-Luc-D3 cells (PerkinElmer) were cultured in McCoy's 5A modified media (Life Technologies). MDA-MB-231-Luc-D3H2LN cells (PerkinElmer) were cultured in Minimum Essential  $\alpha$  Medium (Life Technologies Corporation). Both of the cell culture media contained 10% FBS, 1% GlutaMAX and 1% Penicillin/Streptomycin mixture. Cells were seeded ( $1 \times 10^4$  cells/well) in a black 96-well plate with clear bottoms (Becton Dickinson and Co.). 48 h later, the growth medium was removed and the cells were initially washed with 200  $\mu$ L of PBS, followed by incubation for 5 min with 100  $\mu$ L (150  $\mu$ M, 15  $\mu$ M or 1.5  $\mu$ M) D-cysteine or L-cysteine solution in PBS or PBS alone. Then, 100  $\mu$ L (150  $\mu$ M, 15  $\mu$ M or 1.5  $\mu$ M) solutions of HO-CBT, H<sub>2</sub>N-CBT, D-luciferin or D-aminoluciferin in PBS were added, the cells were immediately placed in IVIS Spectrum and imaged for 1 h with one image acquired every minute. The BLI signal was quantified using region-of-interest (ROI) analysis available on Living Image software 4.4 (Caliper Life Sciences).

**Animals.** FVB-Luc<sup>+</sup> transgenic mice (FVB-Tg(CAG-luc,-GFP)L2G85Chco/J)<sup>[217,218]</sup> were kindly provided by the laboratory of Prof. Christopher Contag at Stanford University, re-derived at UC Davis, and bred at UC Berkeley. The breeding colony was housed in groups of 4-5 mice according to their age and gender with free access to food and water at 22 °C with regular light-dark cycle. All studies were approved and performed according to the guidelines of the Animal Care and Use Committee of the University of California, Berkeley.

**Split luciferin reaction - Animal experiments in FVB-Luc<sup>+</sup> mice.** IVIS Spectrum (Xenogen) was used for BLI imaging in all animal experiments and the resulting data were processed using Living Image software 4.2 (Caliper Life Sciences). All solutions were prepared in sterile DMSO (Sigma-Aldrich) and PBS. Mice were anesthetized via inhalation of isoflurane (Phoenix), that was premixed with medical grade oxygen (Praxair) for both injection and imaging procedure. 6-10 weeks old Female FVB-Luc<sup>+</sup> mice (5 mice per group) were IP injected with either HO-CBT; H<sub>2</sub>N-CBT; D-Cysteine and HO-CBT in equimolar concentrations (1:1); D-Cysteine and H<sub>2</sub>N-CBT in equimolar concentrations (1:1); D-Cysteine and HO-



CBT in 1:10 ratio; D-Cysteine and H<sub>2</sub>N-CBT in 1:10 ratio; D-luciferin; and D-aminoluciferin. All injections were done with one equivalent corresponding to a dose of 0.267 mmol·kg<sup>-1</sup> in 100 µL of PBS (D-Cysteine, 32.34 mg·kg<sup>-1</sup>; D-luciferin, 85.01 mg·kg<sup>-1</sup>) and/or in 20 µL DMSO (HO-CBT, 47.04 mg·kg<sup>-1</sup>; H<sub>2</sub>N-CBT, 46.78 mg·kg<sup>-1</sup>; D-aminoluciferin, 74.58 mg·kg<sup>-1</sup>). The time period of 3 min between IP injection of D-cysteine and CBT derivatives was respected, and the animals were imaged right after the second injection. The animals injected with D-luciferin were imaged right after the injection with the compound.

## 2.6 Supplementary figures

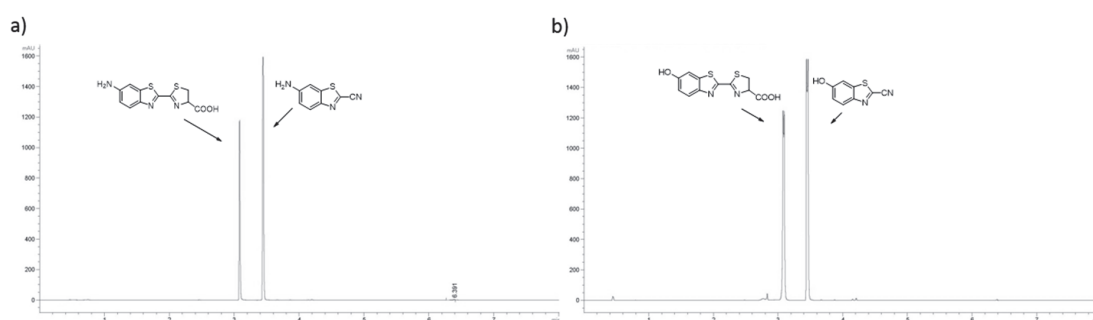


Figure S2.1: In vitro formation of luciferins. (a) HPLC chromatogram of aminoluciferin formation. Condensation reaction between H<sub>2</sub>N-CBT and L-Cysteine was performed with the addition of 100 µL H<sub>2</sub>N-CBT 10mM solution to 50 µL of a 10 mM L-cysteine solution. The resulting mixture was injected into HPLC-MS. (b) HPLC chromatogram of luciferin formation. Condensation reaction between HO-CBT and L-Cysteine was performed with the addition of 100 µL HO-CBT 10mM solution to 50 µL of a 10 mM L-cysteine solution. The resulting mixture was injected into HPLC-MS.

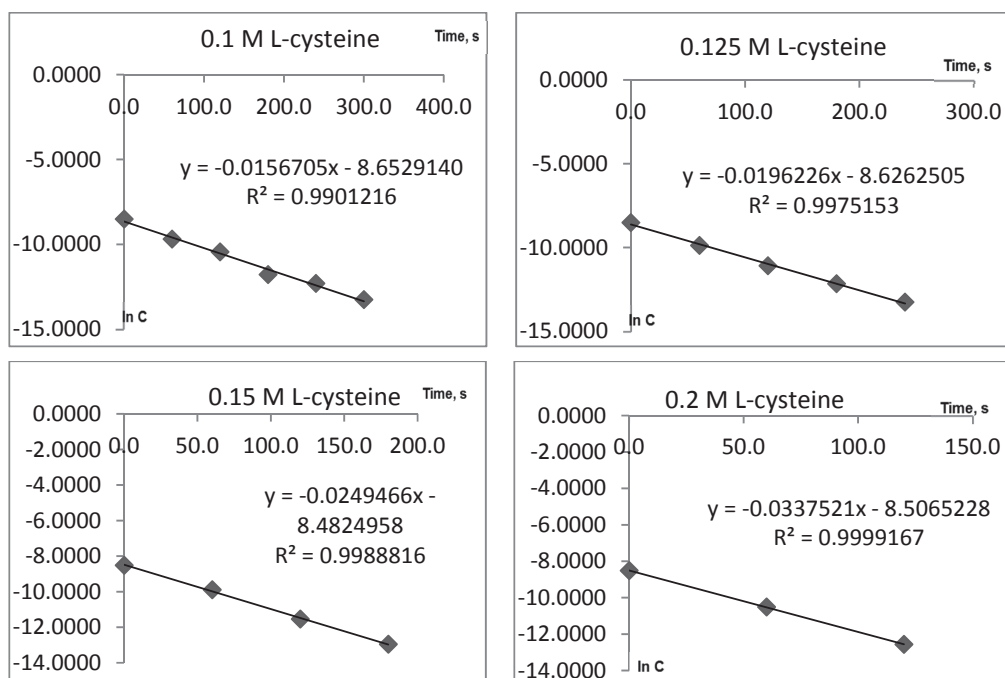


Figure S2.2: Pseudo-first order rate constant determination for the reaction of HO-CBT with different concentrations of L-cysteine.

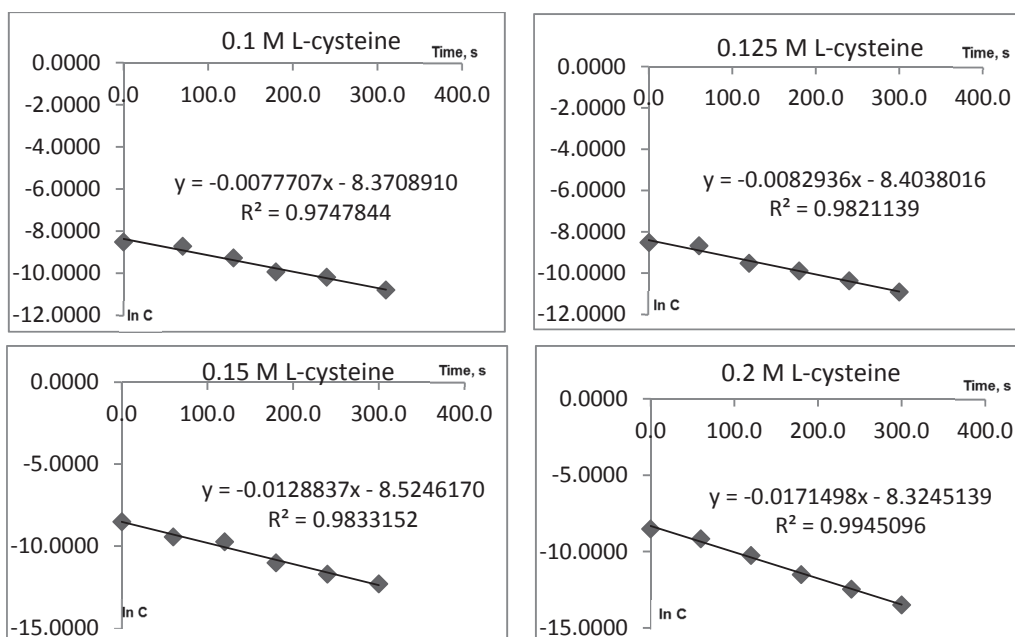


Figure S2.3: Pseudo-first order rate constant determination for the reaction of  $H_2N$ -CBT with different concentrations of L-cysteine.

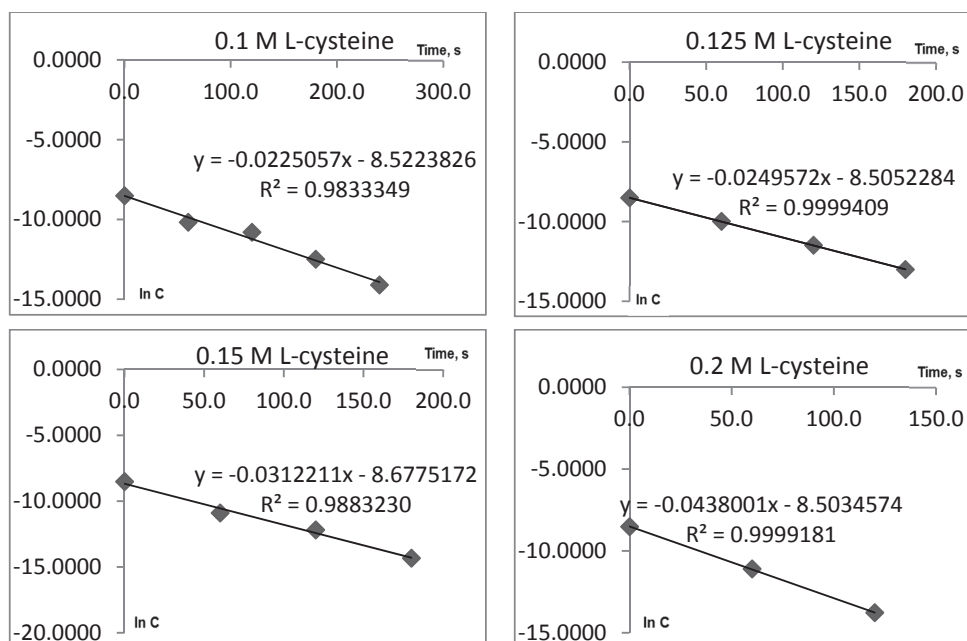


Figure S2.4: Pseudo-first order rate constant determination for the reaction of N-succinamidyl CBT derivative 1 with different concentrations of L-cysteine.

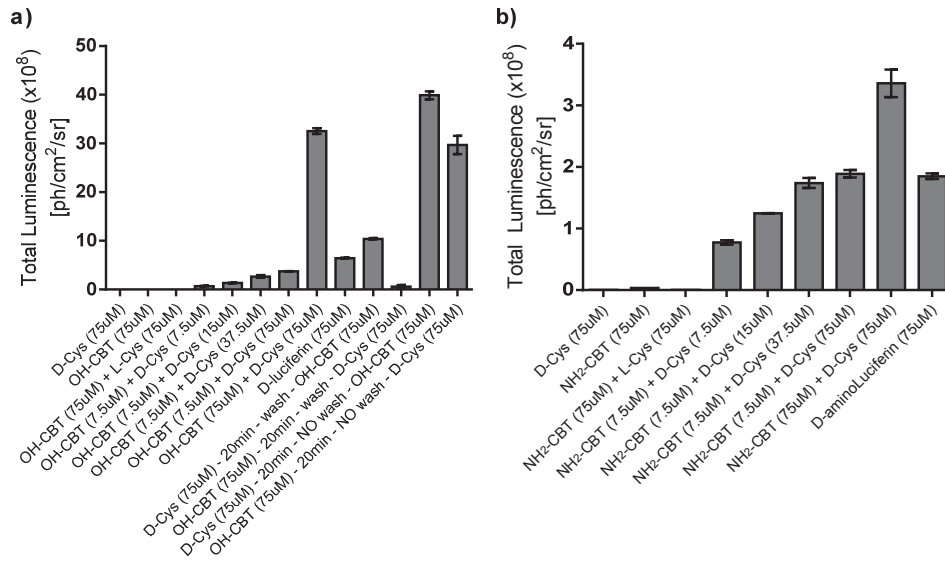


Figure S2.5: Split luciferin ligation reaction in SKOV3-Luc-D3 living cells. (a) Total bioluminescence signal observed over a period of 1 h when cells were incubated with HO-CBT (7.5 or 75  $\mu$ M) and D-cysteine (7.5, 15, 37.5, 75  $\mu$ M) or L-cysteine (75  $\mu$ M). Alternatively, cells were first incubated D-cysteine (75  $\mu$ M) or HO-CBT (75  $\mu$ M) and after 20 min of incubation time, cells were washed with PBS (200  $\mu$ L) and further incubated with the complementary reagent such as HO-CBT (75  $\mu$ M) or D-cysteine (75  $\mu$ M) respectively. (b) Total bioluminescence signal observed over a period of 1 h when cells were incubated with H<sub>2</sub>N-CBT (7.5 or 75  $\mu$ M) and either D-cysteine (7.5, 15, 37.5, 75  $\mu$ M) or L-cysteine (75  $\mu$ M). Error bars are  $\pm$  SD for three measurements.

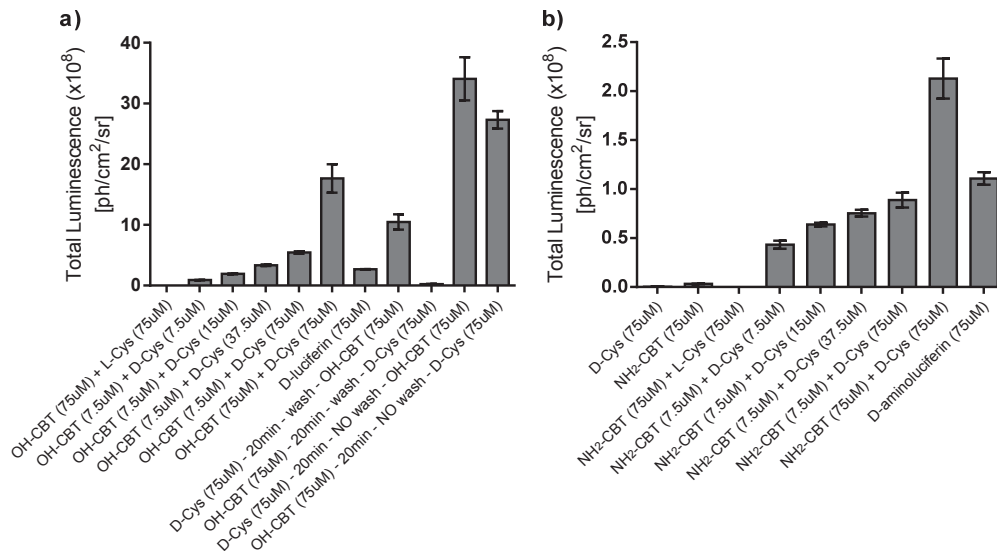


Figure S2.6: Split luciferin ligation reaction in living MDA-MB-231-Luc-D3H2LN cells. (a) Total bioluminescence signal observed over 1 h when cells were incubated with HO-CBT (7.5 or 75  $\mu$ M) and either D-cysteine (7.5, 15, 37.5, 75  $\mu$ M) or L-cysteine (75  $\mu$ M). Alternatively, cells were first incubated D-cysteine (75  $\mu$ M) or HO-CBT (75  $\mu$ M) and after 20 min of incubation time, cells were washed with PBS (200  $\mu$ L) and incubated with the complementary reagent such as HO-CBT (75  $\mu$ M) or D-cysteine (75  $\mu$ M) respectively. (b) Total bioluminescence signal observed over 1 h when cells were incubated with H<sub>2</sub>N-CBT (7.5 or 75  $\mu$ M) and either D-cysteine (7.5, 15, 37.5, 75  $\mu$ M) or L-cysteine (75  $\mu$ M). Error bars are  $\pm$  SD for three measurements.



## Chapter 3 Application of the Split Luciferin Reaction for Non-Invasive Bioluminescent Imaging of Protease Activity

BLI has recently been used to probe molecular signatures of target tissues through caged luciferin substrates, which are uncaged only by a specific biological activity or environment. The underlying principle in the design of these caged luciferin probes is based on the principle that luciferin substituted on the 6'-position oxygen or nitrogen are not capable of light emission (Scheme 1.2, chapter 1).<sup>[84,90,92,99]</sup> This concept was used for the development of probes to sense enzymatic activity (e.g. beta-galactosidase,<sup>[84]</sup> caspases,<sup>[59-62,77]</sup> furin,<sup>[71]</sup> beta-lactamases,<sup>[85]</sup> and nitroreductase<sup>[89]</sup>) that have been used extensively for imaging in living animals. Previously, the caged luciferin approach was also successfully applied to real-time imaging and quantification of fatty acid uptake,<sup>[99]</sup> cell surface glycosylation,<sup>[90]</sup> hydrogen peroxide fluxes,<sup>[92]</sup> as well as to study cell-penetrating peptide conjugates efficiency of delivery, linker release, and biodistribution.<sup>[215]</sup> In addition, the preparation of new red-shifted luciferin derivatives and their corresponding luciferase enzymes for multi-color application of BLI have recently been reported.<sup>[38,40,42,44]</sup>

Although caged luciferin probes are powerful tools for imaging processes *in vivo*, their synthesis can be rather challenging and costly. On the other hand, D-luciferin precursors (i.e. D-cysteine and HO-CBT) and their derivatives are much easier to synthesize and these compounds have higher stability in comparison to luciferins,<sup>[37,58,97,215]</sup> which are known to be sensitive to light, pH and oxygen.<sup>[25,216]</sup> In this chapter, the potential of using the split luciferin reaction for imaging specific biological processes (i.e. protease activity) using the “caging” approach was evaluated. Caged D-cysteine probes were designed, allowing D-luciferin or D-aminoluciferin formation in a protease-dependant manner (**Scheme 3.1**). This methodology was then used to measure the activity of proteases (i.e. thrombin and caspase enzymes) *in vitro* and *in vivo*. Additionally, since both CBT and D-cysteine moieties can be modified with different caging groups simultaneously, the split luciferin approach can be utilized for

dual detection of events *in vivo*. For example, the hydroxy or amino group on the CBT moiety can be caged as a sensor for various biomolecules, similar to the whole luciferin scaffolds (**Scheme 3.2**).<sup>[59-62,71,77,84,85,90,92,99]</sup> At the same time, the amine group on the D-cysteine moiety can be caged with a substrate for proteases including caspases,<sup>[59-62,77]</sup> thrombin,<sup>[77,232]</sup> prostate specific antigen,<sup>[233,234]</sup> and many others that are known to be cleaved after defined peptide sequences.<sup>[77,235]</sup> As a proof of principle, dual imaging of  $\beta$ -galactosidase and caspase 3 activity has been demonstrated *in vitro*, suggesting that the split luciferin reaction could be a valuable tool for imaging multiple biological processes.

### 3.1 *In vitro* imaging of thrombin and caspase 3 protease activity

Caged D-luciferin scaffolds have been previously reported to quantify and visualize activity of various proteases in living cells and animals.<sup>[57-62,77,236,237]</sup> The use of the reaction between HO-CBT or H<sub>2</sub>N-CBT and D-cysteine can be expanded to *in vivo* imaging of protease activity and thus improve applications of this exciting set of tools. The structure of D-cysteine is ideal for being caged with a substrate for proteases, by simply incorporating it on to the end of a protease-specific sequence (**Scheme 3.1, Movie S1**). Importantly, multiple essential mammalian and bacterial proteases are known to cleave after specific *N*-terminal amino acid sequences.<sup>[63,80,86,109,193,238]</sup> While the synthesis of short peptides is cheap and can be readily performed with the help of automated peptide synthesizers,<sup>[239,240]</sup> the synthesis of fully caged luciferin scaffolds involves much more complex and low yielding synthetic procedures.<sup>[38,40,42,44,57,59,71,84,85,89,90,92,99]</sup> The production of caged luciferins is further complicated by the fact that only a few reactions have been reported to work on the full luciferin scaffold. They include TFA deprotection,<sup>[58]</sup> hydrogenation,<sup>[37]</sup> and the formation of a carbonate from the phenolic oxygen.<sup>[97,215]</sup> Moreover, luciferins are known to be inherently more sensitive to light, base, and oxidation.<sup>[25,216]</sup> This greatly limits the production of a broad variety of caged luciferin scaffolds as bioluminescent sensors. Thus, despite many protease-specific sequences known today, very few of them have been used for BLI in the context of caged luciferins<sup>[3,5,47,50,51,58,77,241]</sup> and even fewer are commercially available.<sup>[77]</sup> Since CBTs and cysteine derivatives are easier to manipulate and possess higher intrinsic stabilities to light and pH,<sup>[25,37,97,215,216]</sup> it was reasoned that the use of these precursors might circumvent the significant synthetic challenges posed by caged luciferin scaffolds and therefore significantly expand their applications.

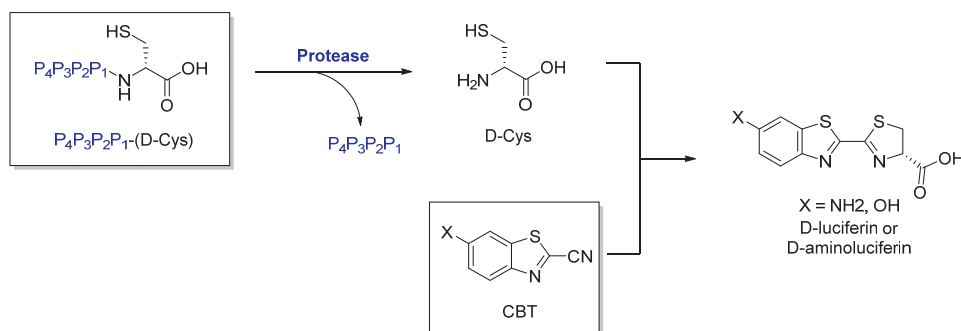
To test the viability of this approach, caspase 3 as well as thrombin protease, which all play important roles in several human pathologies, were selected.<sup>[52,54,55,242]</sup> Activation of both caspase 3 and 7 are directly connected to apoptosis,<sup>[52,53]</sup> which plays a key role in many human pathologies such as cancer and neurodegenerative disease.<sup>[54-56]</sup> Caspases are expressed as zymogen, an inactive form

of the enzyme requiring activation to exercise proteolytic activities. Caspases have been classified in three main groups: initiator (e.g. caspase 8, 9 and 10), executioners (caspase 3, 7 and 6) and inflammatory (e.g. caspase 1 and 4). The initiator group is further divided in two categories that are caspases involved in the intrinsic (caspase 9) or extrinsic (caspase 8 and 10) apoptotic pathway. These pathways consist of a multistep proteolytic cascades where the executioner caspases are activated by the initiators ones via proteolytic cleavage. The intrinsic pathway is a non-receptor mediated process that is triggered by stimuli such as radiation, toxins, free radicals, absence of growth factors or certain hormones. These stimuli will generate mitochondrial-initiated events that will further result in caspase 9 activation. On the other hand, the extrinsic pathway is initiated by transmembrane receptor-mediated interactions involving death receptors and corresponding ligands (e.g. TNFR1/TNF- $\alpha$ , FasR/FasL). The binding of the ligand to the death receptor induces a sequence of event leading to caspase 8 or caspase 10 activation. Both intrinsic and extrinsic pathways lead to the activation of the executioners caspases: caspase 3, caspase 7 and caspase 6.<sup>[243,244]</sup> While there is a difference in substrate preference between the executioners caspases and initiator ones, there is an overlap in activity among each group rendering sometimes difficult to differentiate them with imaging probe.<sup>[245]</sup> The caspase 3 and 7 is a good example as they both share preference for similar substrates. It has been previously reported that DEVD-containing peptides (Asp-Glu-Val-Asp) are selective substrates for caspase 3 and to a lesser extent, caspase 7, with cleavage occurring after the second aspartic acid residue.<sup>[74,246]</sup> Imaging downstream effectors such as caspase 3/7 in cells represent a valuable way for measuring cell death activation. A bioluminogenic caspase 3/7 sensor is commercially available, in which D-aminoluciferin has been introduced at the C-terminus of the DEVD peptide and routinely used to detect apoptosis.<sup>[57-62,77]</sup>

Thrombin is another example of clinically relevant protease that plays a key role in many blood coagulation-related reactions that prevent a variety of mammalian organisms from extensive blood loss.<sup>[247,248]</sup> A thrombin-selective peptide sequence has been previously identified (Gly-Gly-Arg) and utilized in multiple *in vitro* tests to assess activity of the protease.<sup>[76,249]</sup>

Since both caspase 3 and thrombin are known to cleave at the C-terminal end of their corresponding protease-specific sequence of amino acids, the synthesis of these peptides with the addition of D-cysteine at the C-terminal end was performed to yield L(Asp-Glu-Val-Asp)-D-Cys (DEVD-(D-Cys)) and L-(Gly-Gly-Arg)-D-Cys (GGR-(D-Cys)), respectively. These peptides were then incubated with increasing concentrations of their corresponding proteases, followed by addition of HO-CBT or H<sub>2</sub>N-CBT and luciferase buffers sequentially. If the protease is active and could recognize its specific peptide sequence, free D-cysteine would be released in the course of the reaction. Therefore, addition of HO-CBT or H<sub>2</sub>N-CBT would result in the formation of the corresponding D-luciferin or D-aminoluciferin.

Further addition of luciferase would consequently result in significant light production, with more light output from the samples with higher concentrations of proteases (**Scheme 3.1**, **Figure 3.1**, **Figure 3.2**). The efficacy of the peptide specific cleavage can then be estimated by direct comparison of the light output from a D-cysteine caged peptide, with amount of light produced from equimolar amount of free D-cysteine.



Scheme 3.1: Imaging protease activity using the split luciferin reaction. Overall representation of peptidic probe  $P_4P_3P_2P_1$ -(D-Cys) cleavage by the desired protease and further reaction with HO-CBT or  $H_2N$ -CBT to form the corresponding D-luciferin or D-aminoluciferin molecule. P1 to P4 represents amino acids. The choice of P4 to P1 residues will determine the substrate specificity for the desired protease.

Strong bioluminescent signals were observed following incubation of protease-specific peptides with their corresponding proteases, and signal increased with increasing concentration of protease (**Scheme 3.1**, **Figure 3.1**, **Figure 3.2**). For example, concentration-dependent signal was observed when DEVD-(D-Cys) peptide was incubated with increasing amounts of caspase 3 and subsequently treated with  $H_2N$ -CBT-containing luciferase buffer. Importantly, the overall signal produced from DEVD-(D-Cys) peptide incubated with caspase 3 reached 50% of the light output of the signal from the equimolar solution of the free D-cysteine control. This experiment shows that DEVD-(D-Cys) peptide remains a good substrate for caspase 3 even upon addition of a D-cysteine amino acid at the C-terminus of the protease-specific sequence (**Figure 3.1**).



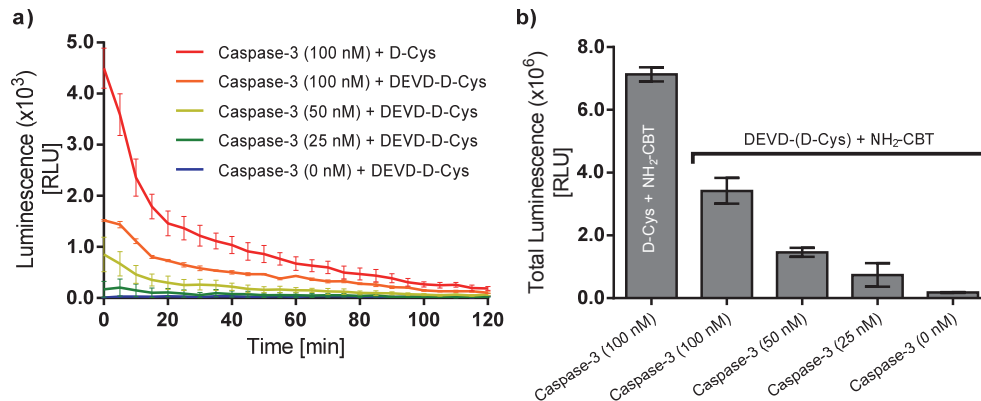


Figure 3.1: *In vitro* enzymatic assay of caspase 3 activity using DEVD-(D-Cys) peptide and H<sub>2</sub>N-CBT. (a) luminescence signal following incubation of DEVD-(D-Cys) peptide with increasing concentrations of caspase 3 (25, 50 and 100 nM) or D-cysteine control (200  $\mu$ M) at 37 °C before addition of H<sub>2</sub>N-CBT (400  $\mu$ M) followed by 1 h incubation at 37°C and subsequent imaging after addition of luciferase buffer. Error bars are  $\pm$  SD of three measurements. (b) Total luminescent signal integrated over 2 h (AUC). Error bars are  $\pm$  SD of three measurements. Statistical analyses were performed with a two-tailed Student's t test. All the groups are statistically significant with each other ( $P < 0.05$ ) except between 25 and 0 nM ( $P=0.12$ ).

Similar results were obtained when D-cysteine was caged with the thrombin-selective peptide GGR (Figure 3.2). A four-fold increase in BL signal over background was observed when the GGR-(D-Cys) peptide was incubated with thrombin protease followed by addition of H<sub>2</sub>N-CBT, and the signal was dependent on the protease concentration (Figure 3.2). The outcome of this *in vitro* enzymatic assays demonstrate the feasibility of using a combination of short D-cysteine-caged amino acid sequences with H<sub>2</sub>N-CBT to study the activity of proteases using bioluminescence.

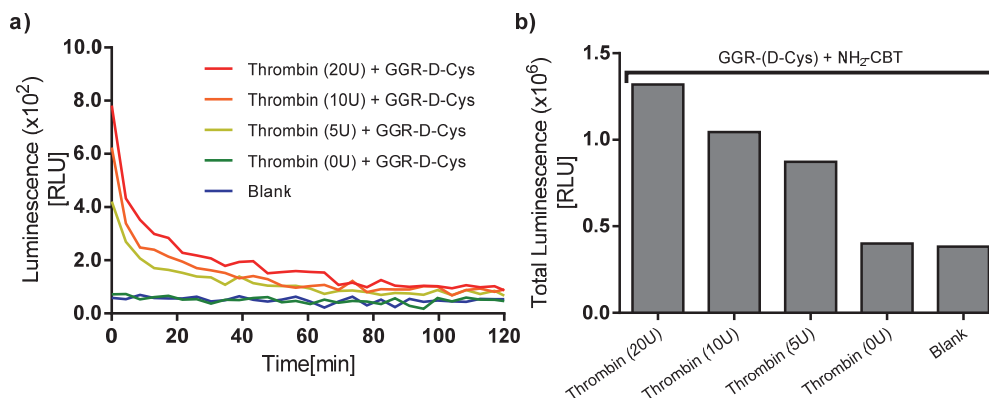


Figure 3.2: *In vitro* enzymatic assay of Thrombin activity using GGR-(D-Cys) peptide and H<sub>2</sub>N-CBT. (a) luminescence signal following incubation of GGR-(D-Cys) peptide (400  $\mu$ M) with varying concentrations of thrombin (20, 10 and 5 units) over 3 h at 37 °C, followed by addition of H<sub>2</sub>N-CBT (400  $\mu$ M in MeOH) and incubation for 1 h at rt. Immediately prior to quantification of bioluminescence emission, 5  $\mu$ L of the reaction solution was added to a luciferase solution (60  $\mu$ g/mL luciferase in 0.1M Tris-HCl, 2 mM ATP, 5 mM MgSO<sub>4</sub>). (b) Total bioluminescent signal integrated over 2 h (AUC). The blank control is luciferase solution alone.

### 3.2 *In vitro* real time imaging of caspase activity

Previous experiments focused on the pre-incubation of the caged peptide probes with the appropriate proteases. To determine if monitoring real-time activation of caspase 3 is possible, the protease, FLuc, peptide probes, HO-CBT and the necessary cofactors were incubated *in vitro*. In other words, all the components necessary for light emission were incubated simultaneously. Following cleavage of the peptide probe by caspase 3, the released D-cysteine moiety reacted with HO-CBT to form D-luciferin, which was subsequently oxidized by luciferase, resulting in caspase-dependent light emission and quantification of bioluminescence emission was performed immediately following addition of the peptide probe. To determine if increasing the concentration of caspase 3 caused an increase in bioluminescence signal, z-DEVD-(D-Cys) peptide, HO-CBT and varying concentrations of caspase 3 were incubated with luciferase and cofactors *in vitro*. The higher the concentrations of caspase 3, the greater the light emission, which resulted in a dose-dependent light emission (**Figure 3.3**). Strikingly, the luminescence generated from 0.1 units per mL (U/mL) of caspase 3 was significantly above the background ( $P = 0.0031$ ). As a control, the peptide probe was replaced by D-cysteine (cage-less peptide probe). Using same concentration of D-cysteine and peptide probe, the total luminescence resulting from D-cysteine and HO-CBT control is equivalent to light potentially emitted by 100% cleavage of the z-DEVD-(D-Cys) peptide by the protease. Therefore, 40 U/mL of caspase 3 was demonstrated to cleave approximately 70% of the peptide probe over 3h (**Figure 3.3b**).

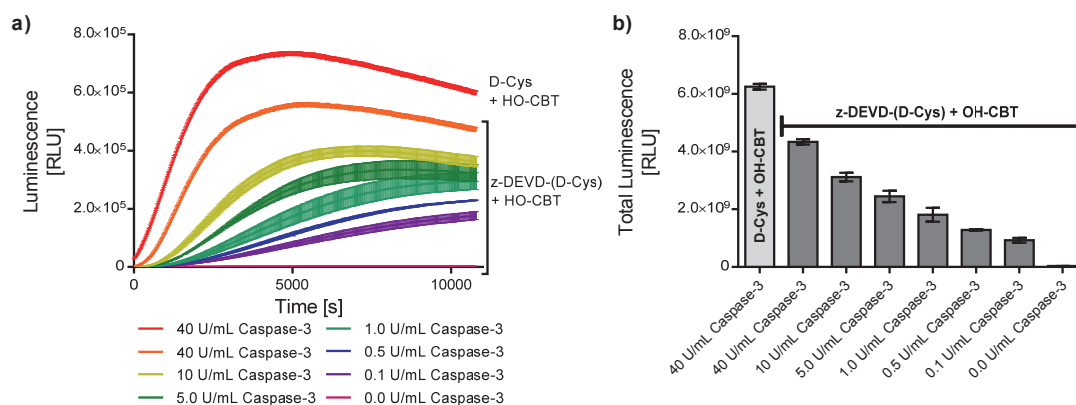


Figure 3.3: *In vitro* enzymatic assay of caspase 3 activity using z-DEVD-(D-Cys) peptide and HO-CBT. (a) luminescence signal following incubation of luciferase (including co-factors), HO-CBT (100  $\mu$ M) and z-DEVD-(D-Cys) peptide in presence of increasing caspase 3 concentrations (0, 0.1, 0.5, 1.0, 5.0, 10 or 40 units/mL) or D-cysteine control (100  $\mu$ M) for 3 h at 37  $^{\circ}$ C. Error bars are  $\pm$  SD of three measurements. (b) Total luminescence integrated over 3 h (AUC). Error bars are  $\pm$  SD of three measurements. Statistical analyses were performed with a two-tailed Student's t test. All the groups are statistically significant with each other ( $P < 0.05$ ) except between 0.5 and 1.0 U/mL ( $P=0.06$ ).

Next, split luciferin based probes for caspase 6, caspase 8 and caspase 9 were developed. These peptide probes were designed to be specific for each caspase by the addition of a D-cysteine moiety at the C-terminal of the caspase cleavage sequences that were reported in the literature. These substrate sequences have also been used for commercially available fluorometric, colorimetric or bioluminescent probes.<sup>[77,250,251]</sup> The z-VEID-(D-Cys), z-LETD-(D-Cys) and z-LEHD-(D-Cys) probes were used for caspase 6, caspase 8 and caspase 9 respectively.<sup>[74,77,246]</sup> Although, it has to be noted that another report has shown that caspase 8 also cleaves LEHD sequence more efficiently than IETD, another caspase 8 substrates.<sup>[250]</sup> The *in vitro* enzymatic evaluation of these probes with the respective caspases are depicted in Figure 3.4.

Results obtained for the caspase 6 probe (z-VEID-(D-Cys)) were comparable to the data obtained for the z-DEVD-(D-Cys)/caspase 3 experiments and resulted in dose-dependent BL emission. Importantly, light emission obtained when the probe was incubated with 40 U/mL of enzyme resulted in approximately 51% of probe cleavage by caspase 6 in 3 h (Figure 3.4).

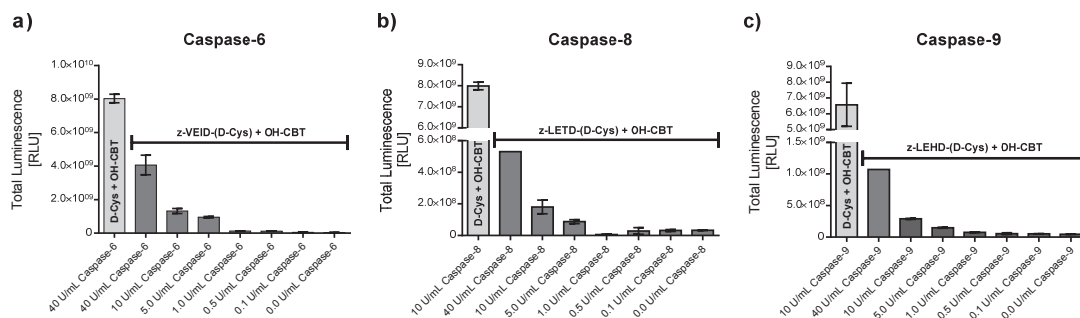


Figure 3.4: *In vitro* enzymatic assay of caspase 6, caspase 8 and caspase 9 activities imaging with respectively z-VEID-(D-Cys), z-LETD-(D-Cys) or z-LEHD-(D-Cys) peptide and HO-CBT. (a) Integrated luminescence signal over 3 h (AUC) resulting from incubation of luciferase (including co-factors), HO-CBT (100  $\mu$ M), z-VEID-(D-Cys) peptide in presence of increasing concentrations of caspase 6 (0, 0.1, 0.5, 1.0, 5.0, 10 and 40 units/mL) or D-cysteine control (100  $\mu$ M) for 3 h at 37  $^{\circ}$ C. (b) Similar results for caspase 8 enzyme using z-LETD-(D-Cys) peptide. (c) Similar results for caspase 9 enzyme using z-LEHD-(D-Cys) peptide. Error bars are  $\pm$  SD of three measurements. The associated luminescence in function of the time data are presented in Figure S3.1. Differences between all groups from 10 to 1 U/mL are statistically significant with each other ( $P < 0.01$ ), and non-significant from 1 to 0 U/mL ( $P > 0.5$ ).

Light emission obtained with the highest concentration of caspase were much lower than for caspase 3 and 6, with approximately 6.7 % and 16.3 % of the probe cleaved for caspase 8 and caspase 9, respectively. These differences in cleavage efficiency could be due to different affinities of the caspases with their respective peptide probe, or due to differences in activity of the caspase. Indeed, the units (U) for each enzyme refers to the value provided by the manufacture (Abcam) for each enzyme. 1 U of caspase is defined as the enzyme activity that cleaves 1 nmol of colorimetric substrate per hour at 37  $^{\circ}$ C in a defined caspase buffer. Thus, the enzymatic activity for each caspase was investigated

using commercially available colorimetric probes in order to determine actual caspases activity, in order to confirm or invalidate manufacture indications. Commercially available colorimetric probes contain a peptide sequence that is specific for the corresponding caspases, with a para-nitroanilide group on the C-terminal. Once released upon caspase cleavage, the para-nitroaniline (pNA) has a high absorbance at 405 nm. By measuring the absorbance, the concentration of released pNA and thus the caspase activity can be determined. Activities of caspase 3, caspase 8 and caspase 9 were measured (**Figure S3.2**). Caspase 3 and caspase 9 have similar activities, with 100% of the probe cleaved after 2.5h. On the other hand, caspase 8 shows very small activity according to the colorimetric assay. If it's estimated that the baseline corresponds to the control group containing 10 U/mL of caspase 8 and no colorimetric probe, approximately 13% of pNA is released over 135 min (**Figure S3.2**). This low activity could explain the results obtained with the BL probe z-LETD-(D-Cys) (**Figure 3.4b**). On the other hand, caspase 9 seems to be very active. Thus the poor cleavage of the LEHD-(D-Cys) peptide compare to caspase 3, could not be explained by the difference in enzymatic activities. This suggests that the probe design may affect the reaction kinetics and that the cleavage of LEHD prior to a D-cysteine moiety may not be optimal for caspase 9, resulting in poor cleavage of the peptide. The carboxybenzyl group on the N-terminal could also influence the substrate affinity to the enzyme.

To further investigate the specificity of the developed bioluminescent probes for caspases, a cross reactivity assay was performed with the four peptide probes and caspases (caspase 1, caspase 2, caspase 3, caspase 4, caspase 5, caspase 6 and caspase 9). Due to the poor activity of caspase 8 (Abcam plc, UK), it was decided not to include this protease in the assay (**Figure 3.5**). This *in vitro* enzymatic assay were performed with simultaneous incubation of caspase and luciferase enzymes, probes and HO-CBT as well as all the necessary cofactors, and subsequent luminescence emission was acquired over 3 hours. The total luminescence integrated over 3 h are depicted in figure 3.5.

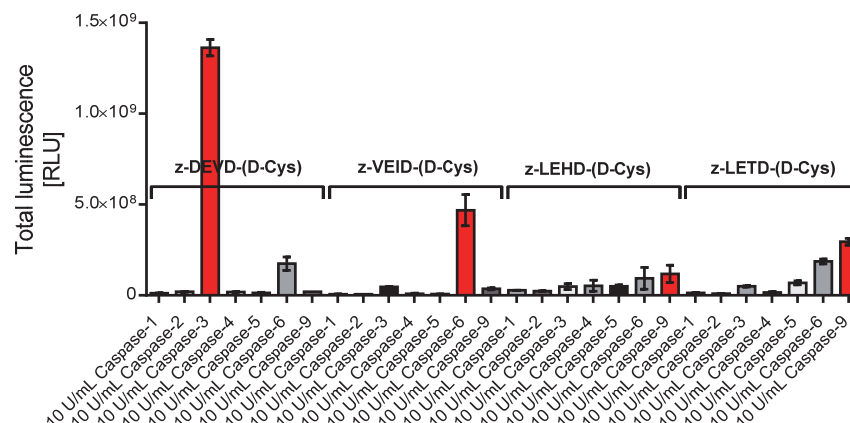


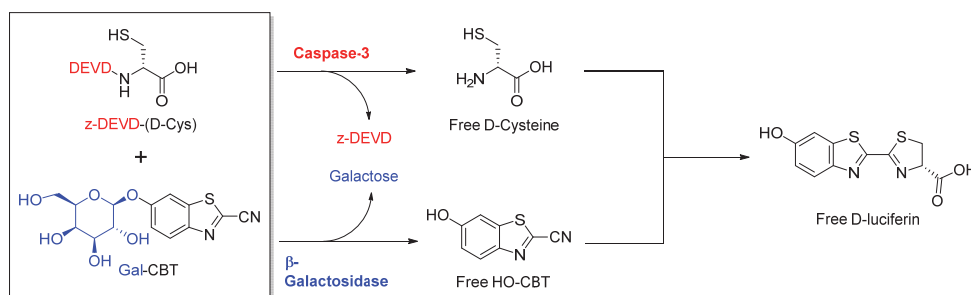
Figure 3.5: Cross reactivity assay of the caspases specific split luciferin probes with different caspases. Integrated luminescent signal over 3 h (AUC) resulting from z-DEVD-(D-Cys), z-VEID-(D-Cys), z-LEHD-(D-Cys) and z-LETD-(D-Cys) probes (100  $\mu$ L) incubated with 10 U/mL of caspase 1 to caspase 6 as well as caspase 9, HO-CBT (100  $\mu$ L) and luciferase enzyme at 37  $^{\circ}$ C. Error bars are  $\pm$  SD of three measurements.

The z-DEVD-(D-Cys) peptide shows specific strong cleavage by caspase 3. This peptide is also cleaved to a lower extent by caspase 6. The caspase 6 specific peptide, z-VEID-(D-Cys), shows also a specific cleavage by caspase 6, with very low light emission resulting incubation with other caspases. The z-LETD-(D-Cys) peptide is cleaved by caspase 9 more efficiently, but a significant amount of this peptide is also cleaved by caspase 6. It is more difficult to draw clear conclusion for that peptide, as this experiment do not include caspase 7 and caspase 8 enzymes. Nevertheless, the z-LETD-(D-Cys) peptide is significantly cleaved by caspase 9 and the signal is surprisingly higher than the one emitted from z-LEHD-(D-Cys) incubation with caspase 9, suggesting that the later would be a better substrate for caspase 9. This results are in contradiction with reported data on substrate specificity using fluorogenic tetrapeptide bearing an aminocoumarin on the C-terminal side.<sup>[246]</sup> But further investigation would be necessary in order to understand this trend and determine if the D-cysteine moiety at C-terminal affects the sequence specificity.<sup>[252,253]</sup> Moreover, the enzyme units used correspond to the manufacturer indication and were not tested in house, and thus variation on activities could vary. In order to have more accurate data, enzyme activities should be determined first using colorimetric probes, allowing to equal activities for every enzyme. This is necessary to have a reliable cross-reactivity assay. But the increased enzyme quantities as well as numerous colorimetric probes necessary is costly and time consuming, makes this assay out of range for a simple control experiment. Nevertheless, activities of caspase 3, 6 and 9 were show to be similar using colorimetric probes. Moreover, these data are useful for comparing cleavage efficiency of different peptides by the same protease. To conclude, these experiments have shown that split luciferin based probes could be used for substrate evaluation, and could potentially be useful for screening peptide libraries as substrates. It also has to

be noted that the caspase substrate specificity were reported to be overlapping and therefore no absolutely specific substrates exist even if there is substrate preferences among caspases.<sup>[244,251]</sup> Caspase 3 was nevertheless found to be one of the efficient target of a large number of short sequence substrate.<sup>[250]</sup> Moreover, the tetrapeptide substrate is important for specificity, but the residue located after the cleavage site also influence rate of cleavage and small residue such as alanine, serine or glycine are preferred.<sup>[254]</sup> Cysteine was not included in this report, but according to properties of preferred amino acids at the P1' position, cysteine should not be problematic. However, isomeric factors were not included and could influence the enzyme/substrate interaction.

### 3.2.1 *In vitro* simultaneous imaging of caspase 3 and $\beta$ -galactosidase using the split luciferin reaction

An interesting feature of the split luciferin reaction, is that both of the luciferin precursors, D-cysteine and CBT, could potentially be caged. By modifying these two molecules, with different molecular patterns that could be removed selectively by distinct biological processes or enzymes, the split luciferin reaction could be an interesting tool for monitoring multiple processes using bioluminescence. To establish the potential use of these probes for dual-process imaging, caging both of the luciferin precursors for different enzymes was performed. This is an advantage that is offered by the use of the split luciferin reaction unlike the classical caged luciferin approach. As a proof of principle, an attempt of imaging  $\beta$ -galactosidase ( $\beta$ -Gal) and caspase 3 at the same time was performed.  $\beta$ -Gal is a hydrolase enzyme that catalyses the hydrolysis of  $\beta$ -galactosides into monosaccharides. It's an essential enzyme in human body also present in some bacteria strains and is widely used as reporter gene in molecular biology.<sup>[255]</sup> A caged-luciferin probe for  $\beta$ -Gal imaging has been reported and consists of a galactoside-luciferin conjugate that has shown to be useful for monitoring  $\beta$ -Gal activity in several experimental set-ups.<sup>[46,84,256,257]</sup> Using a similar approach, an HO-CBT molecules functionalized with a galactoside (Gal-CBT) on the phenolic atom was synthesized. Only if  $\beta$ -Gal is present and active, a free luciferin will be formed after reaction with D-Cysteine. The D-Cysteine moiety will be available for reaction only after cleavage of the DEVD-(D-Cys) peptide by caspase 3. Both  $\beta$ -Gal and caspase 3 enzymes are therefore necessary for the *in situ* formation of a free D-luciferin molecule (**Scheme 3.2**).



Scheme 3.2: Dual caging on luciferin precursors for imaging multiple biomolecular activities using the split luciferin reaction. Galactoside-CBT (Gal-CBT) is selectively cleaved by  $\beta$ -Galactosidase enzyme to generate a free HO-CBT molecule. D-cysteine reactivity towards CBT is masked by the DEVD peptidic sequence. Following cleavage of the z-DEVD-(D-Cys) peptide by caspase 3, the released free D-cysteine reacts with the CBT moiety to yield a D-Luciferin molecule, capable of light emission after reaction with Luciferase.

A sequential assay was performed that consist first of incubating the z-DEVD-(D-Cys) peptide, Gal-CBT, caspase 3 enzyme and  $\beta$ -Gal enzyme in a compatible buffer for 3 hours. The mixture was then added on a Luciferase solution containing all the necessary cofactors for light emission and bioluminescence emission was then measured for 1 h (**Figure S3.3**). Total Luminescence emission over 1 h (AUC) (**Figure 3.6**) was calculated from integration of luminescence in function of the time (**Figure S3.3**). The light emission obtained when the z-DEVD-(D-Cys) peptide and Gal-CBT were incubated simultaneously with both caspase 3 and  $\beta$ -Gal is a lot stronger than the negative controls, when one or both of the enzyme is missing (**Figure 3.6**, grey bars).

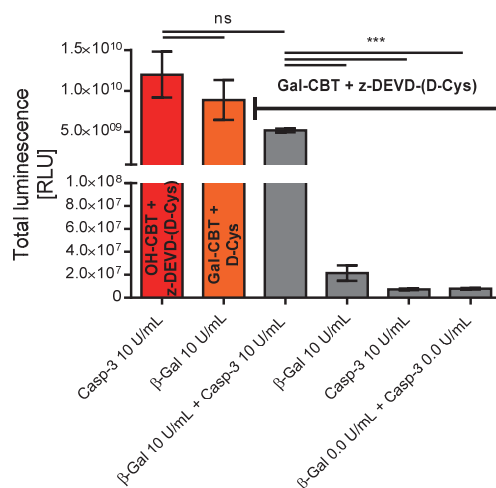


Figure 3.6: Dual enzyme imaging using the split luciferin reaction. Total luminescence emission over 1h (AUC) resulting from Gal-CBT and z-DEVD-(D-Cys) probes (100  $\mu$ M) simultaneous incubation with caspase 3 (10 U/mL) and  $\beta$ -Gal (10 U/mL) enzymes, only  $\beta$ -Gal (10 U/mL), only caspase 3 (10 U/mL) or without any enzymes (grey bars). As a positive control, caspase 3 was incubated with HO-CBT and z-DEVD-(D-Cys) probe or  $\beta$ -Gal with Gal-CBT and D-cysteine. Error bars are  $\pm$  SD of three measurements. Statistical analyses were performed with a two-tailed Student's t test. \*\*\*P < 0.001. ns P > 0.05.

The differences in light emission where both caged components of the split-luciferin are incubated with both enzymes compared to the negative control are important, with an increase in total luminescence ranging from 240 to 700 times. Moreover, the difference with positive control is small and non-significant ( $P > 0.05$ ). It can also be noticed that compared to the positive controls, where Gal-CBT is replaced by free CBT or DEVD-(D-Cys) peptide by free D-Cysteine respectively, light emission is close to the dual imaging light emission. Collectively, these data demonstrate the feasibility of dual enzyme imaging using the split luciferin reaction *in vitro*. Moreover, the good signal to background ratio as well as the intense light emission resulting from simultaneous probe cleavage suggest that this methodology is efficient and selective. Both enzyme have to be present and active for a significant amount of D-luciferin formation.

Of course, this approach does not allow assessment of individual enzyme activity. In a more complex experimental setting, the positive control groups will correspond to measurement of individual activities. Overall, these results suggest that dual caging of the split luciferin reaction can be used for multiple and simultaneous biomolecule activities imaging, with good signal to noise ratio and is promising for potential cell-based and *in vivo* experiments. Moreover, multiple caging could increase the specificity of imaging by introducing several cages selective for different enzymatic markers of the same biological pathway.

For all enzyme/probe pairs tested, light emission was proportional to the enzymatic activity. In particular, split-luciferin probes for caspase 3 and caspase 6 imaging resulted on good signal to noise ratio and excellent cleavage efficiency of the caged D-cysteine probes. Moreover, the split luciferin reaction was efficiently used in *in vitro* enzymatic assay for dual enzyme imaging. Altogether, these data suggest that the Split Luciferin reaction for protease imaging and quantification is versatile and can potentially be applied to a multitude of different protease.

### 3.3 Real time non-invasive imaging of caspase 3/7 activities in living animals

Having already established that the luciferin ligation reaction works efficiently in living transgenic reporter animals, the next step was to establish if this approach was appropriate to quantify the activity of caspase 3/7 in living mice (**Figure 3.7, Figure 3.8**). The focus was set on caspase 3/7 enzymes because a well-characterized mouse model of caspase 3/7 activation was previously reported using the commercially available DEVD-aminoluciferin substrate.<sup>[62,77]</sup> In that study, the activity of caspase 3/7 was induced in the liver of FVB-luc+ mice by administration of lipopolysaccharide (LPS) and D-galactosamine (D-GalN) to the animals, followed by injection of the DEVD-aminoluciferin substrate and



detection of the resulting light production with a CCD camera (**Figure 3.7**).<sup>[62]</sup> D-GalN-sensitized mice treated with LPS were reported to result in fulminant hepatitis, with strong apoptosis generated in liver tissue.<sup>[258]</sup>

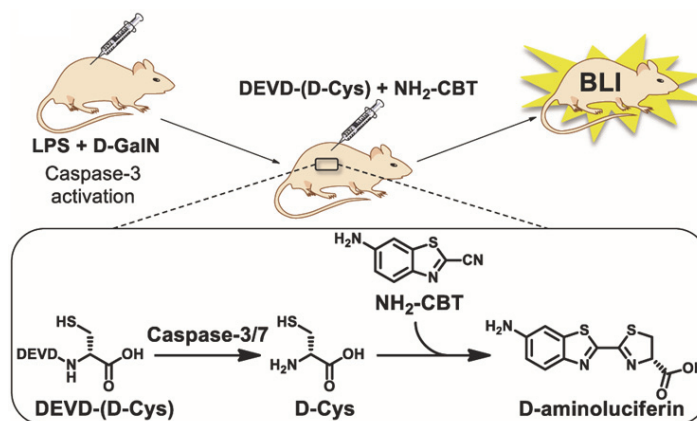


Figure 3.7: Caspase 3/7 activity imaging using luciferin ligation reaction in living transgenic reporter mice. Overall representation of caspase 3 activity imaging with DEVD-(D-Cys) peptide and H<sub>2</sub>N-CBT in a liver failure model *in vivo*.

This previously reported experiment was repeated using a similar mouse strain and DEVD-aminoluciferin substrate as a positive control. FVB-Luc<sup>+</sup> mice were divided into four groups out of which two were injected with equal amounts of D-GalN and LPS followed by either injection of commercial DEVD-aminoluciferin, or a combination of our DEVD-(D-Cys) peptide and H<sub>2</sub>N-CBT. The other two control groups were injected with PBS and a combination of the same imaging reagents. The signals from each D-GalN/LPS treated group were compared to each other and their corresponding PBS controls.

The data shown in Figure 3.8 and Figure 3.9 indicate that a much greater signal was obtained from the two groups of animals treated with D-GalN/LPS in comparison to the control group, treated with PBS. The ratio in average signal observed between the D-GalN/LPS-treated and control groups of mice injected with commercially available substrate was about 3-fold, which was similar to previously reported data<sup>[62]</sup> and statistically significant (P value : 0.00067, **Figure 3.8a**, **Figure 3.9a**).

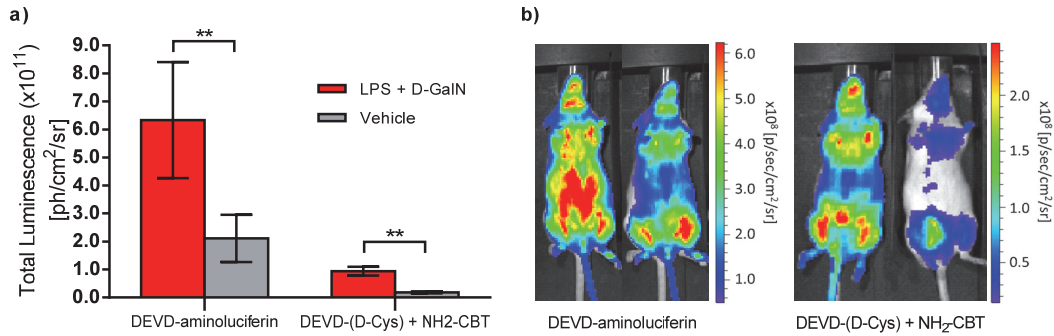


Figure 3.8: Caspase 3/7 activity imaging using luciferin ligation reaction in living transgenic reporter mice. (a) Total luminescence over 1 h from transgenic reporter mice treated with either PBS (control group) or combination of LPS (100  $\mu$ g/kg in 50  $\mu$ L of PBS) and D-GalN (267 mg/kg in 50  $\mu$ L of PBS). Six hours post-treatment, the animals received i.p. injections of either DEVD-aminoluciferin (34 mg/kg in 100  $\mu$ L of PBS) or a combination of DEVD-(D-Cys) peptide (22.6 mg/kg in 100  $\mu$ L of PBS) and H<sub>2</sub>N-CBT (6.8 mg/kg in 20  $\mu$ L of DMSO). Statistical analyses were performed with a two-tailed Student's *t* test. \*\**P* < 0.01 (*n*=8 for DEVD-aminoluciferin groups and *n*=4 for combination of DEVD-(D-Cys) and H<sub>2</sub>N-CBT reagents). Error bars are  $\pm$  SD for 8 and 4 measurements respectively. (b) Representative image of mice, 15 min post-injection of DEVD-aminoluciferin or a combination treatment with DEVD-(D-Cys) and H<sub>2</sub>N-CBT reagents.

At the same time, the ratio between the signals produced from D-GalN/LPS-treated and control groups of mice, injected with combination of DEVD-(D-Cys) peptide and H<sub>2</sub>N-CBT, was about 5.2 fold, higher than the commercial DEVD-aminoluciferin substrate. Importantly, this difference was also statistically significant (*P* value: 0.00258, **Figure 3.8a**, **Figure 3.9b**). This exciting result could arise from proteolytic cleavage being more efficient when it has to cleave between two amino acids. However, when the protease has to cleave between the protease specific sequence and another non-amino acid type of molecule such as D-aminoluciferin, its efficiency might decrease, even when compared with the cleavage at a D-amino acid.

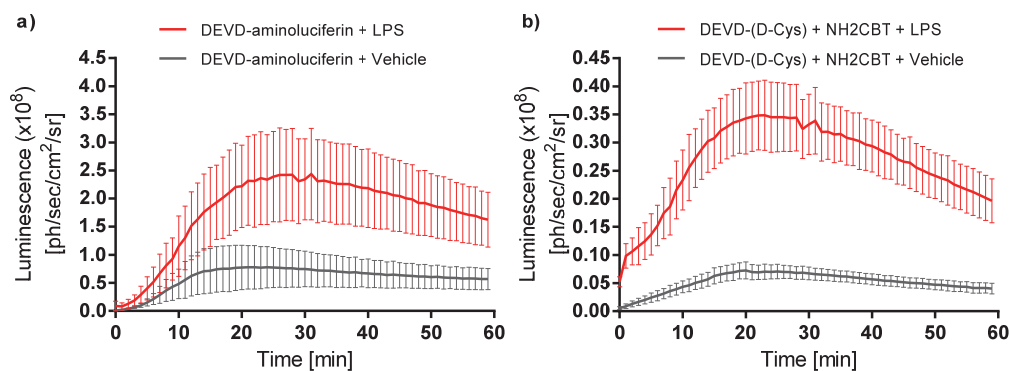


Figure 3.9: Observed luminescence emission as a function of the time from caspase 3/7 selective bioluminescent probes after LPS and D-GalN or vehicle injection of FVB+Luc mice. (a) Luminescence emission in function of the time from i.p. injection of DEVD-aminoluciferin (34 mg/kg in 100  $\mu$ L of PBS, *n*=8) after LPS (100  $\mu$ g/kg in 50  $\mu$ L of PBS) and D-GalN (267 mg/kg in 50  $\mu$ L of PBS) or vehicle (100  $\mu$ L PBS, *n*=8) treatment in FVB-Luc+ mice. Error bars are  $\pm$  SD for eight measurements. (b) Luminescence emission in function of the time from IP injection of DEVD-D-Cys peptide (22.6 mg/kg in 100  $\mu$ L of PBS, *n*=4) and H<sub>2</sub>N-CBT (6.8

mg/kg in 20  $\mu$ L of DMSO, n=4) after LPS and D-GalN or vehicle treatment (n=4) in FVB-luc+ mice. Error bars are  $\pm$  SD for four measurements.

Since the caged split-luciferin approach was successful in a model of hepatic apoptosis, whether this method could be widely applied for studies of caspase 3 and 7 activities in other animal models of apoptosis was investigated. For that, a xenograft animal models, in which human cancer cells were implanted in immune-deficient mice, was used.

In order to establish a successful animal model, two different cancer cell lines were tested for apoptosis induction upon docetaxel treatment, a commonly used anti-cancer drugs for treatment of different type of human cancers, was performed.<sup>[259-262]</sup> Conditions where a majority of cells started to undergo apoptosis upon exposure to the drug were identified for SKOV3-luc-D3 ovarian cancer cells and docetaxel - a drug that has previously been reported to induce apoptosis in this particular cell line (**Figure S3.4**).<sup>[263]</sup> Therefore, this cell line, stably transfected with luciferase, was implanted subcutaneously in nude mice and the tumors were allowed to establish for 6 to 8 weeks.

The animals were then divided in 5 groups (**Figure S3.5a**): two groups injected with commercial DEVD-aminoluciferin substrate with and without docetaxel treatment, two groups that were injected with a combination of DEVD-(D-Cys) peptide and H<sub>2</sub>N-CBT with and without docetaxel treatment, as well as a control group injected with docetaxel and H<sub>2</sub>N-CBT alone. To calibrate for the difference in the tumor size, all the animals were injected with D-luciferin prior and after the treatment with docetaxel or vehicle alone.

The results from the xenograft animal models, in which apoptosis was induced by treatment with docetaxel anticancer drug, were consistent with the ones obtained in the hepatic apoptosis model (P value: 0.0143, **Figure S3.5b**). However, no significant signal to background ratio was observed from the groups of the animals treated with docetaxel or corresponding vehicle followed by injection of commercial DEVD-aminoluciferin substrate (P value: 0.4138). At the same time, 2-fold increase in signal was observed in mice treated with docetaxel in comparison to the vehicle, followed by imaging with combination of DEVD-(D-Cys) peptide and H<sub>2</sub>N-CBT (**Figure S3.5b**).

Together, these results confirm that the combination of D-cysteine caged peptide sequences and H<sub>2</sub>N-CBT represents a valuable tool for quantification and imaging of caspase 3/7 activities directly in living mice. Since BLI is a very sensitive *in vivo* imaging modality, this tool could be used for screening of various proteases activity as well as identification of their new peptide specific substrates *in vitro*. Even though, only the viability of the split luciferin approach for imaging and quantification of caspase 3/7 activity was demonstrated *in vivo*, many other proteases could be studied using this technique.

Based on the results presented here, the split luciferin reaction offers a valuable tool for the development of BLI probes designed for proteases monitoring, both in *in vitro* and *in vivo* set-ups.

### 3.4 Conclusion

Studies of many biological processes in live cells with the help of biocompatible reactions has tremendously advanced our understanding of basic biology.<sup>[133]</sup> However, the great complexity of many human pathologies such as cancer, diabetes, and neurodegenerative diseases requires new tools that would allow studies of biological process on the level of the whole organism. In this chapter, split luciferin based probes for imaging enzymatic activity *in vitro* and in living animals were introduced. The enzymatic activities of multiple caspases as well as thrombin were efficiently imaged in a cell-free and real time set-up. These data demonstrated that the split luciferin approach is efficient and versatile, allowing a greatly improved accessibility of novel bioluminescent probes. It is noteworthy that the synthesis of short peptide sequences with C-terminal D-cysteine can be easily performed with the help of automated peptide synthesis.<sup>[239,240]</sup>

Since caging of D-cysteine can be combined with caging of amino or hydroxy groups on the CBT moiety, this reaction represents a powerful tool where two biological processes may be imaged simultaneously in living mice (**Figure 3.10**). Previously, several probes based on the full luciferin scaffold were reported for sensitive imaging of different biomolecules in live animals, providing a basis for the development of dual imaging approaches.<sup>[57,59,71,84,85,92]</sup> Remarkably, as discussed in chapter 2, the signal produced in cells by the split luciferin reagents was several fold higher than the signal from equimolar amounts of already preformed D-luciferin and D-aminoluciferin (**Figure 2.3**, **Figure 2.4**), providing opportunities for more sensitive imaging of biological processes.

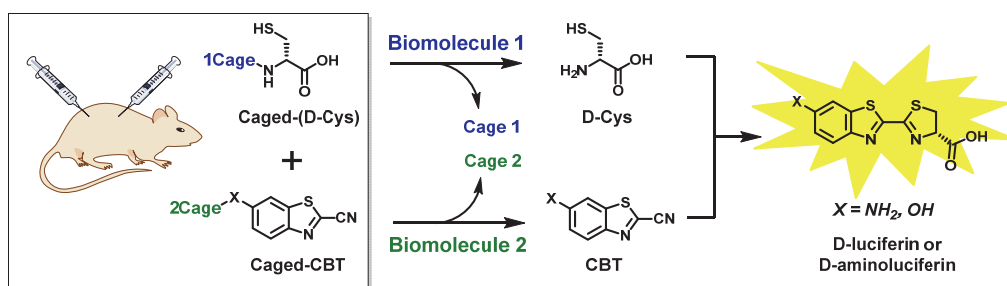


Figure 3.10: Overall representation of the dual imaging concept for luciferin ligation. Both luciferin ligation precursors could be caged as sensors for two different biomolecules. Only when both become uncaged D-luciferin or D-aminoluciferin is formed as the result of split luciferin ligation reaction, allowing the production of light by luciferase.

Furthermore, the properties of the split luciferin reaction are well suited for the development of novel *in vivo* applications. One of them is the real-time imaging of protease activity directly in living animals. In this chapter, successful applications of this technology was demonstrated for real time non-

invasive imaging of caspase 3/7 activity in a hepatic apoptosis model (**Figure 3.6, Figure 3.7, Figure 3.8**) as well as in tumor xenografts upon treatment with docetaxel (**Figure S3.5**). When compared to the commercially available DEVD-aminoluciferin substrate,<sup>[59,71,84,85,92,133,143,234]</sup> the split luciferin ligation reagents had a significantly higher signal to background ratio, demonstrating high potential of this new method for sensitive imaging of apoptosis *in vivo*.

Even though, only the viability of the split luciferin approach for imaging and quantification of caspase 3/7 activity was demonstrated, many other proteases could be immediately studied using this technique. The examples of such proteases and their specific amino acid sequences include caspase 1 (YVAD), caspase 2 (VDVAD) and caspase 12 (ATAD), dipeptidyl peptidase 4 (GP and VP), prostate specific antigen (HSSKLQ) and trypsin (PRNK).<sup>[58,74,77,79,234]</sup> Moreover, this method could also be applied to study wide variety of bacterial, viral and parasite proteases that are essential for the replication and the spread of infectious diseases.<sup>[80]</sup> Examples of these proteases include SARS protease (TSAVLQ), caspase-like (nLPnLD), and trypsin-like (LRR) activity of the proteasome.<sup>[77,81-83]</sup> All of these proteases play a very important role in multiple biological processes and are known to cleave at the end of corresponding specific amino acid sequences. These properties make them ideal candidates for imaging and quantification of their activities in animal models of disease using the split luciferin approach. All together, these results demonstrate high potential of this new *in vivo* ligation strategy for the field of chemical biology and medical research.

**Notes.** Simultaneously to this work, another research group have also been investigating the use of the split luciferin reaction for other bioluminescence applications. Our work was published during the same period.<sup>[230,231]</sup>

### 3.5 Experimental section

**General Material and Methods.** Caged D-cysteine peptides DEVD-(D-Cys) and GGR-(D-Cys) peptides were custom made by Protein and Peptide Chemistry Facility (PPCF) - UNIL (University of Lausanne, Switzerland). Caged D-cysteine peptides z-DEVD-(D-Cys), z-VEID-(D-Cys), z-LETD-(D-Cys) and z-LEHD-(D-Cys) were custom made by Biomatik Corp. The chemicals used in the study were obtained from the following commercial sources and used without further purification. D-cysteine and H<sub>2</sub>N-CBT (Sigma-Aldrich), L-cysteine (Alfa Aesar), HO-CBT (ABCR GmbH), Adenosine 5'-triphosphate disodium salt (ATP, AppliChem GmbH) were used without further purifications. Luciferase (Sigma-Aldrich, prod. number L9506 or SRE0045), human thrombin (Sigma-Aldrich, prod. number T1063) and  $\beta$ -Galactosidase from *Escherichia coli* (Sigma-Aldrich prod. number G4155) were used without further purification. Caspase 3 was kindly provided by Dr. Salvesen at Stanford-Burnham Medical Research Institute,

CA and used for *in vitro* imaging of caspase 3.<sup>[252]</sup> Active human caspase 1, active human caspase 2, active human caspase 3, active human caspase 4, active human caspase 5, active human caspase 6 and active human caspase 9 were purchased from Abcam plc and used for real-time *in vitro* assays. Detailed HRESI-MS measurements were conducted at the EPFL ISIC Mass Spectrometry Service using Micro Mass QTOF Ultima from Waters Corp. Millipore water was used for sample preparation of all the *in vitro*, cellular, and animal assays. Only Luciferase buffer was prepared as following: 60  $\mu\text{g mL}^{-1}$  luciferase in 0.1M Tris-HCl pH=7.4, 2 mM ATP, and 5 mM  $\text{MgSO}_4$ . All *in vitro* and cellular studies were performed in clear bottom black 96 well plates (Becton Dickinson and Co.). Spectramax Gemini (Molecular Devices), IVIS 100 camera (Xenogen) or IVIS Spectrum camera (Xenogen) were used to measure the amount of BLI signal production.

***In vitro* bioluminescent caspase 3 assay with DEVD-(D-Cys) peptide and  $\text{H}_2\text{N-CBT}$ .** Caspase 3 was purified and characterized following the reported procedure (kindly provided by Dr. Salvesen at Stanford University, CA).<sup>[252]</sup> Different concentration solutions of caspase 3 (50, 100 and 200 nM) were prepared in caspase buffer (100 mM HEPES pH 7.4, 0.1% (w/v) CHAPS, 1 mM EDTA, 10 mM DTT, 1% (w/v) sucrose) and were aliquoted in a 96 well-plate (50  $\mu\text{L}$  caspase 3 solution/well). The plate was incubated at 37 °C for 15 min for caspase pre-activation. Following pre-activation, 50  $\mu\text{L}$  of a DEVD-(D-Cys) solution (800  $\mu\text{M}$  in caspase buffer) or 50  $\mu\text{L}$  of a D-Cysteine solution (800  $\mu\text{M}$  in caspase buffer) were added in each well and the plate was incubated at 37 °C for 3 h. After the incubation, 100  $\mu\text{L}$  of a  $\text{H}_2\text{N-CBT}$  solution (400  $\mu\text{M}$  in MeOH) were added to the wells and the plate was incubated for another 1 h at 37°C. Luciferase buffer (60  $\mu\text{g mL}^{-1}$  luciferase in 0.1M Tris-HCl, 2mM ATP, 5 mM  $\text{MgSO}_4$ ) was freshly prepared and aliquoted in a second 96-well plate (115  $\mu\text{L}$ /well). 5  $\mu\text{L}$  of the resulting caspase 3 containing solutions was quickly added to luciferase buffer immediately before reading bioluminescence emission using a Spectramax M5 (Molecular Devices). Bioluminescence signal from the plate was measured with 500 ms integration time for 2 h at 37 °C with 5 min intervals. The observed luminescence over time and the total luminescence collected over the period of 2 h is plotted on **Figure 3.1**.

***In vitro* bioluminescent Thrombin protease assay with GGR-(D-Cys) peptide and amino-CBT.** Solutions of thrombin (20, 10 and 5 Unites) were prepared in thrombin buffer (0.02 M TRIS-HCl pH 8.4, 0.15 M NaCl, 2.5 mM  $\text{CaCl}_2$ ). A solution of Gly-Gly-Arg-(D-Cys) (GGR-(D-Cys)) peptide (400  $\mu\text{M}$ ) was prepared with the different thrombin solutions (20, 10 and 5 Unites) and was incubated at 37°C for 3 h. 20  $\mu\text{L}$  these solutions were added to 20  $\mu\text{L}$  of a  $\text{H}_2\text{N-CBT}$  solution (400  $\mu\text{M}$  in MeOH) and the plate was incubated for another 1 h at rt. A luciferase solution (60  $\mu\text{g/mL}$  luciferase in 0.1 M Tris-HCl, 2 mM ATP, 5 mM  $\text{MgSO}_4$ ) was prepared and aliquoted in a second 96-well plate (115  $\mu\text{L}$ /well). 5  $\mu\text{L}$

of the previously made thrombin, GGR-(D-Cys) and H<sub>2</sub>N-CBT mixture were added on the luciferase solutions immediately before reading bioluminescence emission using a Spectramax Gemini (Molecular Devices, Sunnyvale, CA). Bioluminescence images were taken every 13 s for 2 h at 37 °C.

***In vitro* real time imaging of caspases activities.** Active human caspase 3, active human caspase 6, active human caspase 8 and active human caspase 9 were purchased from Abcam plc and used without further purification. 1 U/μL stock solutions of caspases were prepared in PBS containing 15% glycerol. From the caspase stock solution, the 0.25, 0.125, 0.025, 0.0125, 0.0025 and 0 U/μL dilution were prepared in PBS containing 15% glycerol. Stock solutions of HO-CBT, z-DEVD-(D-Cys) peptide, z-VEID-(D-Cys) peptide, z-LETD-(D-Cys) peptide, z-LEHD-(D-Cys) peptide (10 mM in DMSO) as well as D-cystein stock solution (10 mM in PBS) were prepared. A 60 μg/mL luciferase enzyme solution was prepared in caspase buffer (50 mM HEPES, pH 7.2, 50 mM NaCl, 0.1 % CHAPS, 10 mM EDTA, 5% Glycerol, 10 mM DTT) and supplemented with 2 mM ATP and 5 mM MgSO<sub>4</sub>. In a black 96-well plate, 94 μL per well of the luciferase solution was added. 4 μL per well of the different caspase solutions were added in order to obtain the following final caspase concentrations: 4, 1, 0.5, 0.1, 0.05, 0.01 or 0 U of caspase per well (100 μL). This was followed by the addition of 1 μL of HO-CBT solution in the wells. Finally, 1 μL of the peptide solution or D-cysteine solution was added in the wells containing the corresponding caspase. The plate was then immediately placed in the plate reader and BL acquisition was started. Bioluminescence measurements were performed with 1 min interval on a Tecan Infinite M1000 (Tecan Austria GmbH) plate reader for 3 h at 37°C.

**Colorimetric assay of caspases activities.** Active human caspase 3, active human caspase 8 and active human caspase 9 were purchased from Abcam plc and used without further purification. 1 U/μL stock solutions of caspases were prepared in PBS containing 15% glycerol. Stock solutions of Ac-DEVD-pNA, Ac-LETD-pNA peptide and Ac-LEHD-pNA colorimetric probes (10 mM in DMSO) were prepared. In a transparent 96-well plate, 98 μL of caspase buffer (50 mM HEPES, pH 7.2, 50 mM NaCl, 0.1 % CHAPS, 10 mM EDTA, 5% Glycerol, 10 mM DTT) was added in the wells. 1 μL of the colorimetric probe or pure DMSO was add, followed by the addition of 1 μL of corresponding caspase stock solution or 1 μL of PBS containing 15% glycerol. Immediately after caspase addition, absorbance was measured at 405 nm during 135 min at 15 min interval.

***In vitro* real time cross-reactivity of caspase probes with different caspases.** Active human caspase 1, active human caspase 2, active human caspase 3, active human caspase 4, active human caspase 5, active human caspase 6 and active human caspase 9 were purchased from Abcam plc and used without further purification. 1 U/μL stock solutions of caspases were prepared in PBS containing



15% glycerol. Stock solutions of HO-CBT, z-DEVD-(D-Cys) peptide, z-VEID-(D-Cys) peptide, z-LETD-(D-Cys) peptide and z-LEHD-(D-Cys) peptide (10 mM in DMSO) were prepared. A 60 µg/mL luciferase enzyme solution was prepared in caspase buffer (50 mM HEPES, pH 7.2, 50 mM NaCl, 0.1 % CHAPS, 10 mM EDTA, 5% Glycerol, 10 mM DTT) and supplemented with 2 mM ATP and 5 mM MgSO<sub>4</sub>. In a black 96-well plate, 97 µL per well of the luciferase solution were added. 1 µL per well of the different caspase stock solutions were added. This was followed by the addition of 1 µL of HO-CBT solution in the wells. Finally, 1 µL of the peptide solutions were added in the wells. The plate was then immediately placed in the plate reader and acquisition was started. Bioluminescence measurements were performed on a Tecan Infinite M1000 (Tecan Austria GmbH) plate reader for 3 h at 37°C with 2 min interval.

**Synthesis of 6-(((2S,3R,4S,5R,6R)-3,4,5-trihydroxy-6-(hydroxymethyl)tetrahydro-2H-pyran-2-yl)oxy)benzo[d]thiazole-2-carbonitrile (Cyanobenzothiazolyl β-D-Galactopyranoside, Gal-CBT) (by Dr. Jens Frigell).** Previous reports claimed that basic deacetylation works poorly due to the electrophilic nitrile of the cyanobenzothiazole.<sup>[264]</sup> After experiencing similar troubles, an acidic deacetylation protocol was developed.

2-Cyano-6-(2,3,4,6-tetra-O-acetyl-β-D-Galactopyranosyloxy)benzothiazole (100 mg, 0.197 mmol) was synthesized according to the reported procedure and was then dissolved in CH<sub>2</sub>Cl<sub>2</sub> (5 mL).<sup>[264]</sup> Conc. H<sub>2</sub>SO<sub>4</sub> (0.5 mL) was diluted in MeOH (5 mL) at 0 °C and slowly added to the CH<sub>2</sub>Cl<sub>2</sub> solution. Over 4 h, steady formation of product was seen by LCMS analysis, but also an increase of formation of cyanobenzothiazole (by-product) and the reactions was carefully quenched at 0 °C using NH<sub>4</sub>OH (25%) under rigorous stirring, trying to avoid any yellow/green coloration of the reactions, which indicated by-product formation. This could be avoided by keeping pH at 6 or lower. The white slurry was then diluted with 10 mL 1:1 CH<sub>2</sub>Cl<sub>2</sub>:MeOH and concentrated *in vacuo* (co-evaporating with toluene, 5 mL) resulting in a white solid. 2-Propanol (10 mL) was added and the suspension was sonicated to dissolve all product. The remaining white solid (salts) were filtered off. The clear 2-propanol solution is then concentrated *in vacuo* to give a white solid. The crude material was purified by column chromatography (CHCl<sub>3</sub>:MeOH 8:1) to give Cyanobenzothiazolyl β-D-Galactopyranoside (66.3 mg, 99%) as a white solid, which was lyophilized. <sup>1</sup>H NMR (400 MHz, D<sub>2</sub>O) δ 7.98 (d, *i* = 9.1 Hz, 1H), 7.71 (d, *J* = 2.5 Hz, 1H), 7.39 (dd, *J* = 9.2, 2.5 Hz, 1H), 5.14 (d, *J* = 7.5 Hz, 1H), 4.04 (dd, *J* = 3.2, 1.0 Hz, 1H), 3.97 - 3.79 (m, 5H). <sup>13</sup>C NMR (101 MHz, D<sub>2</sub>O) δ 157.1 (s), 146.8 (s), 137.0(s), 135.6 (s), 125.0 (d), 119.4 (d), 112.9 (s), 107.5 (d), 100.8 (d), 75.6 (d), 72.4 (d), 70.4 (d), 68.4 (d), 60.7 (t). HRMS calcd for C<sub>14</sub>H<sub>14</sub>N<sub>2</sub>O<sub>6</sub>S [MH<sup>+</sup>] 339.0651, found 339.0657.



***In vitro* simultaneous imaging of caspase 3 and  $\beta$ -galactosidase using the split luciferin reaction.** Active human caspase 3 enzyme (Abcam plc) and  $\beta$ -Galactosidase (Sigma-Aldrich) were used without further purification. 1 U/ $\mu$ L stock solution of caspase 3 was prepared in 1 U/ $\mu$ L stock solution of PBS containing 15% glycerol. 1 U/ $\mu$ L stock solution of  $\beta$ -galactosidase was prepared in 1 mM TRIS pH 7.5 containing 1 mM  $MgCl_2$  and 50% glycerol. Stock solutions of HO-CBT, z-DEVD-(DCys) peptide and Gal-CBT (10 mM in DMSO) as well as D-cysteine stock solution (10 mM in PBS) were prepared.

In a 96-well plate, 95  $\mu$ L of reaction buffer (50 mM HEPES, pH 7.2, 150 mM NaCl, 0.1 % CHAPS, 10 mM EDTA, 5% Glycerol, 10 mM DTT) were added. 1  $\mu$ L of Gal-CBT stock solution or HO-CBT stock solution were added, as well as 1  $\mu$ L of z-DEVD-(D-Cys) stock solution or D-cysteine stock solution. 1  $\mu$ L of DMSO was added in the wells where D-cysteine was added and 1  $\mu$ L of PBS was added in all the other wells. These solutions were supplemented with either 1  $\mu$ L of  $\beta$ -galactosidase stock solution or 1  $\mu$ L of caspase 3 stock solution or with both enzyme stock solutions. The plate was then incubated at 37 °C protected from light.

In another black 96-well plate, 80  $\mu$ L of a 60  $\mu$ g/mL luciferase enzyme solution in caspase buffer (50 mM HEPES, pH 7.2, 50 mM NaCl, 0.1 % CHAPS, 10 mM EDTA, 5% Glycerol, 10 mM DTT) and supplemented with 2 mM ATP and 5 mM  $MgSO_4$  were aliquoted. Finally, using a multichannel micropipette, 20  $\mu$ L of the different enzymes solutions were transferred to the luciferase containing 96-well plate. The plate was then immediately placed in the plate reader and luminescence measurement was started. Bioluminescence measurements were performed approx. every minutes on a Tecan Infinite M1000 (Tecan Austria GmbH) plate reader for 3 h at 37°C.

**Animals.** FVB-luc<sup>+</sup> transgenic animals<sup>[217,218]</sup> (full abbreviation: FVB-Tg(CAG-luc,-GFP)L2G85Chco/J) mice were kindly provided by the laboratory of Prof. Christopher Contag at Stanford University, rederived at UC Davis, and bred at UC Berkeley. The breeding colony was housed in groups of 4-5 mice according to their age and gender with free access to food and water at 22 °C with regular light-dark cycle. All studies were approved and performed according to the guidelines of the Animal Care and Use Committee of the University of California, Berkeley.

Experiments in a mouse model of subcutaneous cancer were carried out in strict accordance to the Swiss regulation on animal experimentation and the protocol (VD2363) was approved by the authority of the Canton Vaud, Switzerland (EXPANIM (Expérience sur animaux)–SCAV, Département de la sécurité et de l'environnement, Service de la consommation et des affaires vétérinaires). Swiss nude (swiss nu/nu) mice were obtained from Charles River Labs and were maintained at the EPFL UDP

animal facility under pathogen free conditions and group housed in ventilated cages at 22°C with regular light-dark cycle.

**Real time non-invasive imaging of caspase 3/7 activities in FVB-luc+ mice.** Female FVB-luc+ mice (4 mice per group), were anesthetized with isoflurane and injected IP with either lipopolysaccharides (LPS) purchased from Sigma-Aldrich at concentrations of 100  $\mu\text{g kg}^{-1}$  in 50  $\mu\text{L}$  of PBS followed by injections of D-(+)-Galactosamine hydrochloride (D-GalN) obtained from AppliChem GmbH at concentrations of 267  $\text{mg kg}^{-1}$  in 50  $\mu\text{L}$  of PBS. The control group of mice was injected with 100  $\mu\text{L}$  of PBS (vehicle). Six hours after injection of an LPS/D-GalN combination or vehicle (PBS), mice were treated IP with either DEVD-(D-Cys) peptide (22.6  $\text{mg kg}^{-1}$  in 100  $\mu\text{L}$  of PBS) plus 6-Amino-2-cyanobenzothiazole ( $\text{H}_2\text{N-CBT}$ , 6.8  $\text{mg kg}^{-1}$  in 20  $\mu\text{L}$  of DMSO) or DEVD-aminoluciferin substrate (34  $\text{mg kg}^{-1}$  in 100  $\mu\text{L}$  of PBS) and imaged. A time period of 10 min between injections of DEVD-D-Cys and  $\text{H}_2\text{N-CBT}$  was respected. The mice were imaged using IVIS Spectrum and bioluminescence images were obtained over 1 h at 37°C with 1 min interval. The BLI signal was quantified using region-of-interest (ROI) analysis available on Living Image software 4.2 (Caliper Life Sciences).

**Induction of apoptosis in SKOV3-Luc-D3 ovarian cancer cells by docetaxel treatment.** SKOV-3-Luc-D3 cells (Caliper Life Sciences, Hopkinton, MA) were cultured in McCoy's 5A (modified) medium that contains 10% FBS, 1% GlutaMAX and 1% Penicillin/Streptomycin mixture. Cells were passed and plated in 10 cm petri dishes. Once the cells were 90% confluent, medium was replaced by McCoy's 5A (modified) medium that contains 10% FBS, 1% GlutaMAX, 1% Penicillin/Streptomycin mixture and 10  $\mu\text{M}$  of docetaxel (prepared from a stock solution of 100 $\mu\text{M}$  in EtOH) were added to each well. After a 48 h of incubation, cells were stained either with propidium Iodide, FAM-DEVD-FMK (Vybrant® FAM caspase 8 Assay Kit - for Flow Cytometry, Life Technologies Corp.) or both and flow cytometry assay was performed using a BD SORP LSR II (Becton Dickinson and Company, Franklin Lakes, NJ). Results are presented in Figure S3.4.

**Real time non-invasive imaging of caspase 3/7 activities in tumor xenograft models.** This experiment was designed according to the work published by Hickson et al.<sup>[60]</sup> In the right flank of swiss nude mice, aged 5–6 months,  $4 \times 10^6$  SKOV3-luc-D3 cells were inoculated subcutaneously in a 1:1 mixture of Matrigel and growth medium. Tumor was allowed to establish to an appropriate volume according to Caliper Life Sciences protocol, supplied together with cell line (Xenogen Corporation, Alameda, CA). Animals were then size matched into treatment groups and were injected IP with Docetaxel (60 $\text{mg/kg}$  in 200 $\mu\text{L}$  of a 1:1:3 mixtures tween80/EtOH/saline solution) or vehicle (1:1:3 mixtures tween80/EtOH/saline solution)). 24 h after Docetaxel or vehicle treatment, mice were anesthetized

with isoflurane and injected IP with DEVD-(D-Cys) peptide (166.2 mg/kg in 100  $\mu$ L of PBS) plus H<sub>2</sub>N-CBT (50.24 mg/kg in 40  $\mu$ L of DMSO) or DEVD-aminoluciferin (250 mg/kg in 100  $\mu$ L of PBS) and imaged. A time period of 10 min between injection of DEVD-D-Cys and H<sub>2</sub>N-CBT was respected. Bioluminescence images were acquired over 1.5 h at 37 °C with 1 min interval. The BLI signal was quantified using region-of-interest (ROI) analysis available on Living Image software 4.2 (Caliper Life Sciences). Observed BLI signal was collected from each animal every minute and the total luminescence produced over the course of 1.5 h was calculated (abbreviated as TL-1). 12 h after the first imaging session, mice were imaged again after IP injection of D-luciferin sodium salt (91.3 mg/kg in 100  $\mu$ L of PBS) in order to normalize the caspase 3/7 imaging signal in function of the cancer cell number, because all the animals had different tumor sizes. Observed BLI signal was collected from each animal and the total luminescence produced over the course of 1.5 h was calculated (abbreviated as TL-2). The Logarithmic (Log) values of the integrated total luminescence resulting from injection of the caspase 3/7 probe and D-luciferin (TL-1 and TL-2 respectively) were calculated in order to obtain a linear scale. For every mouse, the Log value of the caspase 3/7 selective probe TL-1 was subtracted by the D-luciferin TL-2 (Plotted Value (**Figure S3.5**) = Log (TL-1) - Log (TL-2)). Therefore, the bigger are the values, the smaller is the normalized light emission and the lower is the caspase 3/7 activity. Statistical analyses were performed with a two-tailed Student's t test. \*P < 0.05 (DEVD-(D-Cys) + H<sub>2</sub>N-CBT: n=9, DEVD-aminoluciferin: n=4) and error bars are  $\pm$  SD.

### 3.6 Supplementary figures

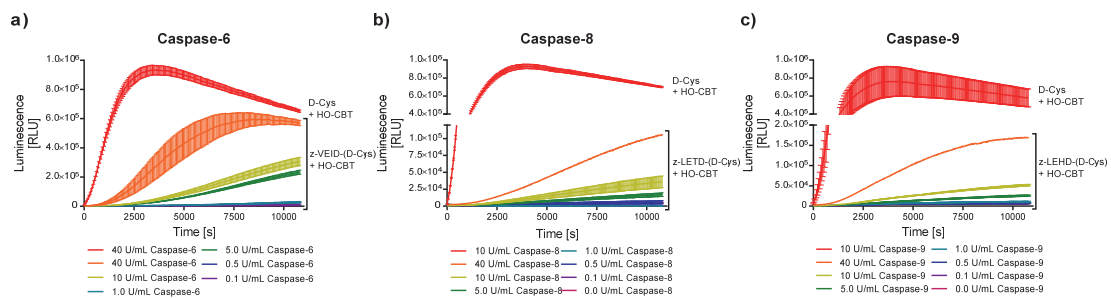


Figure S3.1: *In vitro* enzymatic assay of caspase 6, caspase 8 and caspase 9 activities imaging with respectively z-VEID-(D-Cys), z-LETD-(D-Cys) or z-LEHD-(D-Cys) peptide and HO-CBT. (a) Luminescent signal in function of the time resulting from HO-CBT (100  $\mu$ M) and z-VEID-(D-Cys) peptide or D-cysteine (100  $\mu$ M) incubation in presence of increasing caspase 6 concentrations (0, 0.1, 0.5, 1.0, 5.0, 10 and 40 units/mL) and luciferase enzyme over 3 h at 37 °C. (b) Similar results for caspase 8 enzyme using z-LETD-(D-Cys) peptide. (c) Similar results for caspase 9 enzyme using z-LEHD-(D-Cys) peptide. Error bars are  $\pm$  SD of three measurements.

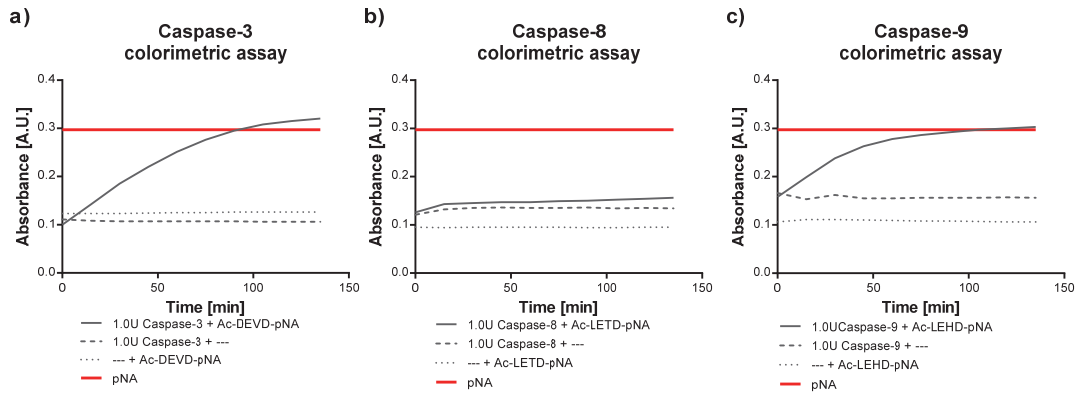


Figure S3.2: Colorimetric assay of caspases activities. (a) Absorbance measured at 405 nm in function of the time during Ac-DEVD-pNA incubation with or without 1 U of caspase 3 enzyme in caspase buffer. (b) Absorbance measured at 405 nm in function of the time during Ac-LETD-pNA incubation with or without 1 U of caspase 8 enzyme in caspase buffer. (c) Absorbance measured at 405 nm in function of the time during Ac-LEHD-pNA incubation with or without 1 U of caspase 9 enzyme in caspase buffer.

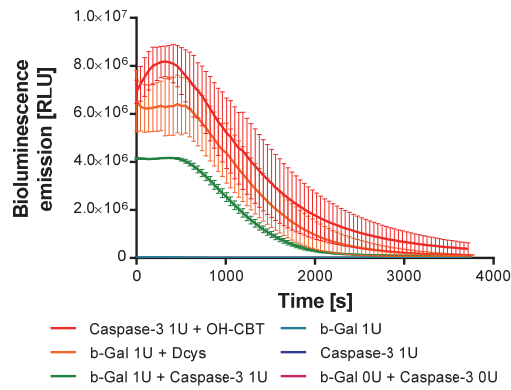


Figure S3.3: Dual enzyme imaging using the split luciferin reaction. Luminescence emission in function of the time resulting from Gal-CBT and z-DEVD-(D-Cys) probes simultaneous incubation with caspase 3 and  $\beta$ -Gal enzymes, only  $\beta$ -Gal, only caspase 3 or without any enzymes (grey bars). As control, caspase 3 was incubated with HO-CBT and z-DEVD-(D-Cys) probe or  $\beta$ -Gal with Gal-CBT and D-cysteine. Error bars are  $\pm$  SD of three measurements.

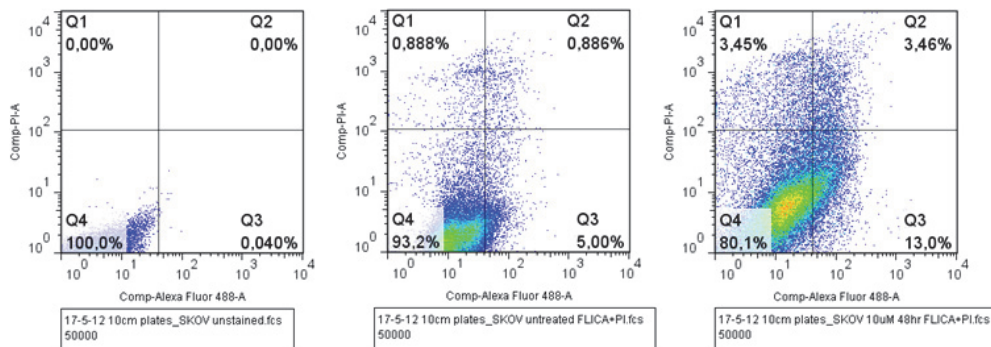


Figure S3.4: Flow cytometry data with a caspase 3/7 activation assay (FAM-DEVD-FMK - Propidium Iodide) on SKOV3 cells lines, 48 h post docetaxel incubations at 10  $\mu$ M concentration.

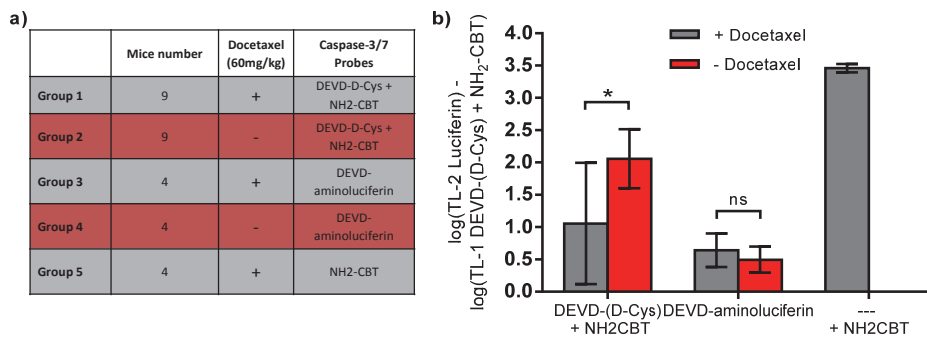
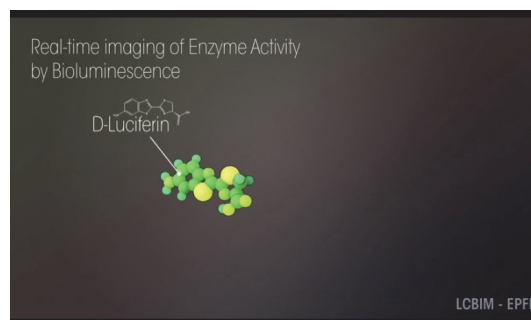


Figure S3.5: Docetaxel treatment on subcutaneous SKOV3-Luc-D3 xenografts model in nude mice for caspase 3/7 activation imaging. (a) Description of experimental groups of animals including number of mice per groups, docetaxel or vehicle treatment and the type of caspase 3/7 selective bioluminescent probes used for imaging. (b) Swiss nude mice (NU(lco)-Foxn1nu (outbred), Charles River Labs) bearing SKOV3-luc-D3 subcutaneous tumor were injected IP with Docetaxel (60 mg/kg in 200  $\mu$ L of a 1:1:3 mixture tween 80/EtOH/saline solution) or only vehicle. 24 h post injection mice were treated IP with either a combination of DEVD-(D-Cys) (166.2 mg/kg in 100  $\mu$ L of PBS) and H2N-CBT (50.24 mg/kg in 40  $\mu$ L of DMSO), DEVD-aminoluciferin (250 mg/kg in 100  $\mu$ L of PBS), or H2N-CBT only (50.24 mg/kg in 40  $\mu$ L of DMSO). A 10 min time period was respected between inj. of DEVD-(D-Cys) and H2N-CBT. The animals were imaged for the period of 1.5 h and the total BLI signal was calculated (TL-1). 12 h after the imaging session, mice were imaged again after IP injection of D-luciferin sodium salt (91.3 mg/kg in 100  $\mu$ L of PBS) in order to normalize the caspase 3/7 imaging signal in function of the cancer cell number. Bioluminescence images were taken every minute during 1.5 h (TL-2). The data shown represent the difference between D-luciferin imaging (proportional to the tumor size) and DEVD-D-Cys and H2N-CBT imaging (proportional to tumor size and caspase 3/7 activation level) on a linear scale. For every mouse, the Log value of the Caspase 3/7 selective probe TL-1 was subtracted by the Log value of D-luciferin TL-2 (Plotted Value = Log (TL-1) - Log (TL-2)). Therefore, the bigger are the values, the smaller is the normalized light emission and the lower is the caspase 3/7 activity. Statistical analyses were performed with a two-tailed Student's t test. \*P < 0.05 (DEVD-(D-Cys) + H2N-CBT: n=9, DEVD-aminoluciferin: n=4) and error bars are  $\pm$  SD.



Movie S3.1: Imaging caspase activity with the split luciferin reaction. First the principle of bioluminescence imaging is depicted. the oxidation of D-aminoluciferin by firefly luciferase enzyme, a process that generates light. In a second sequence, the principle of "classical" caged luciferin is depicted with a DEVD-aminoluciferin probe, that get selectively cleaved by caspase 3 enzyme to release a free amino-D-luciferin molecule, capable of light emission. Then, the split luciferin reaction is animated, showing D-cysteine and H2N-CBT reacting selectively with each other *in vivo* to generate D-aminoluciferin. Finally, the last sequence depicts the caspase 3 dependent release of free D-cysteine from the caspase 3/7 peptide substrate DEVD-(D-Cys) that allows selective reaction with H2N-CBT *in vivo* to form amino-D-luciferin with subsequent light emission from luciferase.<sup>[217,230]</sup>



## Chapter 4 Bioluminescence Imaging of Neutrophil Elastase Activity Using the Split Luciferin Reaction

Neutrophil Elastase (NE), also known as leukocyte elastase, is a chymotrypsin-like serine protease present in high concentration in neutrophil azurophil granules. These granules also contain multiple microbicidal products such as cationic peptides or other proteolytic enzymes such as Proteinase 3 (PR3), Matrix Metalloproteinase 9 and Cathepsin G. Upon activation, neutrophils degranulate, releasing the contents of azurophil granules.<sup>[265,266]</sup> NE displays proteolytic activity and is capable of cleaving elastin and multiple matrix proteins such as fibronectin, laminin or type IV collagen and contributes to defence mechanisms against microbial pathogens. On the other hand, when NE is released in an uncontrolled manner, its proteolytic activity damages healthy tissues leading to organ injury. NE is implicated in a wide variety of diseases such as acute lung injury (ALI), acute respiratory distress syndrome (ARDS), cystic fibrosis (CF), non-small cell lung cancer in addition to other pathological lung conditions. NE activity has also been linked to many other diseases such as chronic wounds or rheumatoid arthritis.<sup>[266-270]</sup>

Imaging NE could have favourable impact on different clinical applications such as diagnosis, monitoring efficiency of a therapy, determining the disease stage or location of neutrophil-mediated inflammation sites.<sup>[265,271,272]</sup> Due to its implication in numerous pathological conditions, non-invasive imaging probes for identification and quantification of NE activity have been developed using different imaging modalities and used for several applications, from *in vitro* enzymatic assay, to *in vivo* imaging on animals models of human pathologies.

Traditionally, NE activity is quantified using colorimetric or fluorogenic synthetic peptide substrates such as N-Methoxysuccinyl-Ala-Ala-Pro-Val-*para*-Nitroanilide (AAPV-pNA) probe or its fluorescent analogues.<sup>[273-275]</sup> These compounds have been extensively used but have only limited applicability

for cell-based or *in vivo* experiments. Chromogenic substrates based on conjugation of a peptide functionalized on the C-terminal with a 4-nitroanilide moiety suffer from poor sensitivity. The corresponding fluorogenic based probes gain in sensitivity but the substrate sequence cannot be modulated with an amino acid after the cleavage site (in direction of the C-terminal) and this approach is limited to certain fluorophores that are not well suited for *in vivo* applications. Different fluorogenic probes based on intramolecular quenched fluorescence have been developed for imaging and measuring NE activity. Förster resonance energy transfer (FRET) based probes were constructed with a fluorescent moiety (i.e. *ortho*-aminobenzoyl, 7-methoxycoumarin-4-yl) positioned on the N-terminal of the peptide substrate and quenched by a fluorescent quencher (i.e. ethylenediamine, N-3-(2,4,-dinitrophenyl)-L-2,3-diaminopropionyl) on the C-terminal. After cleavage of the specific peptide substrate by the enzyme of interest, the quencher is released and the fluorescent group is activated. This methodology was used for identification of specific substrates for NE or PR3 and further used for measuring their respective activities in purified enzyme or cell-based experiments.<sup>[276-280]</sup>

Similar strategies have also been used for the development of quenched fluorescent probes suitable for non-invasive *in vivo* imaging. Probes for fluorescent NE imaging consist of two near-infrared (NIR) fluorescent moieties covalently attached to both N- and C-terminus of a NE specific amino acid sequence (NE 680 FAST, PerkinElmer).<sup>[267]</sup> Using this construct, non-invasive *in vivo* imaging and quantification of NE activity were performed in a mouse model of ALI. Moreover, localization of active NE *ex vivo* in lung sections was confirmed by fluorescence microscopy.<sup>[267]</sup> Furthermore, a significant increase of active NE, in intradermal tumors of mice subjected to photo-dynamic therapy, have been reported *in vivo* using the NE680 FAST probe.<sup>[281]</sup> The same fluorogenic probe was also used for imaging NE activity in a colorectal cancer xenograft model in living mice<sup>[282]</sup> as well as *ex vivo* imaging and quantification of NE activity in white adipose tissue and liver tissue of mice fed a high fat diet.<sup>[283]</sup>

In addition to the optical fluorescence imaging of NE, probes intended for nuclear medicine imaging have been reported for *in vivo* applications. For example, an aptamer inhibitor of NE was radio-labelled with <sup>99m</sup>Tc and used for diagnostic imaging of inflammation in a rat immune reaction model (reverse passive Arthus reaction).<sup>[284]</sup> Furthermore, a NE peptide inhibitor was labelled with <sup>99m</sup>Tc and used for imaging infection and neutrophil-mediated inflammation in monkeys.<sup>[285]</sup>

To date, the probes reported for *in vivo* imaging of NE activity are either based on fluorescence or nuclear medicine imaging modalities. As fluorescence imaging is limited by tissue auto-fluorescence and poor tissue penetration, radioactive tracers suffer from other constraints, as they are dependent



on ionizing radiations that, with the associated costs, synthetic complexity, short half-life and radioactive compounds handling, limit their utilization.<sup>[286,287]</sup> Bioluminescence imaging (BLI) represents a good option for pre-clinical imaging, offering high sensitivity, relatively low cost and ease of implementation, as long as the model under study is expressing luciferase.<sup>[6,114,209]</sup>

Herein, the development of a novel probe for BLI of NE based on the split luciferin reaction is described. To date, no bioluminescent probes for NE imaging have been reported. A pentapeptide containing a D-cysteine residue on the C-terminal was designed, synthesized and further validated for NE imaging using enzymatic assay *in vitro*, primary cell culture of neutrophils and *in vivo* using a model of ALI. Importantly, the *in vivo* experiments demonstrated that the probe could be used for real-time non-invasive imaging and quantification of NE activity in murine model of acute lung inflammation.

## 4.1 Probe design

Since caspase 3/7 activity was successfully imaged using the split luciferin reaction, a similar approach was applied for the development of a NE specific probe. A NE peptide substrate was used to mask the 1,2-aminothiol group of the D-cysteine moiety, blocking its ability to react with CBT. Different NE specific substrates have been reported and used for determining substrate affinity or activity detection of the NE enzyme. This caging strategy requires the D-cysteine amino acid to be placed right after the cleavage site, reducing the choice of amino acid sequence for the design of the NE peptide substrate. Both colorimetric and fluorometric compounds have been reported and used for substrate specificity investigation of NE, revealing that the Ala-Ala-Pro-Val (AAPV) amino acid sequence is one of the most potent substrates when the P<sub>1</sub>' is occupied by a synthetic group.<sup>[273,274]</sup> Moreover, neutrophil PR3 is the closest related protease to NE. These proteases share 54% homology, both are contained in azurophil granules, excreted by activated neutrophils and finally both share substrate preference for a valine residue in the P1 position.<sup>[288]</sup> Without modifying the P' positions, the majority of NE substrate are also, to some extent, cleaved by PR3 protease.<sup>[278]</sup> Nevertheless, Kasperkiewicz et al. reported a synthetic NE substrate composed of unnatural amino acid residues, that is more specific for NE and is cleaved 900-fold more efficiently compared to PR3.<sup>[289]</sup>

To develop a probe for the BLI of NE, investigation started with the AAPV amino acid sequence which is the most commonly used substrate of NE. N-terminal acetylated version of the peptide substrate was synthesized to prevent aminopeptidase cleavage and increase its stability and half-life in serum.<sup>[290-292]</sup> The probe Ac-L(Ala-Ala-Pro-Val)-D-(Cys)-OH (Ac-AAPV-(D-Cys)) was synthesized using Fmoc solid phase peptide synthesis followed by acetate capping and HPLC purification. Upon cleavage of the probe by NE, a free D-cysteine moiety is released, which can subsequently react with 6-hydroxy-

2-cyanobenzothiazole (CBT) moiety, forming D-luciferin molecules. The latter is oxidized by luciferase resulting in light emission. Therefore, D-luciferin formation is dependent on NE activity and the subsequent BL light emission is proportional to its activity (**Figure 4.1**).

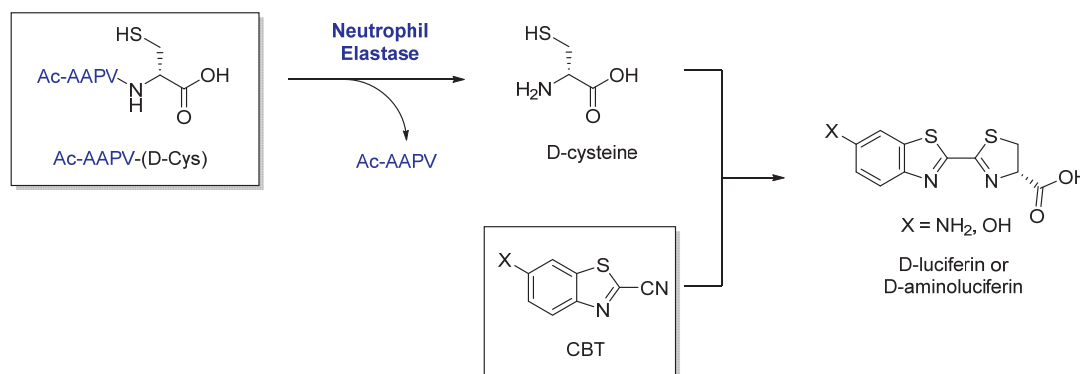


Figure 4.1: Imaging NE activity using a caged split luciferin probe. Overall representation of Ac-AAPV-(D-Cys) peptide probe cleavage by NE and further reaction of the released D-cysteine molecule with HO-CBT or H<sub>2</sub>N-CBT to form the corresponding luciferin molecule.

## 4.2 *In vitro* real time imaging of neutrophil elastase activity in enzymatic assays

The efficiency and specificity of the Ac-AAPV-(D-Cys) probe cleavage was first tested with native purified human neutrophil elastase (HNE) by real-time bioluminescence imaging. Different concentration of HNE were incubated with the Ac-AAPV-(D-Cys) probe, in the presence of HO-CBT and luciferase. To confirm the specificity of D-cysteine release by HNE, these experiments were performed in the presence and absence of sivelestat sodium salt, a specific competitive inhibitor of NE.<sup>[267,293]</sup> The Ac-AAPV-(D-Cys) peptide was efficiently cleaved by HNE. When the peptide was incubated with increasing HNE concentrations, measurements resulted in a dose-dependent light emission (**Figure 4.2**). The higher the concentration of HNE, the greater the light emission from the probe and the signal generated by a concentration of 0.01 µg/mL of HNE is still significantly above light emission of the negative control without HNE ( $P = 0.0254$ ). Moreover, a control experiment was performed where the peptide probe was replaced by D-cysteine (caged-less probe) and incubated with the highest concentration of HNE (**Figure 4.2b**). Since the D-cysteine and peptide concentrations were equivalent, the total luminescence resulting from D-cysteine and HO-CBT control is equivalent to 100% cleavage of the Ac-AAPV-(D-Cys) peptide by the protease and it can be concluded that the luminescence generated from 0.5 µg/mL of HNE cleaves approximately 34 % of the peptide probe over 3h (**Figure 4.2b**).

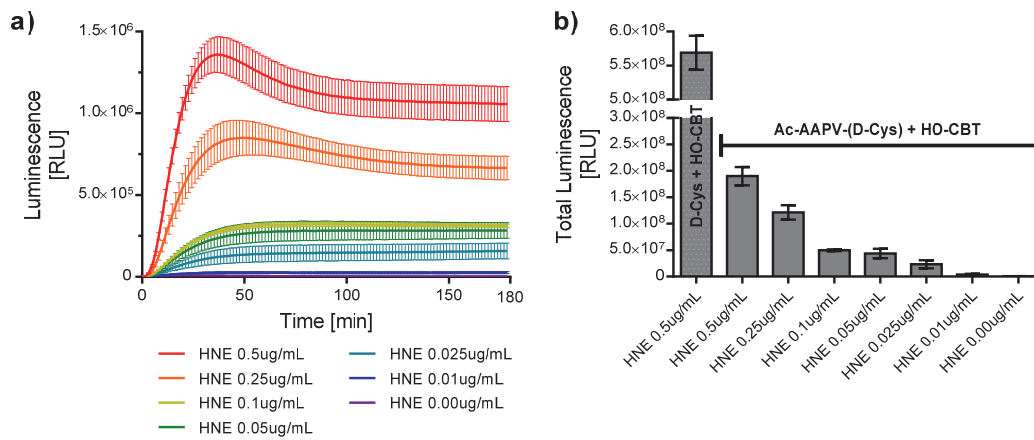


Figure 4.2: *In vitro* enzymatic assay of HNE activity imaging with Ac-AAPV-(D-Cys) and HO-CBT split luciferin probe. (a) luminescent signal over 180 min following incubation of HO-CBT (100  $\mu\text{M}$ ), Ac-AAPV-(D-Cys) peptide (100  $\mu\text{M}$ ) with increasing concentrations of HNE (0, 0.01, 0.025, 0.05, 0.1, 0.25 and 0.5  $\mu\text{g/mL}$ ) and luciferase enzyme at 37  $^{\circ}\text{C}$ . Error bars are  $\pm$  SD of three measurements. (b) Total luminescent signal integrated over 3 h (AUC) following incubation of luciferase, HO-CBT (100  $\mu\text{M}$ ), Ac-AAPV-(D-Cys) peptide with increasing concentrations of HNE (0, 0.01, 0.025, 0.05, 0.1, 0.25 and 0.5  $\mu\text{g/mL}$ ) or D-cysteine as control (100  $\mu\text{M}$ ) over 3 h at 37  $^{\circ}\text{C}$ . Error bars are  $\pm$  SD of three measurements. Statistical analyses were performed with a two-tailed Student's *t* test. Differences between all the groups are statistically significant with each other ( $P < 0.05$ ) except between 0.05 and 0.1  $\mu\text{g/mL}$  ( $P = 0.3$ ).

The negative control (peptide probe without HNE) generates negligible light emission, corresponding to 0.39 % of the total luminescence emitted from 0.5  $\mu\text{g/mL}$  HNE incubated with the probe. These data demonstrate that the uncaging of the NE probe is specific and stable under these experimental conditions. However, in order to confirm the probe specificity further, sivelestat, an inhibitor of HNE, was added to the reaction as control. Subsequently, the probe was incubated with all the necessary material including 0.5  $\mu\text{g/mL}$  of HNE and increasing concentration of sivelestat (Figure 4.3).

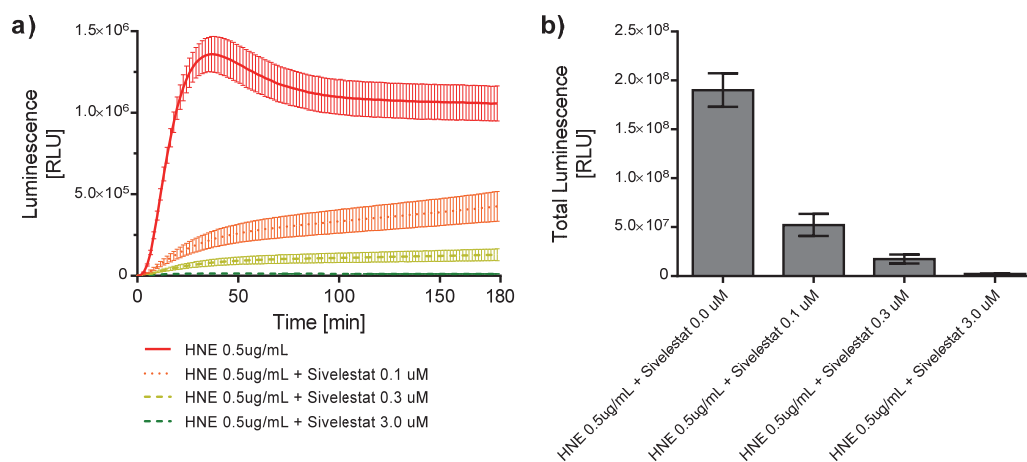


Figure 4.3: *In vitro* enzymatic assay of HNE activity imaging with Ac-AAPV-(D-Cys) peptide and HO-CBT in presence of sivelestat inhibitor. (a) luminescent signal over 3 h following incubation of HO-CBT (100  $\mu$ M), Ac-AAPV-(D-Cys) peptide (100  $\mu$ M), 0.5  $\mu$ g/mL HNE with increasing concentrations of sivelestat (0, 0.1, 0.3 and 3.0  $\mu$ M) and luciferase enzyme at 37  $^{\circ}$ C. Error bars are  $\pm$  SD of three measurements. (b) Total luminescent signal integrated over 3 h (AUC). Error bars are  $\pm$  SD of three measurements. Statistical analyses were performed with a two-tailed Student's t test. Differences between all the groups are statistically significant with each other ( $P < 0.05$ ).

Sivelestat dramatically reduces HNE activity, which results in a strong decrease in light emission. The total luminescence resulting from the probe incubation with HNE was reduced more than 3 times when incubated with 0.1  $\mu$ M sivelestat. That corresponds approximately to 27 % of total luminescence without inhibitor. Moreover, when the sivelestat concentration is increased to 3.0  $\mu$ M, only 1.1 % of the total luminescence emission without inhibitor was observed, highlighting once again the probe specificity to HNE. As an additional control, the effects of HNE on the luciferin/luciferase reaction or the split luciferin reaction were investigated by incubating different HNE concentrations with D-cysteine and HO-CBT (**Figure 4.4**). High concentration of HNE (i.e. 0.5  $\mu$ g/mL) does result in a small decrease in light emission. The total luminescence resulting from the reaction of D-cysteine and HO-CBT was diminished by approximately 17 % if 0.5  $\mu$ g/mL of HNE was present in solution (**Figure 4.4b**). A potential reason for this decrease in light emission, could be due to non-specific proteolytic degradation of luciferase by high HNE concentrations. The light emission from all the other control with smaller HNE concentration resulted in no differences in total luminescence. Only the highest concentration of HNE influenced the signal, meaning that when the Ac-AAPV-(D-Cys) probe is used, the observed luminescence is actually smaller than it should be for a similar amount of luciferin formed.

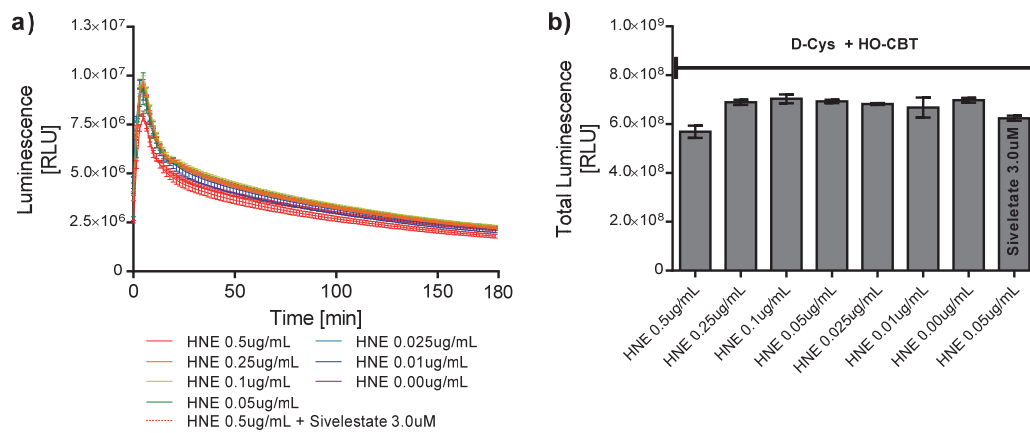


Figure 4.4: *In vitro* enzymatic assay of HNE effect on luminescence emission using the split luciferin reaction. (a) luminescent signal over 3 h following addition of HO-CBT (100 µM) and D-cysteine (100 µM) with increasing concentrations of HNE (0, 0.01, 0.025, 0.05, 0.1, 0.25 and 0.5 µg/mL), sivelestat (3.0 µM) and luciferase enzyme at 37 °C. Error bars are ± SD of three measurements. (b) Total luminescent signal integrated over 3 h (AUC). Error bars are ± SD of three measurements. Statistical analyses were performed with a two-tailed Student's t test. Differences between all the groups are not statistically significant with each other ( $P > 0.05$ ) except between 0.5 and 0.25 µg/mL or between 0.00 and 0.5 µg/mL + sivelestat ( $P > 0.05$ ).

Collectively, these data suggest that the Ac-AAPV-(D-Cys) probe, used in conjugation with HO-CBT, provide an efficient method for both the imaging and quantification of HNE activity. The HNE concentration-dependent signal generated by the probe is selective, with a low detection limit, in the range of 10 ng/ml of enzyme, and suggest that the Ac-AAPV-(D-Cys) peptide could be a good candidate for imaging NE activity in biological environment.

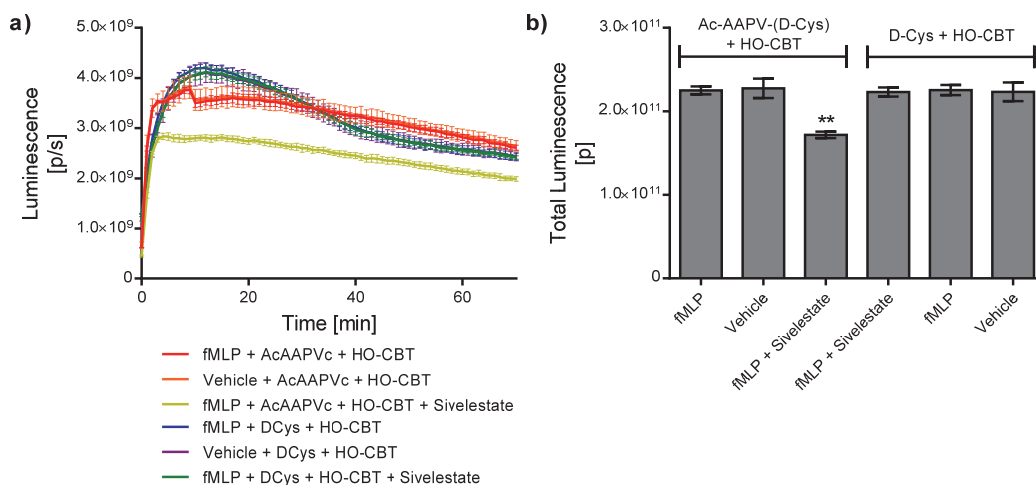
Importantly, it has been reported that PR3 and NE share a bit more than half amino acid homology, and that they can process more or less efficiently similar substrates.<sup>[267,294]</sup> Therefore, for cellular or animals experiments, it has to be accounted that PR3 could be responsible for probe cleavage. However, it's important to note that sivelestat is significantly less potent inhibitor of PR3 than HNE, making the use of this inhibitor a good control to exclude PR3 cleavage in the context of NE imaging experiments.<sup>[267]</sup>

### 4.3 Real time non-invasive imaging and quantification of neutrophil elastase activity in mouse neutrophils using the split luciferin ligation reaction

With promising results *in vitro*, investigation of NE activity imaging in living cells was undertaken using the Ac-AAPV-(D-Cys) peptide and HO-CBT. The experimental design was to activate neutrophils after isolation from mice bone marrow and imaged subsequent NE activity. *N*-Formylmethionyl-leucyl-phenylalanine (fMLP), a bacterial derived peptide, is a chemotactic compound that activates

neutrophils via different intracellular signalling pathways. Among other cellular response, activation results in neutrophil degranulation and superoxide generation.<sup>[295-297]</sup> Release of the granule content provokes excretion of a cocktail of molecules and proteins including serine proteases such as PR3, cathepsin G or NE.<sup>[271]</sup>

Neutrophils extracted from bone marrow of FVB-Luc<sup>+</sup> mice were isolated using density gradient separation by following an adapted reported procedure.<sup>[298]</sup> Unfortunately, after incubation of the extracted neutrophils with D-luciferin, no light emission was observed (data not shown). It was reported that leukocytes display varying levels of Fluc expression depending on the subsets.<sup>[217]</sup> Therefore, Fluc will have to be supplemented exogenously in these experiments. First, extracted neutrophils were incubated with 10  $\mu$ M fMLP or a vehicle control to trigger neutrophil activation and induce the release of granules content, including NE enzyme. The Ac-AAPV-(D-Cys) probe was added to the cell media and incubated for 45 min, followed by HO-CBT. Finally, a luciferase solution containing all necessary cofactors was added to the cell immediately prior imaging. To confirm the specificity of D-cysteine release by HNE, these experiments were performed in the presence and absence of a specific NE inhibitor, sivelestat. Moreover, to confirm that neither fMLP nor sivelestat influence light emission, these experiments were performed with D-cysteine instead of the peptide probe (**Figure 4.5**).



**Figure 4.5:** Imaging NE activity in activated mice neutrophils (a) Observed luminescence over 70 min after activation of neutrophils extracted from FVB-Luc<sup>+</sup> mice bone marrow. After isolation, neutrophils were incubated with fMLP (10  $\mu$ M) or DMSO and Ac-AAPV-(D-Cys) (100  $\mu$ M) peptide or D-cysteine (10  $\mu$ M) for 45 min. HO-CBT was then added to the cells, incubated for 15 min and imaged. (b) Total luminescent signal integrated over 70 min (AUC). Error bars are  $\pm$  SD for three measurements. Statistical analyses were performed with a two-tailed Student's t test. \*\*P < 0.01.

First, light emission emitted when fMLP was used to activate neutrophils is similar than when cells were only treated with vehicle. This is in opposition to the expected results, as NE was supposed

to be released upon fMLP activation and consequently result in an increase in probe cleavage and thus in light emission. Yet, the sivelestat control resulted in a small decrease in light emission, suggesting that the signal observed is dependent on NE activity. This could be the result of neutrophil activation that occurred during the isolation procedure, resulting in no observable effect of fMLP. Moreover, after isolation, neutrophils were kept in RPMI 1640 media. This media contains a large amount of cysteine, that can result in the generation of background following the addition of HO-CBT addition. In order to determine if media could influence the background light emission, HO-CBT was incubated in RPMI 1640, DMEM or DPBS, followed by luciferase addition and subsequent BL measurement. The light emission measured from RPMI media after HO-CBT addition is 17 times higher than similar experiment performed in saline solution (**Figure S4.2**). Therefore, repeating the neutrophil activation experiments with PBS instead of RPMI 1640 could thus improve the conditions, assuming that PBS doesn't influence cell viability and activation. Nevertheless, a high background signal does not explain high light emission from vehicle treated neutrophils imaged with peptide probe (**Figure 4.5**). Interestingly, an alternative hypothesis could be that the probe is cell permeable and can interact with all cellular NE irrespective of neutrophil activation and de-granulation. Further experiments to design a cell impermeable probe as an additional control would help to address this problem.

#### 4.4 Real time non-invasive imaging of neutrophil elastase activity in living animals

It was previously established that the split luciferin reaction has properties that are compatible with bioluminescence imaging in living animals. Using this methodology, caspase 3/7 activity was successfully imaged in a liver apoptosis model in living mice. Since the Ac-AAPV-(D-Cys) peptide has been efficiently used for imaging and quantification of NE activity *in vitro*, this probe could be a good candidate for imaging NE in living animals. Thus, the goal of these *in vivo* studies is to validate the use of the NE split luciferin-based probe for imaging NE activity in living animals.

For the first *in vivo* application of NE bioluminescence imaging using the split luciferin reaction, an acute lung inflammation model was adopted. Lung inflammation can be induced in mice by administration in the lungs of the bacterial pathogen associated molecular patterns (PAMPS) lipopolysaccharides (LPS) and fMLP directly into the lungs.<sup>[267,299]</sup> LPS are large molecules composed of a lipid core conjugated to a carbohydrate chain and decorate the surface of Gram-negative bacteria. LPS is a highly potent antigen, which induces inflammatory responses *in vivo*. fMLP, a bacterial derived peptide, was shown to be a chemotactic compound as well as an activator of macrophages and neutrophils that

results in reactive oxygen species and neutrophil degranulation.<sup>[295]</sup> Whereas intravenous and intraperitoneal (i.p.) administration of LPS in mice have been reported for the development of acute lung injury models, it does not produce neutrophil infiltration in lung parenchyma and as a result is not suited to study the infiltration and activation of neutrophils into the lungs and the corresponding NE activity.<sup>[300-302]</sup> On the other hand, intranasal or intratracheal administration of LPS and fMLP induce a strong inflammatory response via multiple signalling pathways and provoke neutrophil infiltration of pulmonary tissue and as a consequence acute lung injury.<sup>[267,299,303]</sup> Neutrophils bronchoalveolar infiltration is produced by LPS, but the neutrophil activation and thus the neutrophil-associated enzymatic activities is dependent on fMLP treatment in mice.<sup>[299,304]</sup>

As a first report of bioluminescence imaging of NE *in vivo*, an acute lung injury model was induced in mice transiently expressing luciferase enzyme in lung tissue. In order to induce neutrophil-mediated inflammation, a reported procedure was followed with small modifications.<sup>[267,299]</sup> Mice were treated intratracheally with LPS and fMLP, inducing neutrophil recruitment and activation in the lung tissue. The Ac-AAPV-(D-Cys) peptide probe was then administered to the animal, followed by HO-CBT injection and imaging.

BalbC mice were first transfected with a FLuc expression plasmid resulting in luciferase expression in the lung tissue. The luciferase construct, named RedLuc, consists of a codon-optimized luciferase from the *luciola italic* firefly that has a red-shifted emission peak at a wavelength of 617 nm.<sup>[305]</sup> Following transfection, luciferase expression level was measured by imaging mice after injection of D-luciferin. The luciferase expression was determined to be stable from days 4 to 7 post transfection (**Figure S4.3**). Five days after DNA administration, mice were treated intratracheally with LPS, inducing an inflammatory response and neutrophil recruitment in the lung tissue. This was followed 24 h later by intratracheal fMLP treatment resulting in neutrophil activation and degranulation. After a delay of 30 min, the Ac-AAPV-(D-Cys) peptide probe was injected i.p. in the animal. NE is released after activation of recruited neutrophils, and cleaves the probe, releasing free D-cysteine. *In situ* formation of D-luciferin occurs following i.p. administration of HO-CBT 30 min after peptide injection (**Figure 4.6**).



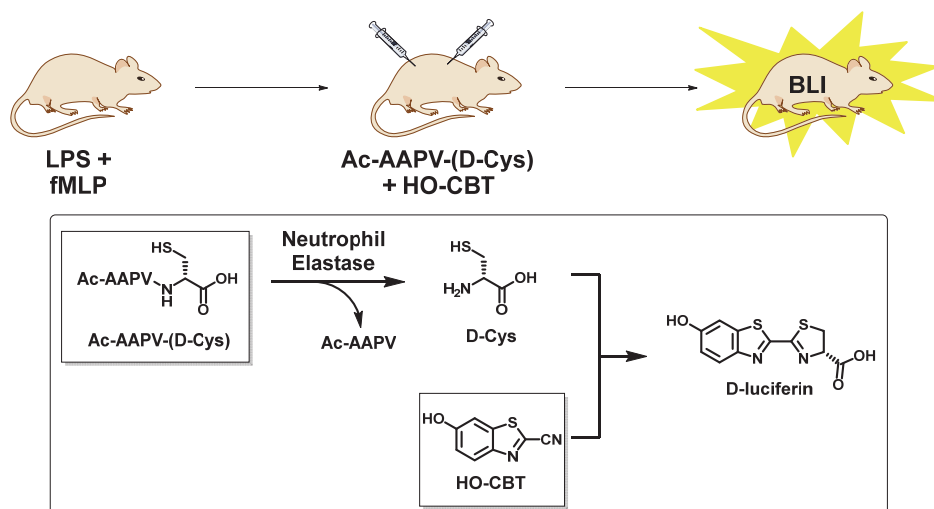


Figure 4.6: NE activity imaging using split luciferin reaction in a mouse model of acute lung injury. Overall representation of mice treatment and NE activity imaging with Ac-AAPV-(D-Cys) peptide and HO-CBT in living animals transiently expressing luciferase enzyme in the lung tissue.

Immediately after CBT administration, mice were placed in the imaging device and bioluminescence was acquired over 1 h. Mice were divided into 3 groups that were all injected with Ac-AAPV-(D-Cys) peptide and HO-CBT, and either received LPS and fMLP administration, LPS only or vehicle only. In order to estimate the intrinsic background generated by HO-CBT administration in this mouse model, one more group just received vehicle and HO-CBT without administration of the peptide probe (Figure 4.7).

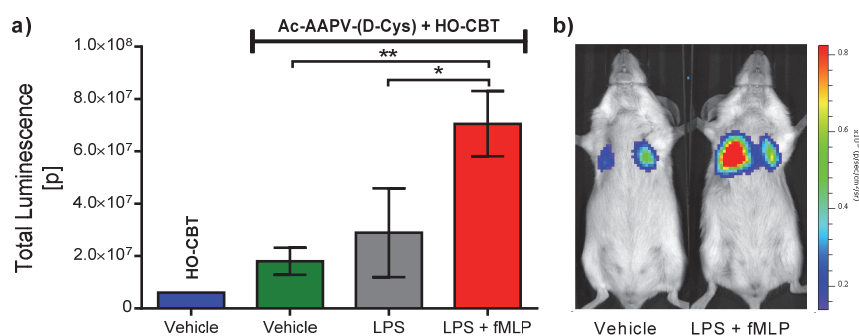


Figure 4.7: Imaging NE activity in a LPS/fMLP induced mouse acute lung injury model. (a) Total luminescence over 1 h from luciferase transfected BalbC mice treated with either vehicle, LPS intratracheally (12.5 µg/mouse in 40 µL PBS) or combination of LPS (12.5 µg/mouse in 40 µL PBS) and fMLP (32 µg/mouse in 40 µL PBS) intratracheally. fMLP was administered 24 hours after LPS treatment. 30 min post fMLP treatment, the animals received i.p. injections of either Ac-AAPV-(D-Cys) peptide (2.363 mg/mouse in 200 µL saline) or vehicle, followed by HO-CBT (0.83 mg/mouse in 400 µL of 25% DMSO in PBS). Statistical analyses were performed with a two-tailed Student's t test. \*\*P < 0.01, \*P < 0.05 (n=3 for all the groups that receive peptide probe and HO-CBT. n=1 for the vehicle group that received only HO-CBT.). Error bars are ± SD for three measurements. (b) Representative image of mice, 30 min post-injection of HO-CBT.

Bioluminescence from the NE probe was greatest in the LPS/fMLP treated group (**Figure 4.7, Figure 4.8**). The ratio in average total light emission between the LPS/fMLP and vehicle treated groups is approximately 4-fold and the difference is statistically significant ( $P = 0.0095$ , **Figure 4.7a**). There is only a 2.4-fold increase in total luminescence between the LPS and the LPS/fMLP group that is also statistically significant ( $P = 0.0305$ ). However, there is no statistical difference between vehicle and LPS treated groups ( $P = 0.3839$ ). It can also be noticed that the light emission acquired over 60 min is increasing in function of the time in LPS/fMLP treated mice, whereas a more constant or low increase is observed in other groups treated with the peptide probe and HO-CBT (**Figure 4.8**).

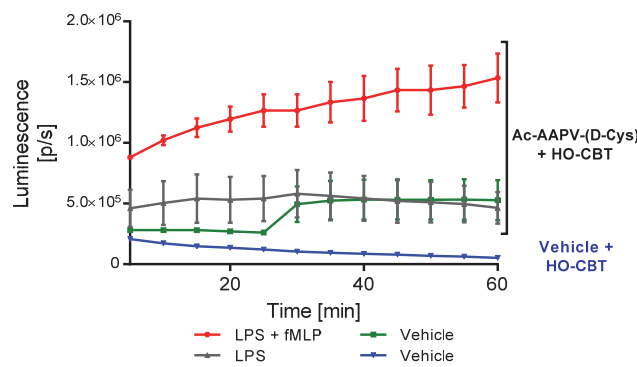


Figure 4.8: Observed luminescence emission over 60 min from NE bioluminescent probes in a LPS/fMLP induced mouse acute lung injury model. Luminescence emission over 60 min following i.p. injection of Ac-AAPV-D-Cys peptide (2.363 mg/mouse in 200  $\mu$ L saline) and HO-CBT (0.83 mg/mouse in 400  $\mu$ L of 25% DMSO in PBS) or only HO-CBT, after intratracheal LPS (12.5  $\mu$ g/mouse in 40  $\mu$ L of PBS) and fMLP (32  $\mu$ g/mouse in 40  $\mu$ L PBS) ( $n=3$ ), only LPS ( $n=3$ ) or vehicle treatment ( $n=3$ ) in luciferase transfected BalbC mice. Error bars are  $\pm$  SD for three measurements.

These data provide strong evidence that NE activity can be efficiently imaged via the split luciferin reaction using Ac-AAPV-(D-Cys) peptide in an acute lung injury model in luciferase expressing mice. A significant increase in signal was observed only under LPS/fMLP treatment compared to the other experimental groups. This is in agreement with previous reports stating that both of these effectors are necessary for neutrophil migration in the lungs and further activation.<sup>[267,299,303]</sup> The lower light emission observed when mice were only treated by LPS is in adequacy with the fact that fMLP is necessary for neutrophils activation that triggers NE release from neutrophil-granules.<sup>[267,304]</sup> Without fMLP, activation of neutrophils is less important, resulting in a lower NE concentration in lung tissues. These results obtained *in vivo* are also in agreement with previous report where NE activity was efficiently imaged in similar neutrophil-mediated lung inflammation using a florigenic probe.<sup>[267]</sup>

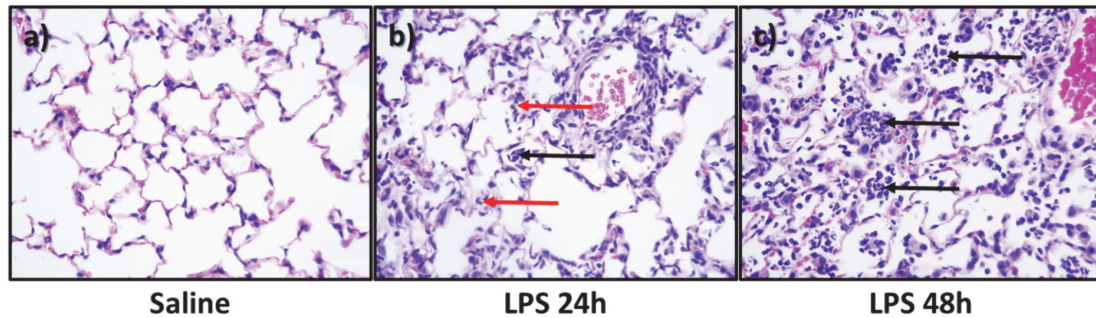


Figure 4.9: Hematoxylin and eosin (HE) staining of formalin fixed paraffin embedded tissue sections from BalbC mice lungs after intratracheal treatment with LPS or saline as control. Histochemical images are representative of the lung tissue per experimental groups (n=3). (a) Negative control, 24 h after administration of 40  $\mu$ l PBS intratracheally. No infiltration of neutrophils is visible (40x, HE). (b) 24 h after administration of LPS intratracheally (12.5  $\mu$ g/mouse in 40  $\mu$ L PBS). Neutrophils are visible within the capillaries in an increased amount (neutrophilia) (red arrows) and accumulate in small numbers within the alveoli (black arrow) (40x, HE). (c) 48 h after administration of LPS intratracheally (12.5  $\mu$ g/mouse in 40  $\mu$ L PBS), neutrophils accumulate in large groups in the alveoli (black arrows) leading to purulent pneumonia (40x, HE).

Analysis of lung sections confirmed that LPS treatment induced neutrophil-mediated inflammation. Lungs from mice administered with LPS or PBS intratracheally were collected 24 and 48 h after treatment. Histological sections of the tissues were analysed after hematoxylin and eosin (HE) staining in collaboration with a pathologist. In lung tissues of control mice treated with PBS, no infiltrated neutrophils were visible (**Figure 4.9a**). However, 24 and 48 h after LPS administration, infiltrated neutrophils are clearly present. At the 24 h time point, neutrophils were principally located in the capillaries (neutrophilia), with a moderate number within the alveoli, whereas at 48 h a large number of neutrophils were mainly found in the lumen of the alveoli (**Figure 4.9b-c**).

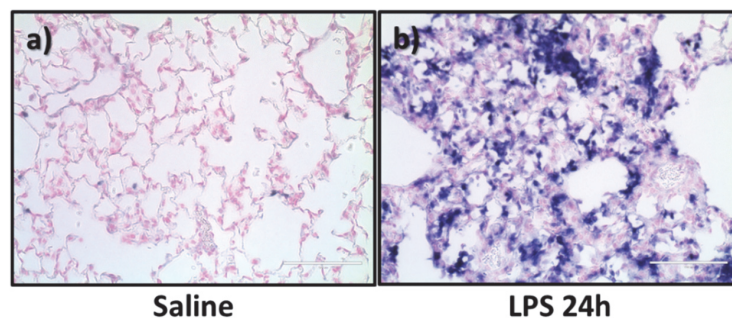


Figure 4.10: Immunohistochemical (IHC) staining of Ly6G antigen revealed by Bluemap on paraffin fixed histology sections from BalbC mice lungs after intratracheal treatment with LPS or saline as control. Immunohistochemical images are representative of whole lung tissue. (a) Negative control, 24 h after administration of 40  $\mu$ l PBS intratracheally. Very low and sprinkled Ly6G staining, mainly located in the capillaries (40x, IHC). (b) 48 h after administration of LPS intratracheally (12.5  $\mu$ g/mouse in 40  $\mu$ L PBS). Strong Ly6G staining of neutrophils (in blue) in the lung alveoli (40x, IHC).

Moreover, the analysis of Ly6G immunohistochemical staining of the tissue section revealed similar observations. Ly6G (Lymphocyte antigen 6 complex locus G6D) is an antigen expressed on granulocytes, also called polymorphonuclear cells. These white blood cells category encompass neutro-

phils, the most abundant granulocytes, but also eosinophils, basophils and mast cells. Thus immuno-histochemical staining of Ly6G demonstrates the presence of this cell population. In healthy lungs, neutrophils and other granulocytes are not present in the alveoli, whereas in inflammation conditions infiltrated granulocytes migrate into the alveoli in large numbers. This exact pattern was observed in mice lung sections where, 48h after LPS intratracheal administration, a large number of Ly6G positive cells are visible in the lung alveoli (**Figure 4.10b**). In contrast, control tissue that only received PBS, only a few Ly6G positive cells, located in capillaries are visible, which is an ordinary observation due to presence of a few granulocytes in the peripheral blood (**Figure 4.10a**). This is in agreement with *in vivo* NE imaging data obtained using the split luciferin approach as well as other reported data<sup>[267,306]</sup> and suggests that neutrophil-mediate inflammation was efficiently induced in the lungs by intratracheal administration of LPS.

In order to confirm these promising results, further investigations of the NE probe Ac-AAPV-(D-Cys) were performed in another mouse strain. The same LPS/fMLP acute lung injury model was induced in ubiquitously luciferase expressing FVB-Luc+ mice, using a slightly different experimental procedure. FVB-Luc+ mice were treated intranasally with LPS, followed 24 h later by intranasal fMLP administration. After a 2 h delay, the Ac-AAPV-(D-Cys) peptide probe was injected i.p. in the animals. *In situ* formation of D-luciferin occurs after HO-CBT i.p. administration, 30 min after peptide injection. Mice were then immediately placed in the imaging system and bioluminescence emission was acquired for 1h. Light emission from the chest region was quantified and luminescence over 60 min as well as the total luminescence (AUC) were calculated (**Figure 4.11**).

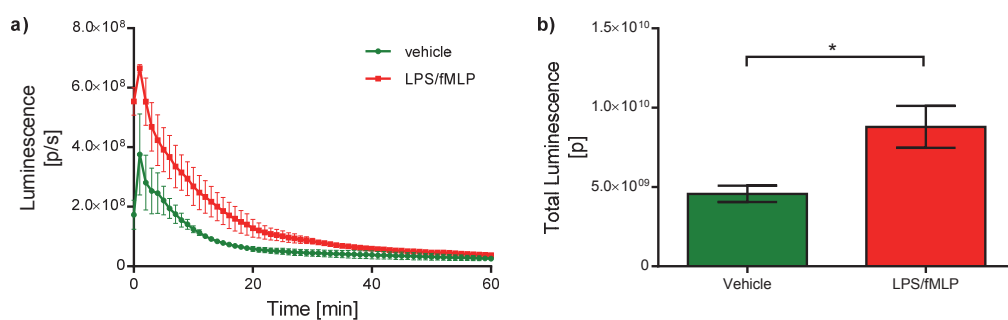


Figure 4.11: Imaging NE activity in a LPS/fMLP induced mouse FVB-Luc+ acute lung injury model. (a) Luminescence emission over 60 min from FVB-Luc+ mice treated with either vehicle or a combination of LPS (100  $\mu$ g/mouse in 40  $\mu$ L PBS) and fMLP (32  $\mu$ g/mouse in 40  $\mu$ L PBS) intranasally. fMLP was administered 24 hours after LPS treatment. 2 h post fMLP treatment, the animals received i.p. injections of either Ac-AAPV-(D-Cys) peptide (0.391 mg/mouse in 200  $\mu$ L saline) or vehicle, followed by HO-CBT (0.136 mg/mouse in 100  $\mu$ L of 20% DMSO in PBS). Error bars are  $\pm$  SD for three measurements. (b) Total luminescence integrated over 1 h (AUC). Statistical analyses were performed with a two-tailed Student's t test. \*P < 0.05 (n=3). Error bars are  $\pm$  SD for three measurements.

Compared to the previous experiments on transfected BalbC strain expressing luciferase enzyme only in the lung tissue, doses and timeline had to be adjusted. The peptide and HO-CBT doses were decreased. High doses were not necessary in FVB-Luc+ animal due to strong ubiquitous luciferase expression. Moreover, due to intranasal administration instead of intratracheal, LPS doses were increased.

The light emission observed in LPS/fMLP treated animals is significantly higher than the vehicle treated controls ( $P = 0.0195$ ). However, total luminescence observed from the LPS/fMLP treated group is approximately two times higher than from vehicle treated group (**Figure 4.10b**). Compared to the experiments performed in transfected BalbC animals, the difference in total luminescence is smaller between both groups of FVB-Luc+ mice.

Overall, these data demonstrate that the Ac-AAPV-(D-Cys) peptide used in combination with HO-CBT allows an efficient, selective and sensitive approach for NE imaging *in vivo*, in mouse models of acute lung injury. Accordingly, the split luciferin based probe for NE could be a valuable tool for imaging neutrophil-mediated inflammation as well as better understanding NE functions in several infection and inflammation models. This confirms that split luciferin based probes are valuable tools for non-invasive imaging of proteases *in vivo*, providing a potent methodology for generation of novel BLI probes.

## 4.5 Conclusion

In this chapter, imaging and quantification of NE using the split luciferin reaction were reported. To our knowledge, this is the first report of BLI of NE activity. Ac-AAPV-(D-Cys) peptide, used in combination with HO-CBT, was validated for the imaging and quantification of NE activity *in vitro* and living animals. *In vitro* experiments with purified NE enzyme revealed that the developed split luciferin-based probe is efficient, selective and sensitive. On the other hand, the cell assay was not conclusive, with high light emission observed from neutrophils that were not activated by incubation with fMLP. However, a small decrease in light emission was observed upon NE inhibitor treatment, suggesting that neutrophils could have been activated during extraction procedure. Alternatively, the probe could be cell permeable and thus could interact with all cellular NE irrespective of neutrophil activation and degranulation. Designing a cell impermeable probe as an additional control would help to understand this problem. Further experiments are thus necessary for a full validation of the probe in a cell-based assay. Moreover, extraction of neutrophils from human blood and subsequent NE imaging experiments could be included in this study.

*In vivo*, NE activity was quantified and imaged in an acute lung inflammation model in two different mouse strains. A significant increase in light emission was observed from mice that received LPS/fMLP administration in the lungs compared to vehicle treated animals. Furthermore, bronchoalveolar lavage (BAL), a medical procedure routinely used for lung disease diagnosis, could be performed on mice challenged with LPS. This would provide evidence that NE can be imaged and quantified using the split luciferin reaction *ex vivo* in BAL fluids. As luciferase enzyme can be added exogenously, this would also provide a method for the quantification of NE activity in non-luciferase expressing animals.

All together, these data provide evidence that NE can be efficiently imaged in a lung inflammation model using the split luciferin reaction. This approach provides an efficient tool for BLI of NE activity in real time, non-invasively and *in vivo*. To date, the split luciferin reaction was used *in vivo* for quantification and visualization of caspase 3/7 activity as well as simultaneous imaging of caspase-8 and hydrogen peroxide.<sup>[230,231,307]</sup> This study provides another report where the split luciferin reaction was used for BLI of protease *in vivo*, highlighting the versatility and good potential of the split luciferin reaction for imaging applications.

## 4.6 Experimental section

**General Material and Methods.** Chemicals were obtained from commercial suppliers and used without further purification. For peptide synthesis, preloaded H-D-Cys(Trt)-2-chlorotrityl resin (particle size 100-200 mesh, loading 0.4 mmol/g, Advanced Chemtech), Fmoc-protected amino acids (Fmoc-L-Valine-OH, Fmoc-Proline-OH and Fmoc-Alanine-OH, purity > 99% Novabiochem), 1-Hydroxy-7-azabenzotriazole (HOAt, purity > 99%, Fluorochem LTD), N,N'-diisopropylcarbodiimide (DIC, purity > 99%, TCI GmbH), N,N'-dimethylformamide (DMF, ReagentPlus grade, Sigma-Aldrich or Technical grade, Thommen-Furler AG), dichloromethane (DCM, Technical grade, Thommen-Furler AG), methanol (MeOH, Technical grade, Thommen-Furler AG), acetonitrile (MeCN, HPLC gradient grade, Fischer Scientific), diethyl ether (Et<sub>2</sub>O, for HPLC, > 99.9%, Sigma-Aldrich), piperidine (purity > 99.9%, Sigma-Aldrich), trifluoroacetic acid (TFA, ReagentPlus, purity 99%, Sigma-Aldrich), triisopropylsilane (TIPS, purity 98%, Aldrich, Sigma-Aldrich), dithiothreitol (DTT, Molecular biology grade, LuBioScience), Acetic anhydride (ReagentPlus, purity 99%, Sigma-Aldrich) and formic acid (FA, LC-MS Ultra grade, Fluka, Sigma-Aldrich) were used.

Human Neutrophil Elastase (HNE) was purchased from Abcam plc, and used without further purification. Luciferase buffer was prepared as following: 60 µg mL<sup>-1</sup> Firefly luciferase (Sigma-Aldrich Chemie GmbH) in 0.1 M Tris-HCl pH = 7.4, 2 mM Adenosine 5'-triphosphate, disodium salt hydrate (ATP, AppliChem GmbH), and 5 mM Magnesium sulfate (MgSO<sub>4</sub>, Sigma-Aldrich). D-Cysteine (D-Cys,



purity >99%, Sigma-Aldrich) and 6-Hydroxy-benzothiazole-2-carbonitrile (HO-CBT, Endotherm GmbH), N-Methoxysuccinyl-Ala-Ala-Pro-Val-*para*-Nitroanilide (AAPV-pNA, NE substrate, Sigma-Aldrich), Lipopolysaccharides from *Escherichia coli* 0111:B4 (LPS, purified by gel-filtration chromatography, Sigma-Aldrich), N-Formyl-Met-Leu-Phe (fMLP, BioXtra, ≥99.0%, Sigma-Aldrich), Dimethyl sulfoxide (DMSO, for molecular biology, Sigma-Aldrich), DPBS (w/o CaCl<sub>2</sub>, w/o MgCl<sub>2</sub>, Life Technologies), 10X HBSS (Life Technologies), FBS (Life Technologies), RPMI 1640 (Life Technologies), N-{2-[(4-[(2,2-Dimethylpropionyl)oxy]phenyl)sulfonyl]amino}benzoyl}glycine sodium salt (sivelestat sodium salt, >98 %, Tocris Bioscience), Phosphate buffered saline (PBS, Life Technologies) and Percoll (pH 8.5-9.5, cell culture tested, Thermo Fisher Scientific Inc.) were used for assays without any further purification. DNA maxiprep kit was purchased from Clontech and JetPEI (*in vivo*-jetPEI) was purchased from Polyplus Transfection.

Millipore water was used for sample preparation of all *in vitro*, cellular, and animal assays. All *in vitro* and cellular studies were performed in clear bottom black 96-well plates that were purchased from Becton Dickinson and Company (Franklin Lakes, NJ). Spectramax Gemini (Molecular Devices) or IVIS Spectrum camera (PerkinElmer) were used to measure the amount of BLI signal production.

UPLC analytical analysis was performed on Water Acquity UPLC system coupled to a Waters Acquity TQ mass detector (Waters Corp., Milford, USA) with Acquity UPLC BEH Shield reverse phase C18 column (2.1x50 mm, 1.7 μm, Waters) using degassed HPLC gradient grade solvents from Fisher Chemicals (Loughborough, UK) and Millipore water both supplemented with 0.1% FA. Semi-preparative HPLC purification was performed using a semi-preparative Waters HPLC system coupled to a Waters Acquity TQ mass detector (Waters Corp., Milford, USA). An XTerra prep MS C18 OBD column (19x50 mm, 5.0 μm, Waters) was used in combination with Degazed MiliQ water supplemented with 0.1% of FA (vol/vol) and MeCN supplemented with 0.1% of FA (vol/vol) as phases for the eluent. HRESI-MS measurements were conducted at the EPFL ISIC Mass Spectrometry Service using Micro Mass QTOF Ultima from Waters Corp.

**Ac-L(Ala-Ala-Pro-Val)-D-(Cys)-OH (Ac-AAPV-(D-Cys)) peptide synthesis.** Peptide was synthesized using Fmoc solid-phase peptide synthesis with a D-cysteine preloaded chloro-trityl resin (H-D-Cys(Trt)-2-Cl-Trt-Resin, 100-200 mesh, 0.4 mmol/g, Advanced Chem Tech) on a 0.4 mmol scale. Sequentially, Fmoc-L-valine, Fmoc-L-proline, and 2 times Fmoc-L-alanine were used. For each coupling, the Fmoc protected amino acid residue (3 eq., 1.2 mmol), 1-hydroxy-7-azabenzotriazole (HOAt, 3 eq., 1.2 mmol) and N,N'-diisopropylcarbodiimide (DIC, 3 eq., 1.2 mmol) and DMF (20 mL) were loaded in a reaction vessel over the resin and stirred at rt for 6 h. The suspension was then filtered and the resin was washed sequentially with DMF, methanol and dichloromethane (DCM). Fmoc deprotection was

performed by resuspending the resin in a 20% (v/v) piperidine solution in DMF (20 mL) for 10 min under stirring at rt. After filtration the solid was washed sequentially with DMF, methanol and DCM. These steps were then repeated until the last amino acid coupling and Fmoc deprotection. Acetate capping was performed by suspending the resin in DMF (20 mL) supplemented with pyridine (3 eq., 94.92 mg, 97.06  $\mu$ L) and acetic anhydride (3 eq., 122.50 mg, 121.69  $\mu$ L) for 30 min at rt under stirring, followed by washing sequentially with DMF, methanol and DCM. Amino acid side-chain deprotection and peptide cleavage from the resin was performed by resuspending 3 times the resin in 10 mL of a DCM/TFA/H<sub>2</sub>O/triisopropylsilane/dithiothreitol (5 mL DCM, 4.5 mL TFA, 0.25 mL H<sub>2</sub>O, 0.25 mL triisopropylsilane and 0.3 mg dithiothreitol) solution for 10 min at rt. Resin was removed by filtration. Combined liquid phases were concentrated under reduced pressure, and the peptide was precipitated with ice-cold diethyl ether (20 mL). The precipitate was recovered and washed twice with ice-cold diethyl ether (20 mL) and dried under reduced pressure. Further purified by semi-preparative HPLC to yield the desired Ac-Ala-Ala-Pro-Val-(D-Cys)-OH product. Purity was confirmed by HRMS and analytical HPLC. HRMS (ESI-TOF)  $m/z$ :  $[M+Na]^+$  calcd for C<sub>21</sub>H<sub>35</sub>N<sub>5</sub>O<sub>7</sub>Na, 524.2155; found, 524.2164. Isolated yield after purification is 51%.

**Bioluminescent Neutrophil Elastase Assay with Ac-AAPV-(D-Cys) Peptide and HO-CBT.** 1  $\mu$ g/ $\mu$ L HNE stock solution was prepared by dissolving the lyophilized Active Human NE (abcam, ab91099) in 50 mM Sodium Acetate pH 5.5 buffer supplemented with 150 mM NaCl. From this stock solution, different HNE solutions were prepared at 0.0, 0.05, 0.025, 0.01, 0.005, 0.0025 and 0.001  $\mu$ g/ $\mu$ L in 100 mM Tris-HCl, pH 7.5, 500 mM NaCl.

In a black flat transparent bottom 96-well plate, 96  $\mu$ L of a Luciferase solution containing 60  $\mu$ g/mL of firefly luciferase enzyme in assay buffer (100 mM Tris-HCl, pH 7.5, 500 mM NaCl, 2 mM ATP, 5 mM MgSO<sub>4</sub>) was added in the wells. 1  $\mu$ L of the HNE solutions were added in the black 96-well, each concentration in triplicates. When necessary, 1  $\mu$ L of sivelestat solutions (3  $\mu$ M, 30  $\mu$ M or 300  $\mu$ M in DMSO) was added to the corresponding wells. Wells that did not receive sivelestat solution, were supplemented with 1  $\mu$ L of DMSO. In every well, either 1  $\mu$ L of a Ac-AAPV-c solution (10 mM in PBS) or 1  $\mu$ L of a D-Cys solution (10 mM in PBS) were added. This was followed by addition of 1  $\mu$ L of a HO-CBT solution (10 mM in DMSO) simultaneously in all the wells. Bioluminescence signal from the plate was immediately measured every 1.5 min with 1000 ms integration time for 3 h at rt.

**Colorimetric assessment of Neutrophil Elastase activity.** 1  $\mu$ g/ $\mu$ L HNE stock solution was prepared by dissolving the lyophilized Active Human NE (abcam, ab91099) in 50 mM Sodium Acetate pH 5.5 buffer supplemented with 150 mM NaCl. In a black flat transparent bottom 96-well plate, 98  $\mu$ L



of NE-buffer (100 mM Tris-HCl, pH 7.5, 500 mM NaCl) were added in the wells. In every wells, either 1  $\mu$ L of a AAPV-pNA solution (10 mM in DMSO) or 1  $\mu$ L of DMSO were added. Absorbance at 405 nm was measured for 15 min. Then, 1  $\mu$ L of the HNE solution were added in the black 96-well. Wells where no HNE was added, received 1  $\mu$ L of vehicle. Absorbance at 405 nm was again measured every 15 min for 4h.

**Animals.** FVB-luc<sup>+</sup> transgenic mice<sup>[217,218]</sup> (full abbreviation: FVB-Tg(CAG-luc,-GFP)L2G85Chco/J) were obtained from The Jackson Laboratory and bred at the EPFL SPF animal facility. The breeding colony was housed in groups of 4-5 mice according to their age and gender with free access to food and water at 22 °C with regular light-dark cycle. All studies were carried out in strict accordance to the Swiss regulation on animal experimentation and the experimental procedure (license VD2969) was approved by the authority of the Canton Vaud, Switzerland (EXPANIM (Expérience sur animaux)–SCAV, Département de la sécurité et de l'environnement, Service de la consommation et des affaires vétérinaires).

Female inbred BalbC (BALB/cAnCrI) mice (7–8 week-old) were housed in groups of 4-5 mice according to their age with free access to food and water at 22 °C with regular light-dark cycle. Experiments were performed in compliance with national and international laws and policies (Guide for the Care and Use of Laboratory Animals, Institute of Laboratory Animal Resources Commission on Life Sciences, National Research Council (1996) Guide for the care and use of laboratory animals. National Academy Press, Washington, DC). Animal studies were approved by the Institutional Animal Care and Use Committee at Chiesi Farmaceutici, Parma, Italy.

**Real time non-invasive imaging and quantification of Neutrophil Elastase activity in mice neutrophils using the split luciferin ligation reaction.** Two 20-22 weeks old FVB-luc<sup>+</sup> female were sacrificed using CO<sub>2</sub> inhalation. Femurs and tibias were collected and put in ice cold PBS. Femurs were separated from tibias at the knee joint. Ends of bones were cut clean with a sharp surgical scissor. Bone marrow (BM) was flushed from bone with 10 mL of ice cold DPBS supplemented with 0.1% FBS using a 29 gauge insulin syringe. BM solution was gently mixed by performing up and downs with a micropipette. Solution was then filtered on a 40  $\mu$ m nylon cell strainer. The recovered solution was centrifuged (12 min, 260 g, 4 °C) and the pellet was resuspended in 4 mL DPBS containing 0.1% FBS. A 90 % percoll stock solution in 10 x HBSS was prepared. 52 %, 64 % and 72 % percoll stock solution (90% in 10 x HBSS) were prepared in DPBS supplemented with 0.1% FBS. In two 15 mL conical tube, 2 mL of each percoll dilution were layered from the more concentrated (72 %, bottom) to the less concentrated one (52 %, top).

top). 2 mL of the BM solution were carefully layered over the 52 % percoll stock solution, and centrifuged for 30 min at 110 g and 4 °C. Neutrophil layer that has formed at the interface between 72 % and 64 % percoll stock solution were harvested and diluted up to 10 mL with DPBS solution containing 0.1 % FBS and centrifuged 5 min at 260 g and 4 °C. Cells were resuspended again in 10 mL DPBS solution containing 0.1 % FBS and centrifuged 5 min at 260 g and 4 °C. This last step was repeated once. Finally, cells were resuspended in 2 mL RPMI 1640 supplemented with 1 % penicillin and streptomycin, counted and diluted to a  $1 \cdot 10^6$  cell per mL.

In a black flat transparent bottom 96-well plate, 100000 cells (100  $\mu$ L) were added in each wells, and cells were placed at 37 °C for 15 min. In every wells, either 1  $\mu$ L of an fMLP solution (1 mM in DMSO) or vehicle was added as well as 1  $\mu$ L of sivelestat solution (3  $\mu$ M in DMSO) or pure DMSO. Then 1  $\mu$ L of Ac-AAPV-(D-Cys) probe solution (10 mM in H<sub>2</sub>O) or 1  $\mu$ L of D-Cys solution (1 mM in H<sub>2</sub>O) were added. The plate was incubated at 37 °C for 45 min and 1  $\mu$ L of HO-CBT solution (10 mM in DMSO) was added in the wells. After another 15 min incubation at 37 °C, 50  $\mu$ L of a 120  $\mu$ g/mL luciferase enzyme solution in luciferase buffer (4 mM ATP, 10 mM MgSO<sub>4</sub> in 100 mM TRIS-HCl pH 8) were added in all the well. The plate was then immediately imaged using an IVIS100 imaging system using automatic settings at 37 °C for 1 h with an acquisition per minute. Photons emitted from the wells were quantified using Living Image® software (Caliper Life Sciences).

**Split luciferin background estimation using different buffers.** In a black flat transparent bottom was used. In every wells, either 99  $\mu$ L of RPMI 1640 supplemented with 1 % penicillin and streptomycin, 99  $\mu$ L of DMEM or 99  $\mu$ L of DPBS were added. One  $\mu$ L of HO-CBT solution (10 mM in DMSO) was added in all the wells and the plate was incubated for 15 min at 37 °C. Then, 50  $\mu$ L of a 120  $\mu$ g/mL luciferase enzyme solution in luciferase buffer (4 mM ATP, 10 mM MgSO<sub>4</sub> in 100 mM TRIS-HCl pH 8) were added in all the well. The plate was then immediately imaged using an IVIS100 imaging system using automatic settings at 37 °C for 1 h with an acquisition per minute. Photons emitted from the wells were quantified using Living Image® software (Caliper Life Sciences).

***In vivo* mice transfection (by Dr. Fabio Stellari and Francesca Ruscitti).** The pLenti-UbC-Red-FLuc-T2A-Puro (RedLuc-puro, Figure S4.4) plasmid was obtained from Perkin Elmert and amplified using Clontech DNA maxiprep kit. *In vivo* JetPEI (Polyplus Transfection) was applied as a carrier for delivering DNA to lung tissues according to manufacturer protocol. Briefly, the plasmid DNA and JetPEI mix were formulated with a final N/P ratio of 7. Forty  $\mu$ g of RedLuc-puro and 7  $\mu$ L of JetPEI were both diluted into 200  $\mu$ L 5% glucose. The two solutions were then mixed and incubated for 15 min at room

temperature. The entire mixture was then injected intravenously into tail vein of BalbC mice. The expression of UbC-Luc was monitored through imaging with an IVIS imaging system 1 day, 4 days, 5 days and 7 days after DNA delivery. Briefly, mice were injected intraperitoneal (i.p.) with luciferin (150 mg/kg) and bioluminescence was measured 15 min following luciferin injection. Mice were anesthetized with 1.5 % isoflurane and images were acquired with an IVIS imaging system. Photons emitted from the chest region were quantified using Living Image® software (Caliper Life Sciences) (Figure S4.3).

**Real time non-invasive imaging of HNE activity in transiently transgenic mice.** 4 days after DNA delivery, the transfected BalbC mice (3 mice per group), were anesthetized with isoflurane and challenged intratracheally with either 12.5 µg/mouse of LPS solubilized in 40 µL PBS or PBS only. After a 24 h delay, mice were administered intratracheally with 32 µg/mouse of fMLP in 40 µL PBS or PBS only. This was followed 30 min later by i.p. injections of the Ac-AAPV-(D-Cys) peptide (2.363 mg/mouse in 200 µL saline). After another 30 min delay, mice were treated i.p. with HO-CBT (0.83 mg/mouse in 400 µL of 25% DMSO solution in PBS) and immediately imaged. Mice were anesthetized with 4.0 % isoflurane and maintained under light anesthesia with 1.5 % isoflurane. Bioluminescence images were acquired with an IVIS lumina II imaging system every 5 min for 1 h at 37°C with exposure time set to 5 min. Photons emitted from the chest region were quantified using Living Image® software (Caliper Life Sciences).

**Preparation of lung tissue for Histology (by Dr. Fabio Stellari and Francesca Ruscitti).** 24 or 48 h after intratracheal LPS administration (12.5 µg/mouse in 40 µL PBS) in female BalbC mice (7–8 week-old), animals were sacrificed and lungs were carefully excised. Lungs were then inflated with a cannula through the trachea by gentle infusion with 0.6 ml of 10 % neutral-buffered formalin solution and were placed in a vial containing 10 % neutral-buffered formalin solution and fixed for at least 48 hours. The whole lungs were dehydrated in graded ethanol series, clarified in xylene and paraffin embedded.

**Hematoxylin and Eosine staining on mice lung tissue.** Preparation of tissue sections and staining procedures were performed at the EPFL histology core facility (HCF). Briefly, dewaxed and rehydrated paraffin sections were placed in Harris Hematoxylin solution for 5 min, washed and differentiated in 1 % acid-alcohol for a few seconds. The slides were then placed in a Eosine-Phloxine solution for 1 min, briefly washed with water, dehydrated, cleared and mounted.

**Immunohistochemical staining of Ly6G antigen on mice lung tissue.** Preparation of tissue sections and Immunohistochemical staining procedures were performed at the EPFL histology core facility

(HCF). Immunohistochemical detection of neutrophils (rat anti Ly6G, clone 1A8, diluted 1:200) was performed using the fully automated Ventana Discovery XT (Roche Diagnostics, Rotkreuz, Switzerland), according to manufacturers instructions. Briefly, dewaxed and rehydrated paraffin sections were pre-treated with heat using standard condition (36 minutes) CC1. The primary antibodies were incubated 1 hour at 37 °C. After incubation with a donkey  $\alpha$ -rat biotin (Jackson ImmunoResearch Laboratories), chromogenic revelation was performed with BlueMap kit (Roche Diagnostics, Rotkreuz, Switzerland) with 32 minutes of substrate incubation.

**Real time non-invasive imaging of HNE activity in FVB-Luc<sup>+</sup> mice.** FVB-Luc<sup>+</sup> mice (3 mice per group), were anesthetized with isoflurane and challenged intranasally with either 100  $\mu$ g/mouse of LPS solubilized in 40  $\mu$ L PBS or vehicle. After a 24 h delay, mice were administered intranasally with 32  $\mu$ g/mouse of fMLP in 40  $\mu$ L PBS or PBS only. This was followed 2 h later by i.p. injections of the Ac-AAPV-(D-Cys) peptide (0.391 mg/mouse in 200  $\mu$ L saline). After another 30 min delay, mice were treated i.p. with HO-CBT (0.136 mg/mouse in 100  $\mu$ L of 20% DMSO solution in PBS) and immediately placed in the imaging system. Mice were anesthetized with 4.0 % isoflurane and maintained under light anaesthesia with 1.5 % isoflurane. Bioluminescence images were acquired with an IVIS Spectrum imaging system every min for 1 h at 37°C with automatic settings. Photons emitted from the chest region were quantified using Living Image<sup>®</sup> software (Caliper Life Sciences).

## 4.7 Supplementary figures

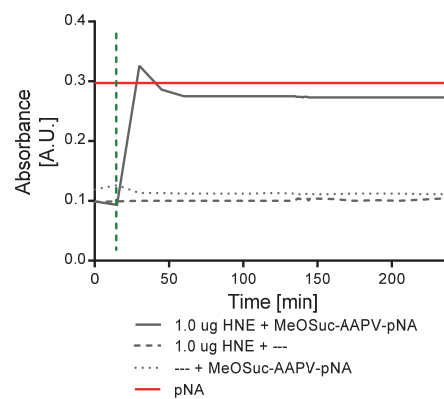


Figure S4.1: Colorimetric assay of HNE activity. Absorbance measured at 405 nm in function of the time during AAPV-pNA incubation with or without 1.0 ug of HNE enzyme in NE-buffer.

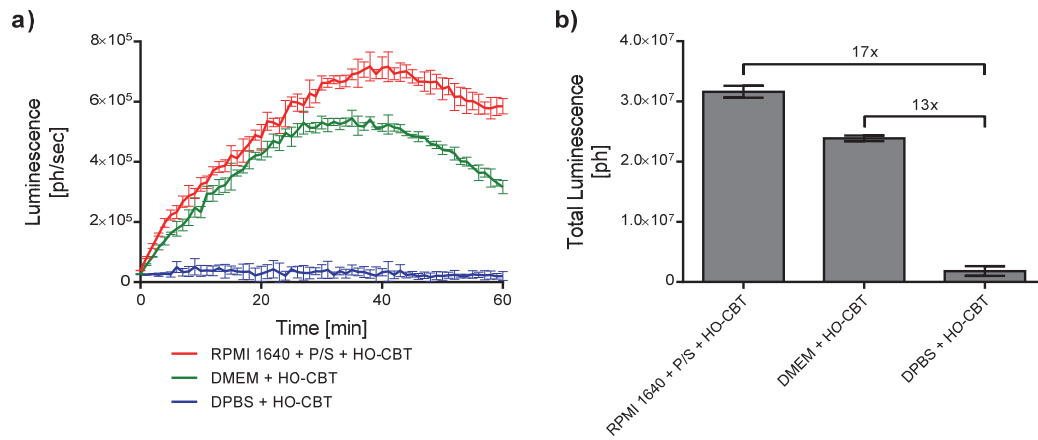


Figure S4.2: Background assessment resulting from the reaction between HO-CBT and cysteine present in different buffers. (a) Observed luminescence as a function of time after HO-CBT (100  $\mu$ M) incubated for 15 min in RPMI 1640 + 1 % penicillin and streptomycin (P/S), DMEM or DPBS. (b) Total luminescent signal integrated over 60 min (AUC). Error bars are  $\pm$  SD for three measurements. Statistical analyses were performed with a two-tailed Student's t test. Differences between all the groups are statistically significant ( $P < 0.002$ ).

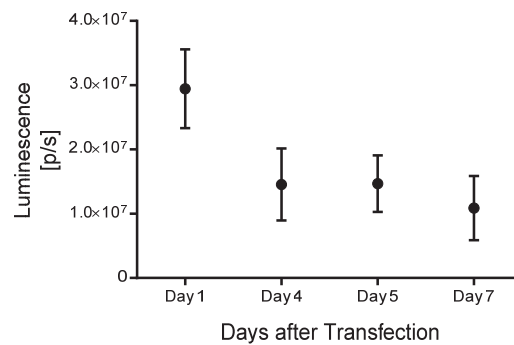


Figure S4.3: Determination of luciferase expression in BalbC transfected mice 1 day, 4 days, 5 days and 7 days after DNA delivery. mice were injected i.p. with D-luciferin (150 mg/kg in 100  $\mu$ L PBS) and bioluminescence was measured 15 min following luciferin injection. Error bars are  $\pm$  SD. Statistical analyses were performed with a two-tailed Student's t test. Differences in light emission between day 4, day 5 and day 7 are not statistically significant ( $P > 0.14$ ).

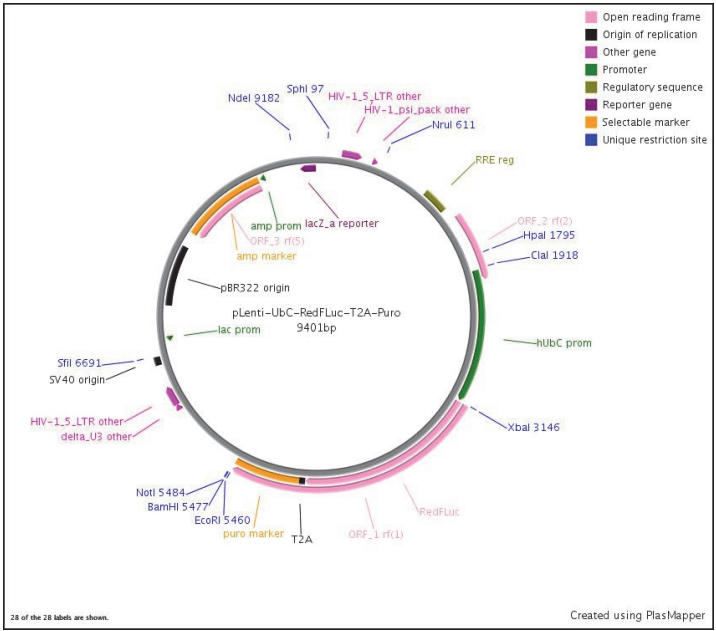


Figure S4.4: Plasmid map of pLenti-UbC-RedFLuc-T2A-Puro (RedLuc-puro) that expresses Luciferase under UbC promoter.

## Chapter 5 Conclusion

Investigation of biological processes in living cells using biocompatible reactions has vastly advanced our understanding of basic biology. Nevertheless, the increased complexity of many human pathologies such as cancer, infections or neurodegenerative diseases requires novel tools to study the biological process on the level of whole organism. However, only a handful of biocompatible reactions have yet been reported to efficiently occur in the complex biological environment of living animals.

The recent focus on 2-cyanobenzothiazole (CBT)-based ligation reaction in the literature has sparked our interest. This reaction has been used for various applications, including fluorescent labeling of proteins and nanostructures formation. Importantly, it was shown to occur selectively in cells.<sup>[197]</sup> As the reaction between D-cysteine and hydroxy- or amino-CBT, named split luciferin reaction, yield the D-luciferin molecule as product, this reaction had substantial potential for BLI applications.

In this work, the split luciferin reaction was shown to efficiently occur in living cells and *in vivo*, generating bioluminescence emission. Remarkably, in cells the signal produced by the split luciferin reagents was several fold higher than the signal from equimolar amounts of already formed D-luciferin and D-aminoluciferin, providing opportunities for more sensitive imaging of biological processes, *in vitro*. The bioluminescence signal produced by the split luciferin reagents *in vivo* was approximately one order of magnitude lower than the light emission generated respectively by D-luciferin or amino-analogue, but still largely above the background. The influence of endogenous L-cysteine on signal was found to be negligible in both living cells and animals within the conditions used in these experiments. In addition, the intensity of the light output with split luciferin reaction can be significantly enhanced by using higher D-cysteine concentration for the *in vivo* studies.

Moreover, the split luciferin approach helps remedy an important problem in the BLI field, which is signal instability of D-luciferin and D-aminoluciferin probes *in vivo*. Important signal variations over short periods of time have been observed utilizing these probes, which in turn induce significant errors for quantification of tumor size or amount of transcriptional activation.<sup>[36,219,220]</sup> The use of split

luciferin approach in animals with D-cysteine and HO-CBT results in major signal stabilization without the use of any specially synthesized expensive reagents or complex procedures.

The split luciferin ligation reaction possesses several unique features which make it highly valuable for a vast variety of imaging applications. The two reagents can be modified (caged) for their use as bioluminogenic probes. D-cysteine modification is very well suited to the development of probes for real-time imaging of protease activity. A successful application of this technology was therefore demonstrated in this study for real time non-invasive imaging of caspase 3/7 activity using a DEVD-(D-Cys) peptide in conjugation with H<sub>2</sub>N-CBT. The probe was validated in a hepatic apoptosis animal model as well as in tumor xenografts model during chemotherapy. When compared to the commercially available DEVD-aminoluciferin substrate, the split luciferin ligation reagents had significantly higher signal to background ratio, demonstrating the high potential of this new method for sensitive imaging of apoptosis. The applicability of this novel tool was further confirmed via studying other proteases (i.e. caspase 6, caspase 8, caspase 9 and thrombin) *in vitro*.

In a further development, another bioluminogenic probe based on the split luciferin approach was developed for imaging and quantification of Neutrophil Elastase (NE) activity. The use of Ac-AAPV-(D-Cys) peptide in combination with HO-CBT yielded an efficient, selective and sensitive *in vitro* quantification method for NE activity. Moreover, imaging of NE activity upon activation of murine neutrophils *ex vivo* was promising, even though further experiments are needed for a complete validation of the probe in cellular assays. The same approach was efficiently applied to NE imaging *in vivo*, in mouse models of acute lung injury. These results conclude that the split luciferin based probe developed in this study is an efficient tool for non-invasive NE imaging *in vivo* and could be a valuable tool for a better understanding of NE function in neutrophil mediated inflammations.

In the present study, we focused on application of the split luciferin approach to monitor caspase 3/7 and NE activities. Furthermore, the same technique could be extended to identify new protease specific peptides as well as to study activities of other proteases.<sup>[80,85,86,109,238]</sup> The examples of such proteases and their specific amino acid sequences include caspase 1 (YVAD), caspase 2 (VDVAD) and caspase 12 (ATAD), dipeptidyl peptidase 4 (GP and VP), tryptase (PRNK) and prostate specific antigen (HSSKLQ).<sup>[58,74,77,79,234]</sup> Moreover, split luciferin method could also be applied to study a wide variety of bacterial, viral and parasite proteases that are essential for the replication and the spread of infectious diseases.<sup>[80]</sup> Examples of these proteases and their specific amino acid sequences include SARS protease (TSAVLQ), caspase-like (nLPnLD), and trypsin-like (LRR) activity of proteasome.<sup>[77,81-83]</sup> All of these proteases mentioned above play important roles in various biological processes and are



known to cleave at the C-terminal of the corresponding specific peptide sequence. Hence, their activities could then be monitored using split luciferin based probes. It is noteworthy to mention that the synthesis of peptide sequences with a C-terminal D-cysteine can be easily performed using automated peptide synthesis,<sup>[239,240]</sup> allowing the generation of a large library of peptide probes to screen substrates for the target of interest.

Since caging of D-cysteine can be combined with caging of amino or hydroxy groups on the CBT moiety, this reaction represents a powerful tool for dual imaging of biological processes. Two biological events could be monitored simultaneously in living mice by using only the two caged luciferin precursors. Previously, multiple probes based on “caging” the luciferin scaffold were reported for sensitive imaging of various biomolecules in live animals, providing a basis for the development of dual imaging approaches.<sup>[50,57,59,71,84,85,92]</sup>

The CBT-based ligation reaction could also be used for bioconjugation in tandem with other biocompatible reactions. Indeed, the CBT-based ligation reagents do not react with azides, and thus could be used in combination with the Staudinger reaction, strain promoted azide-alkyne click reaction or tetrazine reactions with *trans*-cyclooctenes.<sup>[161,187]</sup> This approach could be particularly useful to study simultaneous events in biological systems. Moreover, the kinetics of *in vivo* split luciferin ligation reaction is three orders of magnitude higher than that of Staudinger ligation, opening a wide range of opportunities for the study of fast biological processes.

In summary, this study demonstrates the high potential and versatility of split luciferin reaction for the field of chemical biology and biomedical research. This biocompatible ligation reaction offers a robust methodology for the development of novel bioluminogenic probes with improved accessibility. We sincerely hope that this methodology will prove to be an efficient tool to improve the knowledge on biological systems and disease-associated molecular mechanisms to in turn improve our diagnostic ability of these various diseases and improve the appropriate response to them.



## Chapter 6      References

- (1) Lee, J. J. *Siberian Fed. U.* **2008**, *3*, 194-205.
- (2) Widder, E. A. *Science* **2010**, *328*, 704-708.
- (3) Badr, C. E.; Tannous, B. A. *Trends Biotechnol.* **2011**, *29*, 624-633.
- (4) Wilson, T.; Hastings, J. W. *Annu. Rev. Cell Dev. Biol.* **1998**, *14*, 197-230.
- (5) Keyaerts, M.; Caveliers, V.; Lahoutte, T. *Trends Mol. Med.* **2012**, *18*, 164-172.
- (6) Prescher, J. A.; Contag, C. H. *Curr. Opin. Chem. Biol.* **2010**, *14*, 80-89.
- (7) Haddock, S. H. D.; Moline, M. A.; Case, J. F. *Ann. Rev. Mar. Sci.* **2010**, *2*, 443-493.
- (8) Hall, M. P.; Unch, J.; Binkowski, B. F.; Valley, M. P.; Butler, B. L.; Wood, M. G.; Otto, P.; Zimmerman, K.; Vidugiris, G.; Machleidt, T.; Robers, M. B.; Benink, H. A.; Eggers, C. T.; Slater, M. R.; Meisenheimer, P. L.; Klaubert, D. H.; Fan, F.; Encell, L. P.; Wood, K. V. *ACS Chem. Biol.* **2012**, *7*, 1848-1857.
- (9) Scott, D.; Dikici, E.; Ensor, M.; Daunert, S. *Annu. Rev. Anal. Chem.* **2011**, *4*, 297-319.
- (10) Meighen, E. A. *Annu. Rev. Genet.* **1994**, *28*, 117-139.
- (11) Close, D. M.; Patterson, S. S.; Ripp, S.; Baek, S. J.; Sanseverino, J.; Sayler, G. S. *PLoS One* **2010**, *5*, e12441.
- (12) Luker, K. E.; Luker, G. D. *Antiviral Res.* **2008**, *78*, 179-187.
- (13) Zhao, H.; Doyle, T. C.; Coquoz, O.; Kalish, F.; Rice, B. W.; Contag, C. H. *J. Biomed. Opt.* **2005**, *10*, 041210.
- (14) Miloud, T.; Henrich, C.; Hammerling, G. J. *J. Biomed. Opt.* **2007**, *12*, 054018.
- (15) Bhaumik, S.; Gambhir, S. S. *Proc. Natl. Acad. Sci. USA* **2002**, *99*, 377-382.
- (16) Loening, A. M.; Wu, A. M.; Gambhir, S. S. *Nat. Methods* **2007**, *4*, 641-643.
- (17) Tannous, B. A.; Kim, D. E.; Fernandez, J. L.; Weissleder, R.; Breakefield, X. O. *Mol. Ther.* **2005**, *11*, 435-443.
- (18) Santos, E. B.; Yeh, R.; Lee, J.; Nikhamin, Y.; Punzalan, B.; Punzalan, B.; La Perle, K.; Larson, S. M.; Sadelain, M.; Brentjens, R. J. *Nat. Med.* **2009**, *15*, 338-344.
- (19) Contag, C. H.; Contag, P. R.; Mullins, J. I.; Spilman, S. D.; Stevenson, D. K.; Benaron, D. A. *Mol. Microbiol.* **1995**, *18*, 593-603.
- (20) Rice, B. W.; Cable, M. D.; Nelson, M. B. *J. Biomed. Opt.* **2001**, *6*, 432-440.
- (21) Doyle, T. C.; Wang, Q.; Contag, C. H. *Revealing biomolecular mechanisms through in vivo bioluminescence imaging*. In *Molecular Imaging with Reporter Genes*; Gambhir, S. S., Yaghoubi, S. S., Eds.; Cambridge University Press: **2010**, p 41-69.

- 
- (22) de Wet, J. R.; Wood, K. V.; DeLuca, M.; Helinski, D. R.; Subramani, S. *Mol. Cell. Biol.* **1987**, *7*, 725-737.
- (23) Fraga, H.; Fernandes, D.; Fontes, R.; Esteves da Silva, J. C. G. *FEBS J.* **2005**, *272*, 5206-5216.
- (24) Bai, H. X.; Zhu, P.; Wu, W. X.; Li, J.; Ma, Z.; Zhang, W.; Cheng, Y. N.; Du, L. P.; Li, M. Y. *MedChemComm* **2015**, *6*, 418-424.
- (25) White, E. H.; Worthier, H.; Seliger, H. H.; Mcelroy, W. D. *J. Am. Chem. Soc.* **1966**, *88*, 2015-2019.
- (26) Rhodes, W. C.; Mcelroy, W. D. *J. Biol. Chem.* **1958**, *233*, 1528-1537.
- (27) Fraga, H.; Fernandes, D.; Novotny, J.; Fontes, R.; Esteves da Silva, J. C. G. *ChemBioChem* **2006**, *7*, 929-935.
- (28) Airth, R. L.; Rhodes, W. C.; Mcelroy, W. D. *Biochim. Biophys. Acta* **1958**, *27*, 519-532.
- (29) Fontes, R.; Dukhovich, A.; Sillero, A.; Sillero, M. A. G. *Biochem. Biophys. Res. Commun.* **1997**, *237*, 445-450.
- (30) Lember, N. *Biochem. J* **1996**, *317*, 273-277.
- (31) Nakamura, M.; Maki, S.; Amano, Y.; Ohkita, Y.; Niwa, K.; Hirano, T.; Ohmiya, Y.; Niwa, H. *Biochem. Biophys. Res. Commun.* **2005**, *331*, 471-475.
- (32) Marques, S. M.; Esteves da Silva, J. C. G. *IUBMB Life* **2009**, *61*, 6-17.
- (33) Fraga, H.; Esteves da Silva, J. C. G.; Fontes, R. *Tetrahedron Lett.* **2004**, *45*, 2117-2120.
- (34) Fontes, R.; Ortiz, B.; de Diego, A.; Sillero, A.; Sillero, M. A. G. *FEBS Lett.* **1998**, *438*, 190-194.
- (35) Pinto da Silva, L.; Esteves da Silva, J. C. G. *Photochem. Photobiol. Sci.* **2011**, *10*, 1039-1045.
- (36) Shinde, R.; Perkins, J.; Contag, C. H. *Biochemistry* **2006**, *45*, 11103-11112.
- (37) Woodroffe, C. C.; Shultz, J. W.; Wood, M. G.; Osterman, J.; Cali, J. J.; Daily, W. J.; Meisenheimer, P. L.; Klaubert, D. H. *Biochemistry* **2008**, *47*, 10383-10393.
- (38) Reddy, G. R.; Thompson, W. C.; Miller, S. C. *J. Am. Chem. Soc.* **2010**, *132*, 13586-13587.
- (39) Evans, M. S.; Chaurette, J. P.; Adams, S. T.; Reddy, G. R.; Paley, M. A.; Aronin, N.; Prescher, J. A.; Miller, S. C. *Nat. Methods* **2014**, *11*, 393-395.
- (40) Harwood, K. R.; Mofford, D. M.; Reddy, G. R.; Miller, S. C. *Chem. Biol.* **2011**, *18*, 1649-1657.
- (41) Mofford, D. M.; Reddy, G. R.; Miller, S. C. *J. Am. Chem. Soc.* **2014**, *136*, 13277-13282.
- (42) Conley, N. R.; Dragulescu-Andrasi, A.; Rao, J. H.; Moerner, W. E. *Angew. Chem. Int. Ed.* **2012**, *51*, 3350-3353.
- (43) Woodroffe, C. C.; Meisenheimer, P. L.; Klaubert, D. H.; Kovic, Y.; Rosenberg, J. C.; Behney, C. E.; Southworth, T. L.; Branchini, B. R. *Biochemistry* **2012**, *51*, 9807-9813.
- (44) McCutcheon, D. C.; Paley, M. A.; Steinhardt, R. C.; Prescher, J. A. *J. Am. Chem. Soc.* **2012**, *134*, 7604-7607.
- (45) Branchini, B. R.; Hayward, M. M.; Bamford, S.; Brennan, P. M.; Lajiness, E. J. *Photochem. Photobiol.* **1989**, *49*, 689-695.
- (46) Geiger, R.; Schneider, E.; Wallenfels, K.; Miska, W. *Biol. Chem. Hoppe-Seyler* **1992**, *373*, 1187-1191.
- (47) Adams, S. T.; Miller, S. C. *Curr. Opin. Chem. Biol.* **2014**, *21*, 112-120.
- (48) Berger, F.; Paulmurugan, R.; Bhaumik, S.; Gambhir, S. S. *Eur. J. Nucl. Med. Mol. Imag.* **2008**, *35*, 2275-2285.

- (49) Miska, W.; Geiger, R. *Biol. Chem. Hoppe-Seyler* **1988**, *369*, 407-411.
- (50) Li, J.; Chen, L. Z.; Du, L. P.; Li, M. Y. *Chem. Soc. Rev.* **2013**, *42*, 662-676.
- (51) Razgulin, A.; Ma, N.; Rao, J. H. *Chem. Soc. Rev.* **2011**, *40*, 4186-4216.
- (52) Lakhani, S. A.; Masud, A.; Kuida, K.; Porter, G. A.; Booth, C. J.; Mehal, W. Z.; Inayat, I.; Flavell, R. A. *Science* **2006**, *311*, 847-851.
- (53) Estaquier, J.; Vallette, F.; Vayssiere, J. L.; Mignotte, B. *Adv. Exp. Med. Biol.* **2012**, *942*, 157-183.
- (54) Miyashita, T.; OkamuraOho, Y.; Mito, Y.; Nagafuchi, S.; Yamada, M. *J. Biol. Chem.* **1997**, *272*, 29238-29242.
- (55) Shin, S.; Sung, B. J.; Cho, Y. S.; Kim, H. J.; Ha, N. C.; Hwang, J. I.; Chung, C. W.; Jung, Y. K.; Oh, B. H. *Biochemistry* **2001**, *40*, 1117-1123.
- (56) Rohn, T. T.; Head, E. *Rev. Neurosci.* **2008**, *19*, 383-393.
- (57) Liu, J. J.; Wang, W. G.; Dicker, D. T.; El-Deiry, W. S. *Cancer Biol. Ther.* **2005**, *4*, 885-892.
- (58) O'Brien, M. A.; Daily, W. J.; Hesselberth, P. E.; Moravec, R. A.; Scurria, M. A.; Klaubert, D. H.; Bulleit, R. F.; Wood, K. V. *J. Biomol. Screen.* **2005**, *10*, 137-148.
- (59) Shah, K.; Tung, C. H.; Breakefield, X. O.; Weissleder, R. *Mol. Ther.* **2005**, *11*, 926-931.
- (60) Hickson, J.; Ackler, S.; Klaubert, D.; Bouska, J.; Ellis, P.; Foster, K.; Oleksijew, A.; Rodriguez, L.; Schlessinger, S.; Wang, B.; Frost, D. *Cell Death Differ.* **2010**, *17*, 1003-1010.
- (61) Scabini, M.; Stellari, F.; Cappella, P.; Rizzitano, S.; Texido, G.; Pesenti, E. *Apoptosis* **2011**, *16*, 198-207.
- (62) Biserni, A.; Martorana, F.; Roncoroni, C.; Klaubert, D.; Maggi, A.; Ciana, P. Identification of apoptotic cells in reporter mice using modified luciferin. **2010**. Promega Corporation Web site, <http://ch.promega.com/resources/pubhub/identification-ofapoptotic-cells-in-reporter-mice-using-modified-luciferin/>. Accessed April 2016
- (63) Geiger, G. A.; Parker, S. E.; Beothy, A. P.; Tucker, J. A.; Mullins, M. C.; Kao, G. D. *Cancer Res.* **2006**, *66*, 8172-8181.
- (64) Bassi, D. E.; Fu, J.; Lopez de Cicco, R.; Klein-Szanto, A. J. *Mol. Carcinog.* **2005**, *44*, 151-161.
- (65) Bassi, D. E.; Mahloogi, H.; Klein-Szanto, A. J. *Mol. Carcinog.* **2000**, *28*, 63-69.
- (66) Molloy, S. S.; Anderson, E. D.; Jean, F.; Thomas, G. *Trends Cell Biol.* **1999**, *9*, 28-35.
- (67) Bassi, D. E.; Lopez De Cicco, R.; Mahloogi, H.; Zucker, S.; Thomas, G.; Klein-Szanto, A. J. *Proc. Natl. Acad. Sci. USA* **2001**, *98*, 10326-10331.
- (68) Coppola, J. M.; Bhojani, M. S.; Ross, B. D.; Rehemtulla, A. *Neoplasia* **2008**, *10*, 363-370.
- (69) Hosaka, M.; Nagahama, M.; Kim, W. S.; Watanabe, T.; Hatsuzawa, K.; Ikemizu, J.; Murakami, K.; Nakayama, K. *J. Biol. Chem.* **1991**, *266*, 12127-12130.
- (70) Henrich, S.; Cameron, A.; Bourenkov, G. P.; Kiefersauer, R.; Huber, R.; Lindberg, I.; Bode, W.; Than, M. E. *Nat. Struct. Biol.* **2003**, *10*, 520-526.
- (71) Dragulescu-Andrasi, A.; Liang, G.; Rao, J. *Bioconjugate Chem.* **2009**, *20*, 1660-1666.
- (72) Sapio, M. R.; Fricker, L. D. *Proteomics Clin. Appl.* **2014**, *8*, 327-337.
- (73) Chang, Y. C.; Chao, P. W.; Tung, C. H. *Bioorg. Med. Chem. Lett.* **2011**, *21*, 3931-3934.

- (74) Talanian, R. V.; Quinlan, C.; Trautz, S.; Hackett, M. C.; Mankovich, J. A.; Banach, D.; Ghayur, T.; Brady, K. D.; Wong, W. W. *J. Biol. Chem.* **1997**, *272*, 9677-9682.
- (75) Roy, S.; Sharom, J. R.; Houde, C.; Loisel, T. P.; Vaillancourt, J. P.; Shao, W.; Saleh, M.; Nicholson, D. W. *Proc. Natl. Acad. Sci. USA* **2008**, *105*, 4133-4138.
- (76) van Berkel, S. S.; van der Lee, B.; van Delft, F. L.; Wagenvoort, R.; Hemker, C.; Rutjes, F. P. J. T. *ChemMedChem* **2012**, *7*, 606-617.
- (77) Cosby, N.; Scurria, M.; Daily, W.; Ugo, T. *Cell Notes* **2007**, *18*, 9-11.
- (78) Gorrell, M. D. *Clin. Sci.* **2005**, *108*, 277-292.
- (79) Hedstrom, L. *Chem. Rev.* **2002**, *102*, 4501-4523.
- (80) Wilson, J. W.; Schurr, M. J.; LeBlanc, C. L.; Ramamurthy, R.; Buchanan, K. L.; Nickerson, C. A. *Postgrad. Med. J.* **2002**, *78*, 216-224.
- (81) Huang, C. K.; Wei, P.; Fan, K. Q.; Liu, Y.; Lai, L. H. *Biochemistry* **2004**, *43*, 4568-4574.
- (82) Cheng, S. C.; Chang, G. G.; Chou, C. Y. *Biophys. J.* **2010**, *98*, 1327-1336.
- (83) Kisselev, A. F.; Callard, A.; Goldberg, A. L. *J. Biol. Chem.* **2006**, *281*, 8582-8590.
- (84) Wehrman, T. S.; von Degenfeld, G.; Krutzik, P. O.; Nolan, G. P.; Blau, H. M. *Nat. Methods* **2006**, *3*, 295-301.
- (85) Yao, H.; So, M. K.; Rao, J. *Angew. Chem. Int. Ed.* **2007**, *46*, 7031-7034.
- (86) Zhou, W. H.; Shultz, J. W.; Murphy, N.; Hawkins, E. M.; Bernad, L.; Good, T.; Moothart, L.; Frackman, S.; Klaubert, D. H.; Bulleit, R. F.; Wood, K. V. *Chem. Commun.* **2006**, 4620-4622.
- (87) Zhou, W.; Andrews, C.; Liu, J.; Shultz, J. W.; Valley, M. P.; Cali, J. J.; Hawkins, E. M.; Klaubert, D. H.; Bulleit, R. F.; Wood, K. V. *ChemBioChem* **2008**, *9*, 714-718.
- (88) Rush, J. S.; Beatty, K. E.; Bertozzi, C. R. *ChemBioChem* **2010**, *11*, 2096-2099.
- (89) Vorobyeva, A. G.; Stanton, M.; Godinat, A.; Lund, K. B.; Karateev, G. G.; Francis, K. P.; Allen, E.; Gelovani, J. G.; McCormack, E.; Tangney, M.; Dubikovskaya, E. A. *PLoS One* **2015**, *10*, e0131037.
- (90) Cohen, A. S.; Dubikovskaya, E. A.; Rush, J. S.; Bertozzi, C. R. *J. Am. Chem. Soc.* **2010**, *132*, 8563-8565.
- (91) Sellmyer, M. A.; Bronsart, L.; Imoto, H.; Contag, C. H.; Wandless, T. J.; Prescher, J. A. *Proc. Natl. Acad. Sci. USA* **2013**, *110*, 8567-8572.
- (92) Van de Bittner, G. C.; Dubikovskaya, E. A.; Bertozzi, C. R.; Chang, C. J. *Proc. Natl. Acad. Sci. USA* **2010**, *107*, 21316-21321.
- (93) Tian, X. D.; Li, Z. Y.; Lau, C. W.; Lu, J. Z. *Anal. Chem.* **2015**, *87*, 11325-11331.
- (94) Ke, B. W.; Wu, W. X.; Liu, W.; Liang, H.; Gong, D. Y.; Hu, X. T.; Li, M. Y. *Anal. Chem.* **2016**, *88*, 592-595.
- (95) Shao, Q.; Jiang, T.; Ren, G.; Cheng, Z.; Xing, B. *Chem. Commun.* **2009**, 4028-4030.
- (96) Yang, Y.; Shao, Q.; Deng, R.; Wang, C.; Teng, X.; Cheng, K.; Cheng, Z.; Huang, L.; Liu, Z.; Liu, X.; Xing, B. *Angew. Chem. Int. Ed.* **2012**, *51*, 3125-3129.
- (97) Jones, L. R.; Goun, E. A.; Shinde, R.; Rothbard, J. B.; Contag, C. H.; Wender, P. A. *J. Am. Chem. Soc.* **2006**, *128*, 6526-6527.

- (98) Wender, P. A.; Goun, E. A.; Jones, L. R.; Pillow, T. H.; Rothbard, J. B.; Shinde, R.; Contag, C. H. *Proc. Natl. Acad. Sci. USA* **2007**, *104*, 10340-10345.
- (99) Henkin, A. H.; Cohen, A. S.; Dubikovskaya, E. A.; Park, H. M.; Nikitin, G. F.; Auzias, M. G.; Kazantzis, M.; Bertozzi, C. R.; Stahl, A. *ACS Chem. Biol.* **2012**, *7*, 1884-1891.
- (100) Terai, T.; Nagano, T. *Pflugers Arch.* **2013**, *465*, 347-359.
- (101) Madani, F.; Lindberg, S.; Langel, U.; Futaki, S.; Graslund, A. *J Biophys* **2011**, *2011*, 414729.
- (102) Mishra, A.; Lai, G. H.; Schmidt, N. W.; Sun, V. Z.; Rodriguez, A. R.; Tong, R.; Tang, L.; Cheng, J. J.; Deming, T. J.; Kamei, D. T.; Wong, G. C. L. *Proc. Natl. Acad. Sci. USA* **2011**, *108*, 16883-16888.
- (103) Bechara, C.; Sagan, S. *FEBS Lett.* **2013**, *587*, 1693-1702.
- (104) Hirose, H.; Takeuchi, T.; Osakada, H.; Pujals, S.; Katayama, S.; Nakase, I.; Kobayashi, S.; Haraguchi, T.; Futaki, S. *Mol. Ther.* **2012**, *20*, 984-993.
- (105) Mofford, D. M.; Adams, S. T.; Reddy, G. S. K. K.; Reddy, G. R.; Miller, S. C. *J. Am. Chem. Soc.* **2015**, *137*, 8684-8687.
- (106) Meisenheimer, P. L.; Uyeda, H. T.; Ma, D. P.; Sobol, M.; McDougall, M. G.; Corona, C.; Simpson, D.; Klaubert, D. H.; Cali, J. J. *Drug Metab. Dispos.* **2011**, *39*, 2403-2410.
- (107) Roncoroni, C.; Rizzi, N.; Brunialti, E.; Cali, J. J.; Klaubert, D. H.; Maggi, A.; Ciana, P. *Pharmacol. Res.* **2012**, *65*, 531-536.
- (108) Valley, M. P.; Zhou, W.; Hawkins, E. M.; Shultz, J.; Cali, J. J.; Worzella, T.; Bernad, L.; Good, T.; Good, D.; Riss, T. L.; Klaubert, D. H.; Wood, K. V. *Anal. Biochem.* **2006**, *359*, 238-246.
- (109) Zhou, W. H.; Valley, M. P.; Shultz, J.; Hawkins, E. M.; Bernad, L.; Good, T.; Good, D.; Riss, T. L.; Klaubert, D. H.; Wood, K. V. *J. Am. Chem. Soc.* **2006**, *128*, 3122-3123.
- (110) Contag, C. H. *functional imaging using bioluminescent markers*. In *Molecular Imaging: Principles and Practice*; weissleder, R., Ed.; People's Medical Publishing House: **2010**, p 118-138.
- (111) Edinger, M.; Sweeney, T. J.; Tucker, A. A.; Olomu, A. B.; Negrin, R. S.; Contag, C. H. *Neoplasia* **1999**, *1*, 303-310.
- (112) Hawes, J. J.; Reilly, K. M. *Toxicol. Pathol.* **2010**, *38*, 123-130.
- (113) Contag, C. H.; Spilman, S. D.; Contag, P. R.; Oshiro, M.; Eames, B.; Dennerly, P.; Stevenson, D. K.; Benaron, D. A. *Photochem. Photobiol.* **1997**, *66*, 523-531.
- (114) McCaffrey, A.; Kay, M. A.; Contag, C. H. *Mol. Imaging* **2003**, *2*, 75-86.
- (115) d'Enfert, C.; Vecchiarelli, A.; Brown, A. J. *Virulence* **2010**, *1*, 174-176.
- (116) Luker, K. E.; Smith, M. C.; Luker, G. D.; Gammon, S. T.; Piwnica-Worms, H.; Piwnica-Worms, D. *Proc. Natl. Acad. Sci. USA* **2004**, *101*, 12288-12293.
- (117) Kuchimaru, T.; Iwano, S.; Kiyama, M.; Mitsumata, S.; Kadonosono, T.; Niwa, H.; Maki, S.; Kizaka-Kondoh, S. *Nat. Commun.* **2016**, *7*, 11856.
- (118) Branchini, B. R.; Ablamsky, D. M.; Murtiashaw, M. H.; Uzasci, L.; Fraga, H.; Southworth, T. L. *Anal. Biochem.* **2007**, *361*, 253-262.
- (119) Branchini, B. R.; Ablamsky, D. M.; Davis, A. L.; Southworth, T. L.; Butler, B.; Fan, F.; Jathoul, A. P.; Pule, M. A. *Anal. Biochem.* **2010**, *396*, 290-297.
- (120) Branchini, B. R.; Southworth, T. L.; Khattak, N. F.; Michelini, E.; Roda, A. *Anal. Biochem.* **2005**, *345*, 140-148.

- (121) Liang, Y. J.; Walczak, P.; Bulte, J. W. M. *J. Biomed. Opt.* **2012**, *17*, 016004.
- (122) Tsien, R. Y. *Annu. Rev. Biochem.* **1998**, *67*, 509-544.
- (123) Crivat, G.; Taraska, J. W. *Trends Biotechnol.* **2012**, *30*, 8-16.
- (124) Gautier, A.; Juillerat, A.; Heinis, C.; Correa, I. R.; Kindermann, M.; Beauvils, F.; Johnsson, K. *Chem. Biol.* **2008**, *15*, 128-136.
- (125) Juillerat, A.; Gronemeyer, T.; Keppler, A.; Gendreizig, S.; Pick, H.; Vogel, H.; Johnsson, K. *Chem. Biol.* **2003**, *10*, 313-317.
- (126) Los, G. V.; Encell, L. P.; McDougall, M. G.; Hartzell, D. D.; Karassina, N.; Zimprich, C.; Wood, M. G.; Learish, R.; Ohane, R. F.; Urh, M.; Simpson, D.; Mendez, J.; Zimmerman, K.; Otto, P.; Vidugiris, G.; Zhu, J.; Darzins, A.; Klaubert, D. H.; Bulleit, R. F.; Wood, K. V. *ACS Chem. Biol.* **2008**, *3*, 373-382.
- (127) Griffin, B. A.; Adams, S. R.; Tsien, R. Y. *Science* **1998**, *281*, 269-272.
- (128) Griffin, B. A.; Adams, S. R.; Jones, J.; Tsien, R. Y. *Methods Enzymol.* **2000**, *Volume 327*, 565-578.
- (129) Uttamapinant, C.; White, K. A.; Baruah, H.; Thompson, S.; Fernandez-Suarez, M.; Puthenveetil, S.; Ting, A. Y. *Proc. Natl. Acad. Sci. USA* **2010**, *107*, 10914-10919.
- (130) Rashidian, M.; Dozier, J. K.; Distefano, M. D. *Bioconjugate Chem.* **2013**, *24*, 1277-1294.
- (131) Hang, H. C.; Yu, C.; Kato, D. L.; Bertozzi, C. R. *Proc. Natl. Acad. Sci. USA* **2003**, *100*, 14846-14851.
- (132) Horisawa, K. *Front. Physiol.* **2014**, *5*, 457.
- (133) Sletten, E. M.; Bertozzi, C. R. *Angew. Chem. Int. Ed.* **2009**, *48*, 6974-6998.
- (134) Rogers, A. B. *Gastric Helicobacter spp. in Animal Models: Pathogenesis and Modulation by Extragastric Coinfections*. In *Helicobacter Species: Methods and Protocols*; Houghton, J., Ed.; Humana Press: Totowa, NJ, **2012**, p 175-188.
- (135) LaFerla, F. M.; Green, K. N. *Cold Spring Harb. Perspect. Med.* **2012**, *2*, a006320.
- (136) Peters, M.; Trembovler, V.; Alexandrovich, A.; Parnas, M.; Birnbaumer, L.; Minke, B.; Shohami, E. *J. Neurotrauma* **2012**, *29*, 2831-2834.
- (137) Langdon, S. P. *Curr. Drug Targets* **2012**, *13*, 1535-1547.
- (138) Fedele, M.; Gualillo, O.; Vecchione, A. *J. Biomed. Biotechnol.* **2012**, *2010*, 404130.
- (139) Li, Z. Q.; Zhao, G. P.; Qian, S. Q.; Yang, Z. J.; Chen, X. Y.; Chen, J.; Cai, C.; Liang, X. B.; Guo, J. *J. Ethnopharmacol.* **2012**, *144*, 305-312.
- (140) Agard, N. J.; Baskin, J. M.; Prescher, J. A.; Lo, A.; Bertozzi, C. R. *ACS Chem. Biol.* **2006**, *1*, 644-648.
- (141) Sletten, E. M.; Nakamura, H.; Jewett, J. C.; Bertozzi, C. R. *J. Am. Chem. Soc.* **2010**, *132*, 11799-11805.
- (142) Jewett, J. C.; Sletten, E. M.; Bertozzi, C. R. *J. Am. Chem. Soc.* **2010**, *132*, 3688-3690.
- (143) Chang, P. V.; Prescher, J. A.; Sletten, E. M.; Baskin, J. M.; Miller, I. A.; Agard, N. J.; Lo, A.; Bertozzi, C. R. *Proc. Natl. Acad. Sci. USA* **2010**, *107*, 1821-1826.
- (144) Ning, X. H.; Guo, J.; Wolfert, M. A.; Boons, G. J. *Angew. Chem. Int. Ed.* **2008**, *47*, 2253-2255.
- (145) Stockmann, H.; Neves, A. A.; Stairs, S.; Ireland-Zecchini, H.; Brindle, K. M.; Leeper, F. J. *Chemical Science* **2011**, *2*, 932-936.



- 
- (146) Lin, F. L.; Hoyt, H. M.; van Halbeek, H.; Bergman, R. G.; Bertozzi, C. R. *J. Am. Chem. Soc.* **2005**, *127*, 2686-2695.
- (147) Saxon, E.; Bertozzi, C. R. *Science* **2000**, *287*, 2007-2010.
- (148) Saxon, E.; Armstrong, J. I.; Bertozzi, C. R. *Org. Lett.* **2000**, *2*, 2141-2143.
- (149) Prescher, J. A.; Dube, D. H.; Bertozzi, C. R. *Nature* **2004**, *430*, 873-877.
- (150) Dube, D. H.; Prescher, J. A.; Quang, C. N.; Bertozzi, C. R. *Proc. Natl. Acad. Sci. USA* **2006**, *103*, 4819-4824.
- (151) Nilsson, B. L.; Kiessling, L. L.; Raines, R. T. *Org. Lett.* **2000**, *2*, 1939-1941.
- (152) Hangauer, M. J.; Bertozzi, C. R. *Angew. Chem. Int. Ed.* **2008**, *47*, 2394-2397.
- (153) Chang, P. V.; Prescher, J. A.; Hangauer, M. J.; Bertozzi, C. R. *J. Am. Chem. Soc.* **2007**, *129*, 8400-8401.
- (154) van Berkel, S. S.; van Eldijk, M. B.; van Hest, J. C. M. *Angew. Chem. Int. Ed.* **2011**, *50*, 8806-8827.
- (155) Yang, J.; Seckute, J.; Cole, C. M.; Devaraj, N. K. *Angew. Chem. Int. Ed.* **2012**, *51*, 7476-7479.
- (156) Devaraj, N. K.; Thurber, G. M.; Keliher, E. J.; Marinelli, B.; Weissleder, R. *Proc. Natl. Acad. Sci. USA* **2012**, *109*, 4762-4767.
- (157) Devaraj, N. K.; Weissleder, R.; Hilderbrand, S. A. *Bioconjugate Chem.* **2008**, *19*, 2297-2299.
- (158) Lang, K.; Davis, L.; Wallace, S.; Mahesh, M.; Cox, D. J.; Blackman, M. L.; Fox, J. M.; Chin, J. W. *J. Am. Chem. Soc.* **2012**, *134*, 10317-10320.
- (159) Blackman, M. L.; Royzen, M.; Fox, J. M. *J. Am. Chem. Soc.* **2008**, *130*, 13518-13519.
- (160) Li, Z. B.; Cai, H. C.; Hassink, M.; Blackman, M. L.; Brown, R. C. D.; Conti, P. S.; Fox, J. M. *Chem. Commun.* **2010**, *46*, 8043-8045.
- (161) Liang, Y.; Mackey, J. L.; Lopez, S. A.; Liu, F.; Houk, K. N. *J. Am. Chem. Soc.* **2012**, *134*, 17904-17907.
- (162) Neves, A. A.; Stockmann, H.; Harmston, R. R.; Pryor, H. J.; Alam, I. S.; Ireland-Zecchini, H.; Lewis, D. Y.; Lyons, S. K.; Leeper, F. J.; Brindle, K. M. *FASEB J.* **2011**, *25*, 2528-2537.
- (163) Neves, A. A.; Stockmann, H.; Wainman, Y. A.; Kuo, J. C. H.; Fawcett, S.; Leeper, F. J.; Brindle, K. M. *Bioconjugate Chem.* **2013**, *24*, 934-941.
- (164) Vugts, D. J.; Vervoort, A.; Stigter-van Walsum, M.; Visser, G. W. M.; Robillard, M. S.; Versteegen, R. M.; Vulders, R. C. M.; Herscheid, J. D. M.; van Dongen, G. A. M. S. *Bioconjugate Chem.* **2011**, *22*, 2072-2081.
- (165) Baskin, J. M.; Prescher, J. A.; Laughlin, S. T.; Agard, N. J.; Chang, P. V.; Miller, I. A.; Lo, A.; Codelli, J. A.; Bertozzi, C. R. *Proc. Natl. Acad. Sci. USA* **2007**, *104*, 16793-16797.
- (166) Laughlin, S. T.; Baskin, J. M.; Amacher, S. L.; Bertozzi, C. R. *Science* **2008**, *320*, 664-667.
- (167) Laughlin, S. T.; Bertozzi, C. R. *ACS Chem. Biol.* **2009**, *4*, 1068-1072.
- (168) Dehnert, K. W.; Baskin, J. M.; Laughlin, S. T.; Beahm, B. J.; Naidu, N. N.; Amacher, S. L.; Bertozzi, C. R. *ChemBioChem* **2012**, *13*, 353-357.
- (169) van den Bosch, S. M.; Rossin, R.; Verkerk, P. R.; ten Hoeve, W.; Janssen, H. M.; Lub, J.; Robillard, M. S. *Nucl. Med. Biol.* **2013**, *40*, 415-423.
- (170) Gallo, J.; Kamaly, N.; Lavdas, I.; Stevens, E.; Nguyen, Q. D.; Wylezinska-Arridge, M.; Aboagye, E. O.; Long, N. J. *Angew. Chem. Int. Ed.* **2014**, *53*, 9550-9554.

- (171) Zeglis, B. M.; Sevak, K. K.; Reiner, T.; Mohindra, P.; Carlin, S. D.; Zanzonico, P.; Weissleder, R.; Lewis, J. S. *J. Nucl. Med.* **2013**, *54*, 1389-1396.
- (172) Nichols, B.; Qin, Z. T.; Yang, J.; Vera, D. R.; Devaraj, N. K. *Chem. Commun.* **2014**, *50*, 5215-5217.
- (173) Rossin, R.; Verkerk, P. R.; van den Bosch, S. M.; Volders, R. C. M.; Verel, I.; Lub, J.; Robillard, M. S. *Angew. Chem. Int. Ed.* **2010**, *49*, 3375-3378.
- (174) Rossin, R.; van den Bosch, S. M.; ten Hoeve, W.; Carvelli, M.; Versteegen, R. M.; Lub, J.; Robillard, M. S. *Bioconjugate Chem.* **2013**, *24*, 1210-1217.
- (175) Rossin, R.; van Duijnhoven, S. M. J.; Lappchen, T.; van den Bosch, S. M.; Robillard, M. S. *Mol. Pharm.* **2014**, *11*, 3090-3096.
- (176) Schilling, C. I.; Jung, N.; Biskup, M.; Schepers, U.; Brase, S. *Chem. Soc. Rev.* **2011**, *40*, 4840-4871.
- (177) Debets, M. F.; van der Doelen, C. W. J.; Rutjes, F. P. J. T.; van Delft, F. L. *ChemBioChem* **2010**, *11*, 1168-1184.
- (178) Lemieux, G. A.; de Graffenried, C. L.; Bertozzi, C. R. *J. Am. Chem. Soc.* **2003**, *125*, 4708-4709.
- (179) Kiick, K. L.; Saxon, E.; Tirrell, D. A.; Bertozzi, C. R. *Proc. Natl. Acad. Sci. USA* **2002**, *99*, 19-24.
- (180) Laughlin, S. T.; Bertozzi, C. R. *Nat. Protoc.* **2007**, *2*, 2930-2944.
- (181) Codelli, J. A.; Baskin, J. M.; Agard, N. J.; Berozzi, C. R. *J. Am. Chem. Soc.* **2008**, *130*, 11486-11493.
- (182) Poloukhine, A. A.; Mbua, N. E.; Wolfert, M. A.; Boons, G. J.; Popik, V. V. *J. Am. Chem. Soc.* **2009**, *131*, 15769-15776.
- (183) Debets, M. F.; van Berkel, S. S.; Schoffelen, S.; Rutjes, F. P. J. T.; van Hest, J. C. M.; van Delft, F. L. *Chem. Commun.* **2010**, *46*, 97-99.
- (184) Karver, M. R.; Weissleder, R.; Hilderbrand, S. A. *Bioconjugate Chem.* **2011**, *22*, 2263-2270.
- (185) Taylor, M. T.; Blackman, M. L.; Dmitrenko, O.; Fox, J. M. *J. Am. Chem. Soc.* **2011**, *133*, 9646-9649.
- (186) Devaraj, N. K.; Upadhyay, R.; Hatin, J. B.; Hilderbrand, S. A.; Weissleder, R. *Angew. Chem. Int. Ed.* **2009**, *48*, 7013-7016.
- (187) Knall, A. C.; Slugovc, C. *Chem. Soc. Rev.* **2013**, *42*, 5131-5142.
- (188) Haun, J. B.; Devaraj, N. K.; Hilderbrand, S. A.; Lee, H.; Weissleder, R. *Nat. Nanotechnol.* **2010**, *5*, 660-665.
- (189) Haun, J. B.; Devaraj, N. K.; Marinelli, B. S.; Lee, H.; Weissleder, R. *ACS Nano* **2011**, *5*, 3204-3213.
- (190) Yang, K. S.; Budin, G.; Reiner, T.; Vinegoni, C.; Weissleder, R. *Angew. Chem. Int. Ed.* **2012**, *51*, 6598-6603.
- (191) Budin, G.; Yang, K. S.; Reiner, T.; Weissleder, R. *Angew. Chem. Int. Ed.* **2011**, *50*, 9378-9381.
- (192) White, E. H.; McCapra, F.; Field, G. F. *J. Am. Chem. Soc.* **1963**, *85*, 337-343.
- (193) Ren, H. J.; Xiao, F.; Zhan, K.; Kim, Y. P.; Xie, H. X.; Xia, Z. Y.; Rao, J. *Angew. Chem. Int. Ed.* **2009**, *48*, 9658-9662.
- (194) Liang, G.; Ren, H.; Rao, J. *Nat. Chem.* **2010**, *2*, 54-60.
- (195) Ye, D.; Liang, G.; Ma, M. L.; Rao, J. *Angew. Chem. Int. Ed.* **2011**, *50*, 2275-2279.
- (196) Deng, Y.; Liu, S.; Mei, K.; Tang, A. M.; Cao, C. Y.; Liang, G. L. *Org. Biomol. Chem.* **2011**, *9*, 6917-6919.

- (197) Yuan, Y.; Liang, G. L. *Org. Biomol. Chem.* **2014**, *12*, 865-871.
- (198) Yuan, Y.; Zhang, J.; Wang, M. J.; Mei, B.; Guan, Y. F.; Liang, G. L. *Anal. Chem.* **2013**, *85*, 1280-1284.
- (199) Nguyen, D. P.; Elliott, T.; Holt, M.; Muir, T. W.; Chin, J. W. *J. Am. Chem. Soc.* **2011**, *133*, 11418-11421.
- (200) Cui, L.; Rao, J. 2-Cyanobenzothiazole (CBT) Condensation for Site-Specific Labeling of Proteins at the Terminal Cysteine Residues. In *Site-Specific Protein Labeling: Methods and Protocols*; Gautier, A., Hinner, J. M., Eds.; Springer New York: New York, NY, **2015**, p 81-92.
- (201) Cheng, Y. F.; Peng, H. J.; Chen, W. X.; Ni, N. T.; Ke, B. W.; Dai, C. F.; Wang, B. H. *Chem. Eur. J.* **2013**, *19*, 4036-4042.
- (202) Wang, P.; Zhang, C. J.; Chen, G. C.; Na, Z. K.; Yao, S. Q.; Sun, H. Y. *Chem. Commun.* **2013**, *49*, 8644-8646.
- (203) Wang, H. C.; Yu, C. C.; Liang, C. F.; Huang, L. D.; Hwu, J. R.; Lin, C. C. *ChemBioChem* **2014**, *15*, 829-835.
- (204) Cao, C. Y.; Chen, Y.; Wu, F. Z.; Deng, Y.; Liang, G. L. *Chem. Commun.* **2011**, *47*, 10320-10322.
- (205) Miao, Q. Q.; Bai, X. Y.; Shen, Y. Y.; Mei, B.; Gao, J. H.; Li, L.; Liang, G. L. *Chem. Commun.* **2012**, *48*, 9738-9740.
- (206) Liang, G. L.; Ronald, J.; Chen, Y. X.; Ye, D. J.; Pandit, P.; Ma, M. L.; Rutt, B.; Rao, J. H. *Angew. Chem. Int. Ed.* **2011**, *50*, 6283-6286.
- (207) Jeon, J.; Shen, B.; Xiong, L. Q.; Miao, Z.; Lee, K. H.; Rao, J.; Chin, F. T. *Bioconjugate Chem.* **2012**, *23*, 1902-1908.
- (208) Inkster, J. A.; Colin, D. J.; Seimbille, Y. *Org. Biomol. Chem.* **2015**, *13*, 3667-3676.
- (209) Massoud, T. F.; Gambhir, S. S. *Genes Dev.* **2003**, *17*, 545-580.
- (210) Oballa, R. M.; Truchon, J. F.; Bayly, C. I.; Chauret, N.; Day, S.; Crane, S.; Berthelette, C. *Bioorg. Med. Chem. Lett.* **2007**, *17*, 998-1002.
- (211) McBean, G. J.; Flynn, J. *Biochem. Soc. Trans.* **2001**, *29*, 717-722.
- (212) Knickelbein, R. G.; Seres, T.; Lam, G.; Johnston, R. B.; Warshaw, J. B. *Am. J. Physiol. Lung Cell. Mol. Physiol.* **1997**, *273*, L1147-L1155.
- (213) Chen, Z.; Fei, Y. J.; Anderson, C. M. H.; Wake, K. A.; Miyauchi, S.; Huang, W.; Thwaites, D. T.; Ganapathy, V. J. *Physiol.* **2003**, *546*, 349-361.
- (214) Shikano, N.; Nakajima, S.; Kotani, T.; Ogura, M.; Sagara, J. I.; Iwamura, Y.; Yoshimoto, M.; Kubota, N.; Ishikawa, N.; Kawai, K. *Nucl. Med. Biol.* **2007**, *34*, 659-665.
- (215) Goun, E. A.; Pillow, T. H.; Jones, L. R.; Rothbard, J. B.; Wender, P. A. *ChemBioChem* **2006**, *7*, 1497-1515.
- (216) White, E. H.; Steinmetz, M. G.; Miano, J. D.; Wildes, P. D.; Morland, R. J. *Am. Chem. Soc.* **1980**, *102*, 3199-3208.
- (217) ACS Chemical Biology Website. <http://pubs.acs.org/doi/suppl/10.1021/cb3007314> (April 17, **2016**)
- (218) Cao, Y. A.; Wagers, A. J.; Beilhack, A.; Dusich, J.; Bachmann, M. H.; Negrin, R. S.; Weissman, I. L.; Contag, C. H. *Proc. Natl. Acad. Sci. USA* **2004**, *101*, 221-226.
- (219) Gross, S.; Piwnicka-Worms, D. *Nat. Methods* **2005**, *2*, 607-614.
- (220) Chandran, S. S.; Williams, S. A.; Denmeade, S. R. *Luminescence* **2009**, *24*, 35-38.
- (221) Vieira, J.; Pinto da Silva, L.; Esteves da Silva, J. C. G. *J. Photochem. Photobiol., B* **2012**, *117*, 33-39.
- (222) Kelkar, M.; De, A. *Curr. Opin. Pharmacol.* **2012**, *12*, 592-600.

- (223) Welsh, D. K.; Noguchi, T. *Cold Spring Harb. Protoc.* **2012**, 2012, 852-866.
- (224) Kim, S. B. *Protein Eng. Des. Sel.* **2012**, 25, 261-269.
- (225) Zinn, K. R.; Chaudhuri, T. R.; Szafran, A. A.; O'Quinn, D.; Weaver, C.; Dugger, K.; Lamar, D.; Kesterson, R. A.; Wang, X. D.; Frank, S. J. *ILAR J.* **2008**, 49, 103-115.
- (226) Chaudhari, A. J.; Darvas, F.; Bading, J. R.; Moats, R. A.; Conti, P. S.; Smith, D. J.; Cherry, S. R.; Leahy, R. M. *Phys. Med. Biol.* **2005**, 50, 5421-5441.
- (227) King, M.; Wagner, A. *Bioconjugate Chem.* **2014**, 25, 825-839.
- (228) Patterson, D. M.; Nazarova, L. A.; Prescher, J. A. *ACS Chem. Biol.* **2014**, 9, 592-605.
- (229) Rossin, R.; Robillard, M. S. *Curr. Opin. Chem. Biol.* **2014**, 21, 161-169.
- (230) Godinat, A.; Park, H. M.; Miller, S. C.; Cheng, K.; Hanahan, D.; Sanman, L. E.; Bogoy, M.; Yu, A.; Nikitin, G. F.; Stahl, A.; Dubikovskaya, E. A. *ACS Chem. Biol.* **2013**, 8, 987-999.
- (231) Van de Bittner, G. C.; Bertozzi, C. R.; Chang, C. J. *J. Am. Chem. Soc.* **2013**, 135, 1783-1795.
- (232) McLaughlin, J. N.; Patterson, M. M.; Malik, A. B. *Proc. Natl. Acad. Sci. USA* **2007**, 104, 5662-5667.
- (233) Ito, K.; Nishimura, W.; Maeda, M.; Gomi, K.; Inouye, S.; Arakawa, H. *Anal. Chim. Acta* **2007**, 588, 245-251.
- (234) Denmeade, S. R.; Lou, W.; Lovgren, J.; Malm, J.; Lilja, H.; Isaacs, J. T. *Cancer Res.* **1997**, 57, 4924-4930.
- (235) Monsees, T.; Miska, W.; Geiger, R. *Anal. Biochem.* **1994**, 221, 329-334.
- (236) Ray, P.; De, A.; Patel, M.; Gambhir, S. S. *Clin. Cancer. Res.* **2008**, 14, 5801-5809.
- (237) Laxman, B.; Hall, D. E.; Bhojani, M. S.; Hamstra, D. A.; Chenevert, T. L.; Ross, B. D.; Rehemtulla, A. *Proc. Natl. Acad. Sci. USA* **2002**, 99, 16551-16555.
- (238) Cali, J. J.; Ma, D. P.; Sobol, M.; Simpson, D. J.; Frackman, S.; Good, T. I.; Daily, W. J.; Liu, D. *Expert Opin. Drug Metab. Toxicol.* **2006**, 2, 629-645.
- (239) Merrifield, R. B. *Science* **1965**, 150, 178-185.
- (240) Merrifield, R. B.; Stewart, J. M. *Nature* **1965**, 207, 522-523.
- (241) Paley, M. A.; Prescher, J. A. *MedChemComm* **2014**, 5, 255-267.
- (242) Jurisicova, A.; Antenos, M.; Varmuza, S.; Tilly, J. L.; Casper, R. F. *Mol. Human Reprod.* **2003**, 9, 133-141.
- (243) Elmore, S. *Toxicol. Pathol.* **2007**, 35, 495-516.
- (244) Pop, C.; Salvesen, G. S. *J. Biol. Chem.* **2009**, 284, 21777-21781.
- (245) Nicholls, S. B.; Hyman, B. T. *Methods Enzymol.* **2014**, 544, 251-269.
- (246) Thornberry, N. A.; Ranon, T. A.; Pieterse, E. P.; Rasper, D. M.; Timkey, T.; GarciaCalvo, M.; Houtzager, V. M.; Nordstrom, P. A.; Roy, S.; Vaillancourt, J. P.; Chapman, K. T.; Nicholson, D. W. *J. Biol. Chem.* **1997**, 272, 17907-17911.
- (247) Donahue, B. S.; Gailani, D.; Higgins, M. S.; Drinkwater, D. C.; George, A. L. *Circulation* **2003**, 107, 1003-1008.
- (248) Angelillo-Scherrer, A.; de Frutos, P. G.; Aparicio, C.; Melis, E.; Savi, P.; Lupu, F.; Arnout, J.; Dewerchin, M.; Hoylaerts, M. F.; Herbert, M.; Collen, D.; Dahlback, B.; Carmeliet, P. *Nat. Med.* **2001**, 7, 215-221.

- 
- (249) Seife, C. *Science* **1997**, *277*, 1602-1603.
- (250) McStay, G. P.; Salvesen, G. S.; Green, D. R. *Cell Death Differ.* **2008**, *15*, 322-331.
- (251) Timmer, J. C.; Salvesen, G. S. *Cell Death Differ.* **2007**, *14*, 66-72.
- (252) Stennicke, H. R.; Salvesen, G. S. *Methods* **1999**, *17*, 313-319.
- (253) Stennicke, H. R.; Salvesen, G. S. *Apoptosis* **2000**, *322*, 91-100.
- (254) Stennicke, H. R.; Renatus, M.; Meldal, M.; Salvesen, G. S. *Biochem. J* **2000**, *350*, 563-568.
- (255) Husain, Q. *Crit. Rev. Biotechnol.* **2010**, *30*, 41-62.
- (256) Masuda-Nishimura, I.; Fukuda, S.; Sano, A.; Kasai, K.; Tatsumi, H. *Lett. Appl. Microbiol.* **2000**, *30*, 130-135.
- (257) Yang, X. Y.; Janatova, J.; Andrade, J. D. *Anal. Biochem.* **2005**, *336*, 102-107.
- (258) Mignon, A.; Rouquet, N.; Fabre, M.; Martin, S.; Pages, J. C.; Dhainaut, J. F.; Kahn, A.; Briand, P.; Joulin, V. *Am. J. Respir. Crit. Care Med.* **1999**, *159*, 1308-1315.
- (259) Lyseng-Williamson, K. A.; Fenton, C. *Drugs* **2005**, *65*, 2513-2531.
- (260) Dieras, V. *Oncology* **1997**, *11*, 31-33.
- (261) Fulton, B.; Spencer, C. M. *Drugs* **1996**, *51*, 1075-1092.
- (262) Michael, A.; Syrigos, K.; Pandha, H. *Prostate Cancer Prostatic Dis.* **2009**, *12*, 13-16.
- (263) Halder, J.; Landen, C. N.; Lutgendorf, S. K.; Li, Y.; Jennings, N. B.; Fan, D.; Nelkin, G. M.; Schmandt, R.; Schaller, M. D.; Sood, A. K. *Clin. Cancer. Res.* **2005**, *11*, 8829-8836.
- (264) Amess, R.; Baggett, N.; Darby, P. R.; Goode, A. R.; Vickers, E. E. *Carbohydr. Res.* **1990**, *205*, 225-233.
- (265) Shapiro, S. D. *Am. J. Respir. Cell Mol. Biol.* **2002**, *26*, 266-268.
- (266) Lee, W. L.; Downey, G. P. *Am. J. Respir. Crit. Care Med.* **2001**, *164*, 896-904.
- (267) Kossodo, S.; Zhang, J.; Groves, K.; Cuneo, G. J.; Handy, E.; Morin, J.; Delaney, J.; Yared, W.; Rajopadhye, M.; Peterson, J. D. *Int. J. Mol. Imaging.* **2011**, *2011*, 581406.
- (268) Kawabata, K.; Hagio, T.; Matsuoka, S. *Eur. J. Pharmacol.* **2002**, *451*, 1-10.
- (269) Korkmaz, B.; Horwitz, M. S.; Jenne, D. E.; Gauthier, F. *Pharmacol. Rev.* **2010**, *62*, 726-759.
- (270) Moroy, G.; Alix, A. J. P.; Sapi, J.; Hornebeck, W.; Bourguet, E. *Anticancer Agents Med. Chem.* **2012**, *12*, 565-579.
- (271) Pham, C. T. N. *Nat. Rev. Immunol.* **2006**, *6*, 541-550.
- (272) Lee, W. L.; Downey, G. P. *The role of Neutrophils in acute lung injury*. In *Etiology and Treatment of Acute Lung Injury: From Bench to Bedside*; Matalon, S., Sznajder, J. I., Eds. **2001**; Vol. 336, p 113-123.
- (273) Castillo, M. J.; Nakajima, K.; Zimmerman, M.; Powers, J. C. *Anal. Biochem.* **1979**, *99*, 53-64.
- (274) Nakajima, K.; Powers, J. C.; Ashe, B. M.; Zimmerman, M. *J. Biol. Chem.* **1979**, *254*, 4027-4032.
- (275) Janoff, A. *Biochem. J* **1969**, *114*, 157-159.

- (276) Korkmaz, B.; Attucci, S.; Hazouard, E.; Ferrandiere, M.; Jourdan, M. L.; Brillard-Bourdet, M.; Juliano, L.; Gauthier, F. *J. Biol. Chem.* **2002**, *277*, 39074-39081.
- (277) Korkmaz, B.; Hajjar, E.; Kalupov, T.; Reuter, N.; Brillard-Bourdet, M.; Moreau, T.; Juliano, L.; Gauthier, F. *J. Biol. Chem.* **2007**, *282*, 1989-1997.
- (278) Koehl, C.; Knight, C. G.; Bieth, J. G. *J. Biol. Chem.* **2003**, *278*, 12609-12612.
- (279) Korkmaz, B.; Attucci, S.; Jourdan, M. L.; Juliano, L.; Gauthier, F. *J. Immunol.* **2005**, *175*, 3329-3338.
- (280) Korkmaz, B.; Attucci, S.; Juliano, M. A.; Kalupov, T.; Jourdan, M. L.; Juliano, L.; Gauthier, F. *Nat. Protoc.* **2008**, *3*, 991-1000.
- (281) Mitra, S.; Modi, K. D.; Foster, T. H. *J. Biomed. Opt.* **2013**, *18*, 101314.
- (282) Ho, A. S.; Chen, C. H.; Cheng, C. C.; Wang, C. C.; Lin, H. C.; Luo, T. Y.; Lien, G. S.; Chang, J. S. *Oncotarget* **2014**, *5*, 473-480.
- (283) Talukdar, S.; Oh, D. Y.; Bandyopadhyay, G.; Li, D. M.; Xu, J. F.; McNelis, J.; Lu, M.; Li, P. P.; Yan, Q. Y.; Zhu, Y. M.; Ofrecio, J.; Lin, M.; Brenner, M. B.; Olefsky, J. M. *Nat. Med.* **2012**, *18*, 1407-1412.
- (284) Charlton, J.; Sennello, J.; Smith, D. *Chem. Biol.* **1997**, *4*, 809-816.
- (285) Rusckowski, M.; Qu, T.; Pullman, J.; Marcel, R.; Ley, A. C.; Ladner, R. C.; Hnatowich, D. J. *J. Nucl. Med.* **2000**, *41*, 363-374.
- (286) Leblond, F.; Davis, S. C.; Valdes, P. A.; Pogue, B. W. *J. Photochem. Photobiol., B* **2010**, *98*, 77-94.
- (287) Rahmim, A.; Zaidi, H. *Nucl. Med. Commun.* **2008**, *29*, 193-207.
- (288) Rao, N. V.; Hoidal, J. R. *Chapter 589 - Myeloblastin*. In *Handbook of Proteolytic Enzymes*; Salvesen, N. D. R., Ed.; Academic Press: **2013**, p 2666-2675.
- (289) Kasperkiewicz, P.; Poreba, M.; Snipas, S. J.; Parker, H.; Winterbourn, C. C.; Salvesen, G. S.; Drag, M. *Proc. Natl. Acad. Sci. USA* **2014**, *111*, 2518-2523.
- (290) Jenssen, H.; Aspino, S. *Serum Stability of Peptides*. In *Peptide-Based Drug Design*; Otvos, L., Ed.; Humana Press: **2008**; Vol. 494, p 177-186.
- (291) Powell, M. F.; Stewart, T.; Otvos, L.; Urge, L.; Gaeta, F. C. A.; Sette, A.; Arrhenius, T.; Thomson, D.; Soda, K.; Colon, S. M. *Pharm. Res.* **1993**, *10*, 1268-1273.
- (292) Sato, A. K.; Viswanathan, M.; Kent, R. B.; Wood, C. R. *Curr. Opin. Biotechnol.* **2006**, *17*, 638-642.
- (293) Kawabata, K.; Suzuki, M.; Sugitani, M.; Imaki, K.; Toda, M.; Miyamoto, T. *Biochem. Biophys. Res. Commun.* **1991**, *177*, 814-820.
- (294) Wiesner, O.; Litwiller, R. D.; Hummel, A. M.; Viss, M. A.; McDonald, C. J.; Jenne, D. E.; Fass, D. N.; Specks, U. *FEBS Lett.* **2005**, *579*, 5305-5312.
- (295) Sato, T.; Hongu, T.; Sakamoto, M.; Funakoshi, Y.; Kanaho, Y. *Mol. Cell. Biol.* **2013**, *33*, 136-145.
- (296) Nick, J. A.; Avdi, N. J.; Young, S. K.; Knall, C.; Gerwins, P.; Johnson, G. L.; Worthen, G. S. *J. Clin. Invest.* **1997**, *99*, 975-986.
- (297) Sandborg, R. R.; Smolen, J. E. *Lab. Invest.* **1988**, *59*, 300-320.
- (298) Boxio, R.; Bossenmeyer-Pourie, C.; Steinckwich, N.; Dournon, C.; Nüsse, O. *J. Leukocyte Biol.* **2004**, *75*, 604-611.
- (299) Corteling, R.; Wyss, D.; Trifilieff, A. *BMC Pharmacol.* **2002**, *2*, 1-8.

- (300) Lefort, J.; Singer, M.; Leduc, D.; Renesto, P.; Nahori, M. A.; Huerre, M.; Creminon, C.; Chignard, M.; Vargaftig, B. B. *J. Immunol.* **1998**, *161*, 474-480.
- (301) Miotla, J. M.; Teixeira, M. M.; Hellewell, P. G. *Am. J. Respir. Cell Mol. Biol.* **1998**, *18*, 411-420.
- (302) Asti, C.; Ruggieri, V.; Porzio, S.; Chiusaroli, R.; Melillo, G.; Caselli, G. F. *Pulm. Pharmacol. Ther.* **2000**, *13*, 61-69.
- (303) Chen, L. Y.; Pan, W. W.; Chen, M.; Li, J. D.; Liu, W.; Chen, G. Q.; Huang, S.; Papadimos, T. J.; Pan, Z. K. *J. Immunol.* **2009**, *182*, 2518-2524.
- (304) Panaro, M. A.; Mitolo, V. *Immunopharmacol. Immunotoxicol.* **1999**, *21*, 397-419.
- (305) Branchini, B. R.; Southworth, T. L.; DeAngelis, J. P.; Roda, A.; Michelini, E. *Comp. Biochem. Physiol. B, Biochem. Mol. Biol.* **2006**, *145*, 159-167.
- (306) Kawabata, K.; Hagio, T.; Matsumoto, S.; Nakao, S.; Orita, S.; Aze, Y.; Ohno, H. *Am. J. Respir. Crit. Care Med.* **2000**, *161*, 2013-2018.
- (307) Godinat, A.; Budin, G.; Morales, A. R.; Park, H. M.; Sanman, L. E.; Bogoy, M.; Yu, A.; Stahl, A.; Dubikovskaya, E. A. *Curr. Protoc. Chem. Biol.* **2014**, *6*, 169-189.





# Chapter 7 Annexes

## 7.1 Curriculum Vitae

### CONTACT INFORMATION

Name and Address	<b>Aurélien Godinat</b> Chemin de la Forêt 6 1024 Ecublens Switzerland
Phone number	+41 (0)79 786 61 73
E-mail address	aurelien.godinat@epfl.ch, aurelien.godinat@gmail.com

### PERSONAL INFORMATION

Nationality	Swiss / French
Date & place of birth	October 30th, 1984, Nyon (VD), Switzerland

### EDUCATION

11.2011-11.2016	Ph.D. studies in chemical biology Laboratory of bioorganic chemistry and molecular imaging (LCBIM) Swiss Federal Institute of Technology, Lausanne (EPFL) under the supervision of Prof. Elena A. Dubikovskaya
11.2009-02.2011	Master of Science (M.Sc.) in biological and molecular Chemistry Swiss Federal Institute of Technology, Lausanne (EPFL)
10.2004-08.2009	Bachelor of Science (B.Sc.) in Chemistry Swiss Federal Institute of Technology, Lausanne (EPFL)
08.2001-06.2004	High school - Swiss cantonal scientific maturity (biology and chemistry)

## PROFESSIONAL QUALIFICATIONS

Languages	French: native English: full professional proficiency German: limited professional proficiency Italian: basic notions
Certificate	Animal Experimentation certificate (Module 1, Introductory Course in Laboratory Animal Science, theoretical and practical)

## AWARDS

- *European Society of Molecular Imaging Young Investigator Award 2013* - (May 2013, Turin, Italy)
- *Runners-up best poster presentation at the Swiss Chemical Society Fall Meeting 2013* - (September 2013, Lausanne, Switzerland)

## PUBLICATIONS

- Vorobyeva, A. G.; Stanton, M.; Godinat, A.; Lund, K. B.; Karateev, G. G.; Francis, K. P.; Allen, E.; Gelovani, J. G.; McCormack, E.; Tangney, M.; Dubikovskaya, E. A. *PlosOne*, **2015**, 10, e0131037.
- Geissbuehler, S.; Sharipov, A.; Godinat, A.; Bocchio, N. L.; Sandoz, P. A.; Huss, A.; Jensen, N. A.; Jakobs, S.; Enderlein, J.; Van der Goot, F. G.; Dubikovskaya, E. A.; Lasser, T.; Leutenegger, M. *Nature Communications*, **2014**, 5, 5830.
- Godinat, A.; Budin, G.; Morales, A. R.; Park, H. M.; Sanman, L. E.; Bogyo, M.; Yu, A.; Stahl, A.; Dubikovskaya, E. A. *Curr. Prot. Chem. Biol.* **2014**, 6, 169–189.
- Godinat, A.; Park, H. M.; Miller, S. C.; Cheng, K.; Hanahan, D.; Sanman, L. E.; Bogyo, M.; Yu, A.; Nikitin, G. N.; Stahl, A.; Dubikovskaya, E. A. *ACS Chem. Biol.* **2013**, 8, 987–999.
- Vechorkin, O.; Godinat, A.; Scopelliti, R.; Hu, X. *Angew. Chem. Int. Ed.* **2011**, 50, 11777–11781.
- Borcard, F.; Godinat, A.; Staedler, D.; Comas Blanco, H.; Dumont, A.-L.; Chapuis-Bernasconi, C.; Scaletta, C.; Applegate, L. A.; Krauss Juillerat, F.; Gonzenbach, U.; Gerber-Lemaire, S.; Juillerat-Jeanerret, L. *Bioconjugate Chem.* **2011**, 22, 1422–1432.
- Thommes, K.; Fernandez-Zumel, M. A.; Buron, C.; Godinat, A.; Scopelliti, R.; Severin, K. *Eur. J. Org. Chem.* **2011**, No. 2, 249–255.

## PATENTS APPLICATIONS

- Dubikovskaya, E. A.; Godinat, A. Precursor molecule for the synthesis of d-luciferin. PCT Int. Appl. **2013**. Patent number WO2014057139 A3.
- Sinisi, R.; Dubikovskaya, E.; Budin, G.; Karateev, G.; Frigell, J.; Konovalova, A.; Godinat, A. Bioluminescence imaging of small biomolecules, PCT Int. Appl. **2014**. Patent number WO2014111906 A1.

## BOOK CHAPTER

- Godinat, A.; Karatas, H.; Budin, G.; Dubikovskaya, E. A. (Submitted for publication) *Chemical ligation for molecular imaging*. In *Chemical Ligation: Tools for Biomolecule Synthesis and Modification.*; D'Andrea, L.; Romanelli, A., Eds.; John Wiley & Sons.
- Karatas, H.; Godinat, A.; Budin, G.; Dubikovskaya, E. A. (Manuscript in preparation) *Modified luciferins for sensing molecular changes in vivo*. In *Visualizing Chemical Communications Among Migratory Cells In Vivo.*; Contag, C. H.; Kusy, S.; Prescher, J. A., Eds.; Springer.

## PROFESSIONAL MEMBERSHIPS

- Member of the European Society of Molecular Imaging
- Member of the Swiss Chemical Society



